UNIVERSIDADE ESTADUAL PAULISTA "JÚLIO DE MESQUITA FILHO"

FACULDADE DE ENGENHARIA

CAMPUS DE ILHA SOLTEIRA

RODRIGO BORGES SANTOS

AN ALTERNATIVE APPROACH TO DESIGN PERIODIC RODS

Ilha Solteira

2018

RODRIGO BORGES SANTOS

AN ALTERNATIVE APPROACH TO DESIGN PERIODIC RODS

Doctoral Thesis presented to the School of Mechanical Engineering of Ilha Solteira of the São Paulo State University (UNESP) in partial fulfillment of the requirements for the degree of Doctor in Mechanical Engineering, in the Area of Solid Mechanics and Mechanical Design.

Prof. Dr. Douglas Domingues Bueno
Advisor

Prof. Dr. Michael John Brennan
Co-advisor

Prof. Dr. Vicente Lopes Junior
Co-advisor

Ilha Solteira
2018

FICHA CATALOGRÁFICA
Desenvolvido pelo Serviço Técnico de Biblioteca e Documentação

Santos, Rodrigo Borges.
S237a An alternative approach to design periodic rods / Rodrigo Borges Santos. -- Ilha Solteira: [s.n.], 06/03/2018
93 f. : il.

Tese (doutorado) - Universidade Estadual Paulista. Faculdade de Engenharia. Área de conhecimento: Solid Mechanics, 2018

Orientador: Douglas Domingues Bueno
Co-orientador: Michael John Brennan And Vicente Lopes Júnior
Inclui bibliografia

1. Periodic rods design. 2. Wave transmission equation. 3. Vibration Attenuation.

Sandra Maria Clemente de Souza
DSTBD/STRAUD
Bibliotecária
CRB 8-4740

UNIVERSIDADE ESTADUAL PAULISTA

Câmpus de Ilha Solteira

CERTIFICADO DE APROVAÇÃO

TÍTULO DA TESE: AN ALTERNATIVE APPROACH TO DESIGN PERIODIC RODS

AUTOR: RODRIGO BORGES SANTOS
ORIENTADOR: DOUGLAS DOMINGUES BUENO
COORIENTADOR: VICENTE LOPES JUNIOR
COORIENTADOR: MICHAEL JOHN BRENNAN

Aprovado como parte das exigências para obtenção do Título de Doutor em ENGENHARIA MECÂNICA, área: MECANICA DOS SÓLIDOS pela Comissão Examinadora:

Prof. Dr. DOUGLAS DOMINGUES BUENO
Departamento de Matemática / Faculdade de Engenharia de Ilha Solteira

Prof. Dr. AMARILDO TABONE PASCHOALINI
Departamento de Engenharia Mecânica / Faculdade de Engenharia de Ilha Solteira

Prof. Dr. MARCIO ANTONIO BAZANI
Departamento de Engenharia Mecânica / Faculdade de Engenharia de Ilha Solteira

Prof. Dr. JOSÉ ROBERTO DE FRANÇA ARRUDA
Departamento de Mecanica Computacional / Universidade Estadual de Campinas - UNICAMP

Prof. Dr. PAULO JOSÉ PAUPITZ GONÇALVES
Departamento de Engenharia Mecânica / Faculdade de Engenharia de Bauru

Ilha Solteira, 06 de março de 2018

Para minha amada família, minha esposa Maria Regina, minha mãe Juraci e meu irmão Wamer. Em memória de meu querido pai, João.

AGRADECIMENTOS

Em primeiro lugar, gostaria de expressar minha profunda gratidão ao meu orientador, prof. Dr. Douglas D. Bueno, por sua amizade, ensinamentos, direcionamentos, encorajamento, suporte e paciência.

Meu sincero obrigado ao meu co-orientador Prof. Dr Michael J. Brennan pela generosa contribuição nesta tese com muitas sugestões, direcionamentos e suporte técnico. Também, agradeço ao meu co-orientador Prof. Dr. Vicente Lopes Júnior pela sua confiança, amizade e por abrir as portas para o desenvolvimento desta tese.

Eu também sou muito grato à minha família por sempre me apoiar, incentivar e aconselhar nos meus objetivos. Em especial, agradeço a minha esposa Maria Regina Ap. de Lima por estar sempre do meu lado em todas as situações de minha vida. A concretização desta tese é um sonho realizado. Obrigado Maria Regina por ter contribuído na realização deste sonho.

Gostaria também de agradecer a todos colegas do Grupo de Materiais e Sistemas Inteligentes (GMSINT) da UNESP/Ilha Solteira, em especial, a Camila G. Gonsalez Bueno, pela amizade, incentivos, discussões técnicas e momentos de descontração.

Obrigado a todos da Universidade Federal da Grande Dourados (UFGD) que contribuíram para o meu afastamento desta universidade durante 1 ano, possibilitando a dedicação exclusiva no desenvolvimento desta tese.

Finalmente e mais importante, eu **agradeço a Deus** por ser o guia de minha vida e por me dar proteção, esperança, oportunidades, sabedoria, paciência, força, paz e saúde. É através Dele que todas as coisas são possíveis em minha vida.

“Sonhos determinam o que você quer,
Ação determina o que você conquista.”
Aldo Novak

ABSTRACT

The reduction of structural vibration has been an important topic for many engineering applications. In traditional projects different passive control techniques involving viscoelastic materials and dynamic absorbers and, more recently, active control methodologies including actuators and sensors have been successfully employed. Different researches have demonstrated that vibration reduction can be obtained using the concept of periodicity. The periodic structures involve identical elements or parts connected repeatedly. The design of periodic structures can be employed to get frequency band without elastic waves propagation, i.e., stop bands, introducing an effect similar to the filter. In this context, the present work introduces an alternative approach for designing periodic rods. This alternative involves the modeling of an infinite hybrid type periodic rod in which a finite periodic structure is connected between two semi-infinite rods. It is used a methodology that relates state vector and wave amplitudes. The main proposal of this work is to develop a relation between the transmitted and incident longitudinal waves amplitudes in terms of physical and geometrical properties of a generic candidate structure to simplify the process of designing. Based on this approach is shown that a periodic rod can be designed to satisfy requirements of a vibration suppression. A hypothetical problem is proposed and numerical and experimental results show the stop bands obtained to solve the problem. It shows that this approach is an important tool for designing this type of structures.

Keywords: Periodic rods design. Wave transmission equation. Vibration attenuation.

RESUMO

A redução de vibração estrutural tem sido um importante tópico para muitas aplicações de engenharia. Nos projetos tradicionais, diferentes técnicas de controle passivo envolvendo materiais visco-elásticos e absorvedores dinâmicos e, mais recentemente, metodologias de controle ativo incluindo atuadores e sensores têm sido empregado com sucesso. Diferentes pesquisas tem demostrado que redução de vibração pode ser obtida usando o conceito de periodicidade. As estruturas periódicas envolvem elementos idênticos ou partes conectadas repetidamente. O projeto de estruturas periódicas pode ser empregado para conseguir bandas de frequências em que não há propagação de ondas elásticas, denominadas de "*stop bands*", introduzindo um efeito similar ao de um filtro. Neste contexto, o presente trabalho apresenta uma abordagem alternativa para o projeto de barras periódicas. Esta alternativa envolve a modelagem de uma barra periódica do tipo híbrida infinita na qual uma estrutura periódica finita é conectada entre duas barras semi-infinitas. Para isto, é utilizada uma metodologia que relaciona vetor de estados e amplitude de ondas. A principal proposta deste trabalho é desenvolver uma relação entre as amplitudes de ondas longitudinais transmitidas e incidentes em termos das propriedades físicas e geométricas de uma genérica estrutura periódica para simplificar o processo do projeto. Usando esta formulação mostra-se que uma barra periódica pode ser projetada para satisfazer os requisitos de uma supressão de vibração. Um problema hipotético é proposto e resultados numéricos e experimentais mostram os "*stop bands*" obtidos para resolver o problema. Isto mostra que esta abordagem é uma importante ferramenta para o projeto deste tipo de estruturas.

Palavras-chave: Projeto de barras periódicas. Equação da transmissão de ondas. Atenuação de vibração.

LIST OF FIGURES

LIST OF ABBREVIATIONS AND SYMBOLS

Matrices and Vectors

$\mathbf{a}$	wave amplitude vector
$\mathbf{h}$	states vector
$\mathbf{H}$	transformation matrix
$\tilde{\mathbf{H}}$	matrix of size 2×2
$\mathbf{I}$	identity matrix
$\mathbf{T}$	spatial transformation matrix
$\tilde{\mathbf{T}}$	transfer matrix
γ	matrix of size 2×2
μ	matrix of size 2×2

Latin Letters

A	wave amplitude
b	term of the transmission and reflection equation
C	coefficient of power
c	constant value
dx	length of differential rod element
dB	Decibel unit
E	Young's modulus
F	external longitudinal force
j	imaginary number ($\sqrt{-1}$)
k	longitudinal wavenumber
L	length of a segment
m	positive or negative integer number
N	number of cells
P	average power transfered per cycle
p	instantaneous power
q	body force per unit volume
S	cross-section area
t	time variable
T	temporal period
u	longitudinal displacement

$\dot{u}$	longitudinal velocity
v	wave propagation velocity
x	space variable and direction of wave propagation in one-dimensional
Z	mechanical impedance

Greek Letters

ω	angular frequency
Ω	non-dimensional frequency
λ	wavelength
ψ	Bloch parameter (or propagation constant)
Λ	eigenvalue of the transfer matrix
ϕ	phase angle of the wave
σ	axial stress
ε	axial strain
ρ	mass density
α	term of the transmission and reflection equations
β	term of the transmission and reflection equations
η	term of the transmission and reflection equations
τ	ratio of propagation times
κ	ratio of impedance
φ	angle relative to the phase velocity curve
θ	angle relative to the group velocity curve
ξ	damping loss factor

Superscripts

Re	relative to the real part
Im	relative to the imaginary part

Subscripts

a	relative to the first segment of the periodic cell
Al	relative to the aluminum material
b	relative to the homogeneous part of the rod
c	relative to the second part of the periodic cell
cb	relative to the geometric or physical parameters ratio of a and b segments
ca	relative to the geometric or physical parameters ratio of c and a segments
cb	relative to the geometric or physical parameters ratio of c and b segments

$cell$	relative to the periodic cell
G	relative to the global periodic structure
g	relative to the group velocity
i	relative to the incident waves
inc	relative to the incoming waves
k	relative to the each wavenumber value
Δk	relative to the each wavenumber interval
L	relative to the left side segment or left-going waves (depending on context)
ny	relative to the nylon material
out	relative to the outgoing waves
p	relative to the phase velocity
PR	relative to the reflection power
PT	relative to the transmission power
R	relative to the right side segment or right-going waves (depending on context)
r	relative to the reflected waves
S	relative to the specific impedance
$steel$	relative to the steel material
t	relative to the transmitted waves

Acronyms

BW	Bandwidths
PB	Pass Band
SB	Stop Band
$WFEM$	Wave Finites Elements Method
$WSEM$	Wave Spectral Element Method

Special Notations

$[\quad]$	matrix
$\{\quad\}$	vector
$\lvert\quad\rvert$	absolute value of a number
$\sqrt{\quad}$	square root of a number
$min(\ )$	minimum value of a number
$max(\ )$	maximum value of a number
$det(\ )$	determinant function
$\ln(\ )$	natural logarithmic of a number
$\frac{\partial(\ )}{\partial t}$	first-order partial differential relative to time variable
$\frac{\partial(\ )}{\partial x}$	first-order partial differential relative to spatial variable

$\frac{\partial^2(\ )}{\partial t^2}$ second-order partial differential relative to time variable

$\frac{\partial^2(\ )}{\partial x^2}$ second-order partial differential relative to spatial variable

CONTENTS

1 INTRODUCTION

This chapter presents a brief description of the context in which this work is based on, as well as publications regarding periodic structures whose aim is to attenuate structural vibration. Furthermore, this chapter presents the objectives, contributions achieved, and how the text of this thesis is organized.

1.1 CONTEXT OF THE WORK

The reduction of structural vibration has been a very important topic for many engineering applications. In traditional projects, different passive control techniques involving viscoelastic materials and dynamic absorber design and, also, active control methodologies involving actuators and sensors have been successfully employed.

Different researches have demonstrated that vibration reduction can be obtained using the concept of periodicity. These works have designed periodic structures based on geometrical and physical properties. The structures involve identical elements or parts connected repeated times. This idea has been applied for designing panels of satellites, aircraft fuselage and wings, truss structures, pipelines, train tracks, and others (NARISETTI, 2010; MEAD, 1996). The design of periodic structures can be employed to get frequency band without elastic wave propagation i.e, stop bands, introducing an effect similar to the filter.

In engineering, some vibration problems consist of a vibration source with higher dominant intensity, such as seismic events (XIONG et al., 2012). Other common sources are industrial machines (electric generators, turbines, compressors, pumps, among others) that in some cases are assembled upon supports or structures made of rods and produce vibrations and noise at high levels, which may even be harmful to human health. In the context of this work, these applications are called “unilateral source problems”, since, particularly, a formulation for rods is developed. Besides, many of these problems present predominantly unidimensional vibration propagation, as shown by (SINGH et al., 2004; ASIRI et al., 2005; XIUCHANG et al., 2011; CHEN; WU, 2016), among others.

In particular for aeronautical applications, the helicopter gearbox is a significant source of vibration and cockpit noise. The frequency range noise (in general 500 - 2000 Hz) is primarily transmitted to fuselage through rigid connections. The use of a periodic-layered elastomer and metal isolators can result an important noise reduction into the cockpit, as shown by (SZEFI, 2003a; SZEFI et al., 2003b; SZEFI et al., 2004). Also, for the naval industry, the

inclusion of a periodic structure in a floating raft isolation system (extensively applied in ships and submarines) can result in significant attenuation of vibration and noise caused by resonant substructures (SONG et al., 2015; WANG; MAK, 2018). In the automotive industry, vehicles can use periodic viscoelastic materials to minimize vibration transmission from their engines to the chassis. This type of structure keeps comfort also working in higher rotational levels in comparison with conventional designs (ASIRI, 2007; JUNG et al., 2010). In addition, in the civil engineering, periodic foundations can be used to achieve a much more effective seismic isolation (GAOFENG; ZHIFEI, 2010; XIANG et al., 2012; CHENG; SHI, 2017).

For practical engineering applications in general it is defined a frequency range in which vibration must be reduced. Commonly it is the first step to design a structure, which can satisfy requirements of maximum admissible vibration level. The design can also consider limitations for geometrical and physical properties of the structure. At this point, the main task is to define the material and geometry to get the desired result using a periodic structure. However, in the literature it is easier to find methodologies of analysis of periodic structures, especially based on *Wave Finites Elements Method - WFEM* (DUHAMEL et al., 2006; MACE et al., 2005; MENCIK, 2014; NOBREGA et al., 2016; SILVA et al., 2015) and *Wave Spectral Element Method - WSEM* (SOLAROLI et al., 2003). For these ones in general a structure must be previously defined and just after this definition the stop bands can be found. In this context, the use of this kind of strategy may make the structural design an exhaustive loop of unsuccessful attempts.

In this context, the present work introduces an approach to design periodic rod type structures. The main proposal is to present a relation between transmitted and incident longitudinal waves amplitudes in terms of physical and geometrical properties of a generic candidate structure shown in figure 1. The approach considers incident waves from the left side structure and a problem with an one side source of vibration and a dominant one dimensional vibration transmission and the objectives and contributions of this work are shown below.

Figure 1 - Scattering of longitudinal waves by a periodic structure. Incident (A_i), reflected (A_r) and (A_t) transmitted longitudinal waves.

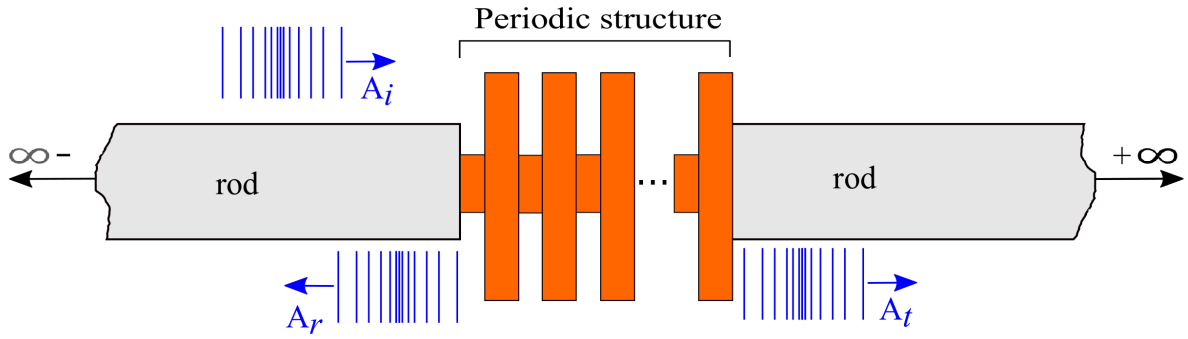

Source: elaborated by the author.

1.2 OBJECTIVES

The main objective of this thesis is to develop a methodology that involves the amplitude ratio of incident and transmitted longitudinal waves that propagate in a periodic rod structure. In addition, the secondary objectives are presented below:

- to model a periodic rod referred to as *hybrid infinite* in this work, consisting of a periodic finite structure embedded in an infinite rod;
- to evaluate the transmission and reflection of waves that propagate in structures whose periodicity is geometrical;
- to find out, through numeric simulations, the number of periodic cells needed to represent the dominant dynamics of a structure with periodic cells along all its extension;
- to make explicit the influence of physical properties and structural geometrical parameters on stop bands formation, as well as their characteristics, such as: location, bandwidth and attenuation levels, in order to assist the process of designing this structure.

1.3 CONTRIBUTIONS TO KNOWLEDGE

The following presents some of the contributions of this work in the context of periodic structures design meeting requirements of permissible vibration levels, frequency bands with stop bands, as well as geometrical constraints:

- scalar equations for transmission and reflection of longitudinal waves are developed as an alternative to classic solutions regarding matrix systems of equations;
- some practical aspects of periodic structures design are discussed considering explicit physical and geometrical parameters in order to assist the analyst's understanding;
- it is shown that by using 3 to 4 periodic cells, it is possible to obtain vibration attenuation levels equivalent to those of structures whose periodic cells are present along all their extension, which entails a great simplification when manufacturing this kind of structure;
- a strategy to apply the formulation developed in this work is presented for infinite structures in practical engineering problems (finite structures).

1.4 THESIS OUTLINE

Chapter 1 presents the context of this work, the objectives and the contributions achieved in this research. The basic theoretical foundation involved in the study of the harmonic motion of waves is described in chapter 2. Basic concepts are presented, such as periodic structures filtering properties, and dispersion in periodic systems. Furthermore, the longitudinal wave's equation is obtained, the concept of wave impedance is defined and the analysis of transmission, reflection and waves energy flow in a discontinuity is presented.

In chapter 3 an approach to design periodic rods is presented. Equations for transmission and reflection of longitudinal waves are obtained, and the transfer matrix eigenvalue problem is discussed.

Chapter 4 presents the results for the numeric simulations using the transmission and reflection relations proposed. The simulations are presented for different structure configurations with geometrical periodicity.

Chapter 5 discusses practical aspects of designing periodic rods, a hypothetical condition of a practical vibration problem is presented, and candidate solutions are discussed. Additionally, experimental tests are carried out to verify the methodology employed in this work. The conclusions and future work suggestions are described in chapter 6.

2 BASIC THEORETICAL FOUNDATION

This chapter aims to present the basic theoretical foundation involved in this work. Initially, it approaches the concept of periodic structures, as well as their filtering properties, and dispersion in periodic systems. Afterwards, important concepts regarding the harmonic motion of waves are described, such as some types of waves, wave number and length, phase and group velocity, among others. At last, the longitudinal wave's equation is obtained, the wave impedance is discussed, and the analysis of transmission, reflection and energy flow in a discontinuity is presented.

2.1 PERIODIC STRUCTURES

A periodic structure is composed of a number of identical structural elements, also named as *cells*, which are joined together end to end and/or side to side to form the whole structure (MEAD, 1996). These structures can be made by man and can exist naturally like in crystalline graphene sheet and honeycomb. In engineering there are also easily known in multi-storey buildings, support truss of bridges, aircraft structures, train tracks, and others.

2.1.1 Filtering properties

The design of period structures can be used to generate frequency ranges in which waves do not propagate or are highly attenuated through the structure. The characteristics of these systems make them potential candidates to act as passive vibro-acoustic filters. The filtering properties exhibited by these ones as well as the frequency ranges positioning within a particular range depend on the structural conception and arrangement of the periodic cells. The frequency ranges in which these structures allow waves propagate are called *pass bands* (PB) and, in another hand, frequency ranges in which there is waves attenuations are called *stop bands* (SB) or *band gaps* (BRILLOUIN, 1953). This effect of attenuation is generated due internal reflection of waves caused by the impedance variations (difference of material properties or geometrical discontinuities).

The frequency pass and stop bands are formed through the constructive and destructive waves interference inside a unit cell, respectively. According to Manktelow (2013) the incident wave is reflected and transmitted (partially) at an interface and each one of them repeat the same process. At frequencies within the stop band, the waves reflected act to cancel the incident wave resulting a transmitted wave with significant attenuation. On the other hand, at

frequencies within the pass band, the transmitted waves are not significantly attenuated (SZEFI, 2003a). A typical example of responses obtained from periodic structures analysis are showed by vibration transmission curves. Figure 2 shows an illustration of this curve obtained by the relation between the displacements u_R/u_L measured at the ends of the periodic structure when a external force F is applied at the left end, where u_R and u_L are respectively the displacement spectral amplitudes in the right and left sides of the periodic part of the rod.

Figure 2 - Illustration for transmission of the one-dimensional periodic structure.

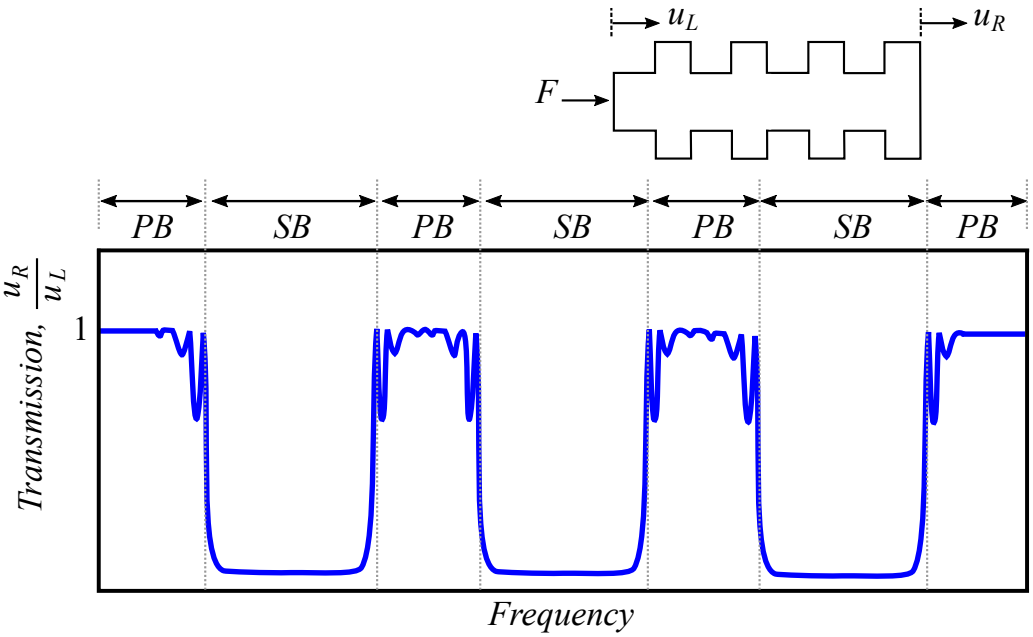

Source: elaborated by the author.

2.1.2 Dispersion in periodic systems

Consider a periodic structure composed of N cells arranged along of the axis x as shown in figure 3, where A_R represents right-going waves while A_L indicates the left-going waves.

Figure 3 - Illustration of the one-dimensional periodic structure composed of N cells.

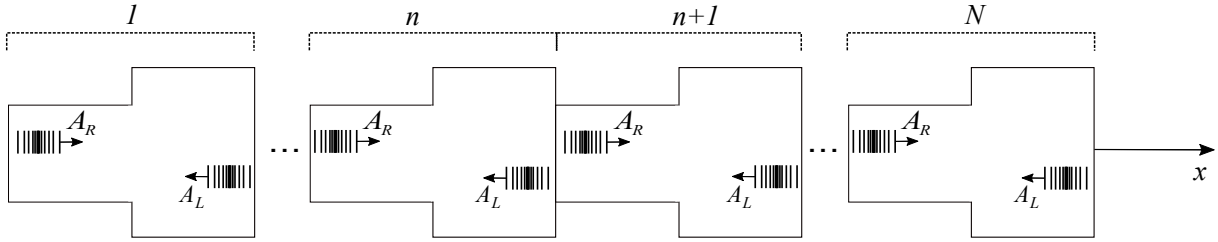

Source: elaborated by the author.

According to the literature, the Bloch's theorem for a periodic system shows that wave amplitudes between two consecutive cells n and $(n+1)$ are given by (MENCIK, 2010; GAZALET et al., 2013)

$$A^{(n+1)} = \Lambda A^{(n)} \tag{1}$$

where, $n = 1, ..., N$ and

$$\Lambda = e^{\psi} \tag{2}$$

and A is the wave amplitude, $\psi = \ln(\Lambda)$ is the Bloch parameter (or also called *propagation constant*), $\ln(\ )$ is the natural logarithmic and Λ is the eigenvalue of the transfer matrix (root of the characteristic Eq. 98), discussed in section 3.4. For each frequency can be extracted a pair of Λ such that $\Lambda_1\Lambda_2 = 1$ (HVATOV; SOROKIN, 2015). Therefore, the eigenvalues can be classified by two groups, i.e., $|\Lambda_1| \leq 1$ which corresponds to waves traveling to the right and $|\Lambda_2| \geq 1$ which corresponds to waves traveling to the left side of the structure.

This theory states that for any structure with repetitive identical units, the change in wave amplitude across a unit cell does not depend upon the location of the unit cell within the structure, i.e., a wave propagating in a periodic structure can be described by the motion of a single cell. Thus, as result of this theorem, it is possible to understand the wave propagation though an entire structure just by considering the wave motion in a single unit cell (PHANI et al., 2006) .

The Bloch parameters are complex numbers given by $\psi = \psi^{Re} + i\psi^{Im}$. This one controls the nature of elastic wave propagation in periodic structures. The real part ψ^{Re} is the *attenuation factor* and represents the amplitude decay of a wave propagation from one cell to the next one. The imaginary part ψ^{Im} is the *phase constant* and represent the phase difference in two adjacent cells, i.e, is a measurement of the phase changing across one unit cell. If ψ is purely imaginary (real part is zero) the absolute value of Λ is unit ($|\Lambda| = 1$) and waves propagating without attenuation (zone of pass band). However, if a real part exists ($|\Lambda| \neq 1$) the attenuation of the wave's amplitude is observed (zone of stop band) (GAN et al., 2016; SOLAROLI et al., 2003; SINGH et al., 2004).

The relationship between frequency and Bloch parameter, described by $\omega(\psi)$, is named the dispersion relation for a periodic system. An important characteristic of Bloch wave dispersion relationships is the periodicity such that $\omega(\psi) = \omega(\psi + 2m\pi)$, where m is a positive or negative integer number (BRILLOUIN, 1953). This means that the frequency ω is a periodic function of ψ and also leads to the definition of a *first Brillouin zone* that corresponds to the domain conventionally defined by $\psi \in [-\pi, \pi]$. Moreover, the dispersion relationship also follows the symmetry relationship $\omega(\psi) = \omega(-\psi)$ that leads to the definition of an *irreducible*

Brillouin zone that corresponds to $\psi \in [0, \pi]$. A common representation for a dispersion curve is illustrated by figure 4.

Figure 4 - Illustration of the propagation constants for the longitudinal wave, where *PB* and *SB* respectively represent the pass and stop band.

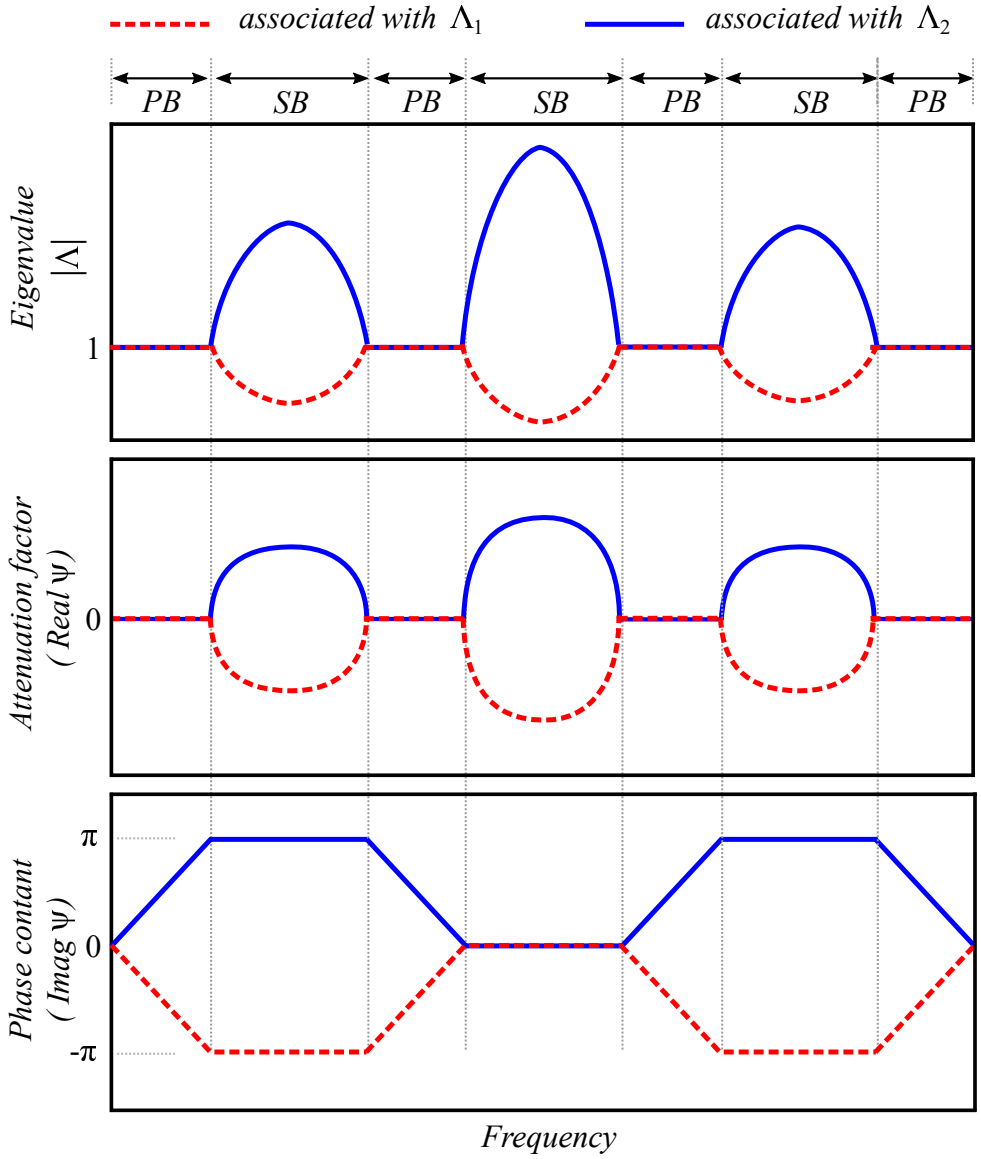

Source: elaborated by the author.

2.2 SOME DEFINITIONS OF HARMONIC WAVE MOTION

2.2.1 Waves in one-dimensional structures

An elastic wave motion is a phenomenon in which a physical quantity (for instance, energy or pressure) propagates through a medium, without transport of matter (FAHY; GARDONIO, 2007). The main types of waves propagating in a one-dimensional structure are illustrated in figure 5.

In *longitudinal* or *compression wave* the particles motion of the medium are parallel to the direction of wave propagation, the particles vibrate about their individual equilibrium positions. In this type of wave motion there is some out-of-plane displacement due to the Poisson ratio effect (i.e. lateral strains) as showed in figure 5 (a). In the *transversal* or *shear wave* the particles motion are perpendicular to the direction of wave propagation, see figure 5 (b). The other type of wave is the *flexural* or *bending waves* in witch there is translational displacement and rotation, see figure 5 (c). In this wave motion, bending moment and the shear force govern the deformation of medium. Note that, shear and bending waves are examples of out-of-plane waves.

Figure 5 - Illustrative representations for the deformation patterns of three types of wave motions in one-dimensional structures.

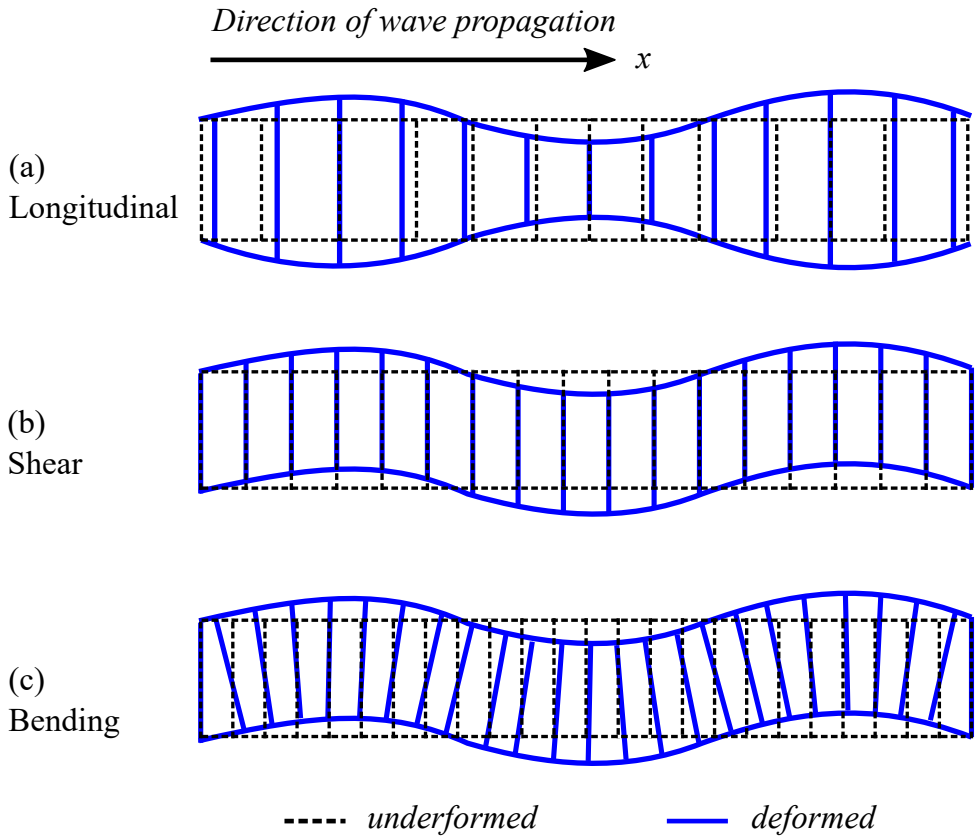

Source: adapted from Fahy and Gardonio (2007).

2.2.2 Wavenumber and wavelength

The harmonic wave motion in time and space can be represented by (BRENNAN et al., 2016)

$$u(x,t) = A\cos(\omega t \pm kx) \tag{3}$$

or

$$u(x,t) = A\sin(\omega t \pm kx) \tag{4}$$

where A is the amplitude of the wave, k is the wavenumber, ω is the angular frequency, x is the space variable and t is the time variable. The wavenumber is *spatial frequency* and is inversely proportional to the spatial period, i.e., to the wavelength λ (CREMER et al., 2005)

$$k = \frac{2\pi}{\lambda} \tag{5}$$

Also, the angular or *temporal frequency* is inversely proportional to the duration T (period) of a cycle

$$\omega = \frac{2\pi}{T} \tag{6}$$

The analogy between temporal frequency and the wavenumber is illustrated in figure 6. The wavenumber is fundamental for understanding the harmonic wave motion. Physically, it represents the phase change per unit increase of distance, in the same way as ω represents the phase change per unit increase of time.

Figure 6 - Analogy between temporal frequency and spatial frequency (wavenumber).

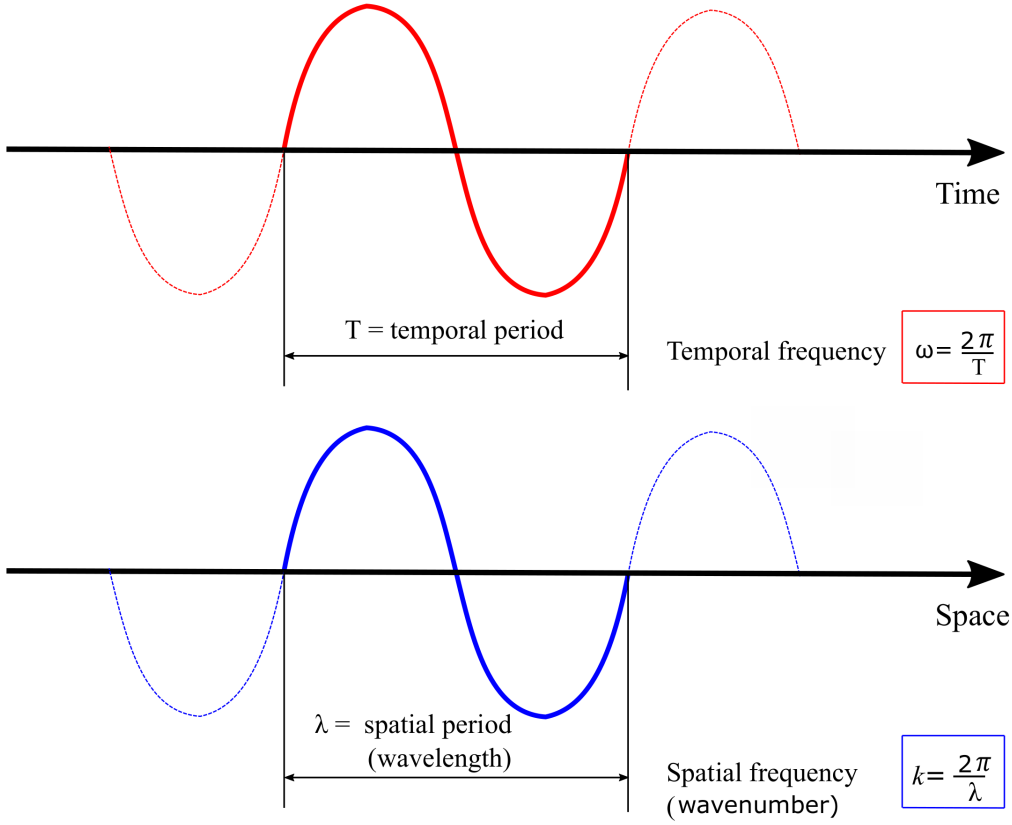

Source: adapted from Fahy and Gardonio (2007).

2.2.3 Direction of propagation

Consider a wave motion represented by equation (3) or (4). The argument of those functions is designate as *phase* ϕ of this wave, i.e., $\phi = \omega t \pm kx$. When the second term of that argument is negative ($-kx$) as time increases, x must increase positively in order to keep a constant ϕ and, thus, a wave propagating through the positive x direction. Otherwise, for $+kx$, x must increase negatively and the wave propagating in the negative x direction. Figure 7 shows an illustration of wave propagation in the positive and negative direction for a particular wavenumber.

Figure 7 - Illustration of wave propagation in the positive and negative direction.

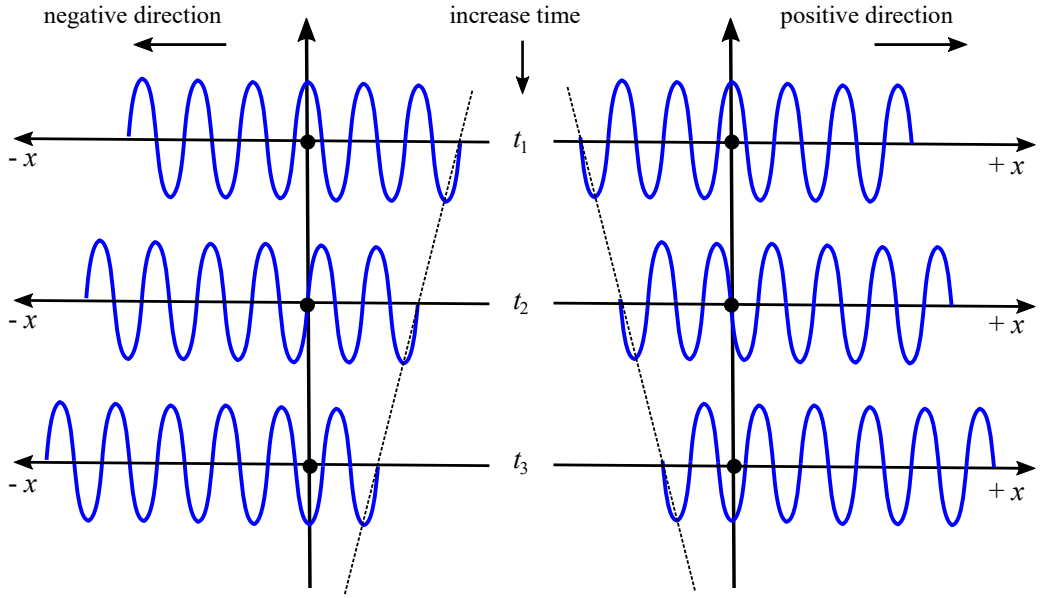

Source: adapted from Fahy and Gardonio (2007).

2.2.4 Phase velocity

Considering a wave propagating to the right side structure, i.e., phase this wave is $\phi = \omega t - kx$. For the constant phase ($\omega t - kx = constant$), we can be write (OSTACHOWICZ et al., 2012)

$$x = \left(\frac{\omega}{k}\right) t - \frac{constant}{k} = \left(\frac{\omega}{k}\right) t + c_k \tag{7}$$

where c_k is a constant for each k.

The relationship between temporal frequency ω and spatial frequency k of the propagating waves is defined as *phase velocity* (v_p) of the wave

$$v_p = \frac{\omega}{k} \tag{8}$$

Thus, a point of constant phase moves with this velocity and if an observer travelling in the direction of wave propagation at this velocity sees no change of phase (FAHY; GARDONIO, 2007). The harmonic wave propagating to the right with phase velocity v_p is presented in figure 8.

Figure 8 - Harmonic wave propagating with phase velocity v_p.

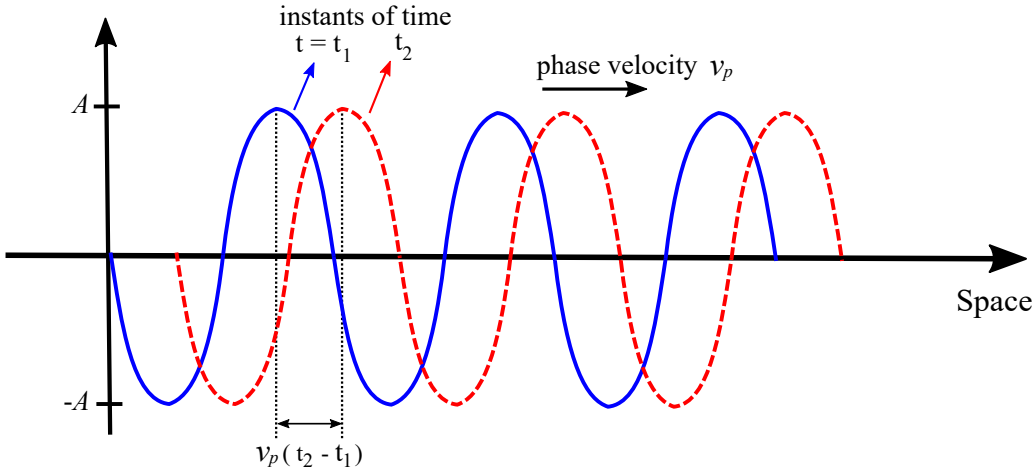

Source: elaborated by the author.

2.2.5 Group velocity

Consider two waves propagating to the right side structure, with amplitudes A, but different frequencies and wavenumber, i.e., waves propagation with phase velocity v_{p1} and v_{p2}, respectively, as presented in figure 9 (a).

The sum of these waves, figure 9 (b) can be described by

$$u(x,t) = A[\sin(\omega_1 t - k_1 x) + \sin(\omega_2 t - k_2 x)] \tag{9}$$

Application of trigonometric identities for the sum of sinus functions

$$u(x,t) = \bar{U} \sin\left[\left(\frac{\omega_1 + \omega_2}{2}\right) t - \left(\frac{k_1 + k_2}{2}\right) x\right] \tag{10}$$

where

$$\bar{U} = 2A\cos\left[\left(\frac{\omega_1 - \omega_2}{2}\right) t - \left(\frac{k_1 - k_2}{2}\right) x\right] = 2A\cos\left[(\Delta\omega)t - (\Delta k)x\right] \tag{11}$$

In equation (10), one term is associated with modulation (cosine term) and another is associated with carrier wave (sine term). The superposition of a carrier wave and a modulation wave is called of *wave packet* or group of waves, as presented in figure 10.

Figure 9 - Illustration of sum of waves propagating in the same direction. (a) two waves propagating with same amplitudes, different frequencies and wavenumber (b) wave propagating packet with velocity v_g.

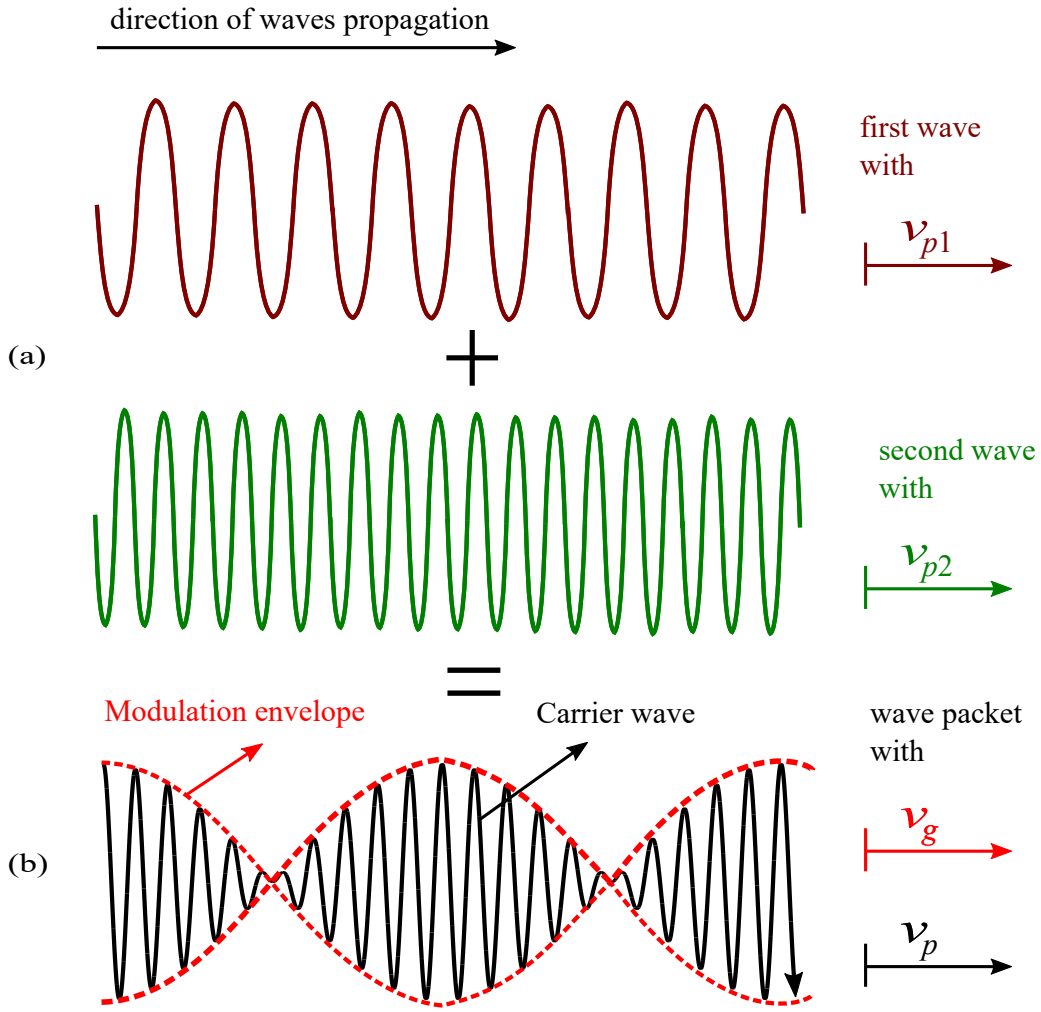

Source: adapted from Brennan et al. (2016).

Figure 10 - Wave packet as the superposition of a carrier wave and a modulating wave.

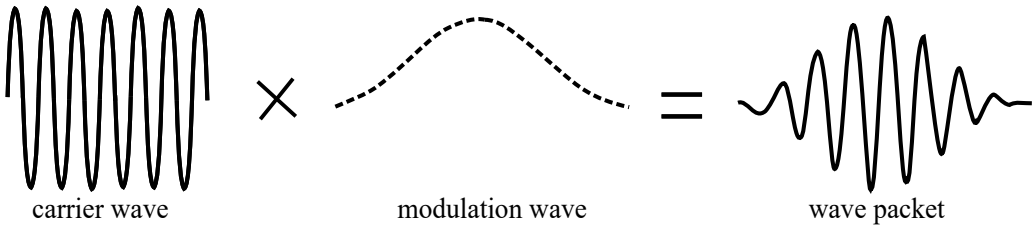

Source: adapted from Ostachowicz et al. (2012).

The phase velocity of the combined wave, figure 9 (b), is give by (BRENNAN et al., 2016)

$$v_p = \frac{\omega_1 + \omega_2}{k_1 + k_2} \tag{12}$$

The waves packet does not propagate at the phase velocity. It propagates at the *group velocity* that is defined by propagation velocity of modulation wave ($\bar{U}$ term). For a constant phase ($\Delta\omega t - \Delta k x = constant$), we can be write (OSTACHOWICZ et al., 2012)

$$x = \left(\frac{\Delta\omega}{\Delta k}\right) t - \frac{constant}{\Delta k} = \left(\frac{\Delta\omega}{\Delta k}\right) t + c_{\Delta k} \tag{13}$$

where $c_{\Delta k}$ is a constant for each Δk.

Thus, the *group velocity*, which is the velocity at which the energy in the combined wave is transported, is given by

$$v_g = \frac{\omega_1 - \omega_2}{k_1 - k_2} = \frac{\Delta\omega}{\Delta k} \tag{14}$$

In the limit transition $\Delta\omega \longrightarrow 0$ and $\Delta k \longrightarrow 0$, the equation (14) becomes

$$v_g = \frac{d\omega}{dk} \tag{15}$$

Note that the group velocity is the rate of change of frequency with respect to the wavenumber.

2.2.6 Dispersion relation

The relationship between k and ω, i.e, $\omega = \omega(k)$ is defined as *dispersion relation*. It is a property of each wave type and of the type of wave-supporting medium (FAHY; GARDONIO, 2007). If it is a linear function, the medium is called non dispersive, and otherwise the medium is dispersive. The figure 11 illustrates the dispersion relation for dispersive and non-dispersive medium.

A non-dispersive medium presents a group velocity that is equal to the phase velocity that is frequency independent (such as tension waves in strings and compressional waves in rods). In this case, the wavenumbers are proportional to frequency. In the dispersive medium the group and phase velocities are different and they are frequency dependent (such as bending waves in beams and plates). In this case, for each frequency the wave packet travels in a different velocity and deform during the propagation.

Figure 11 - Illustration of the dispersion curves for a dispersive and non-dispersive medium.

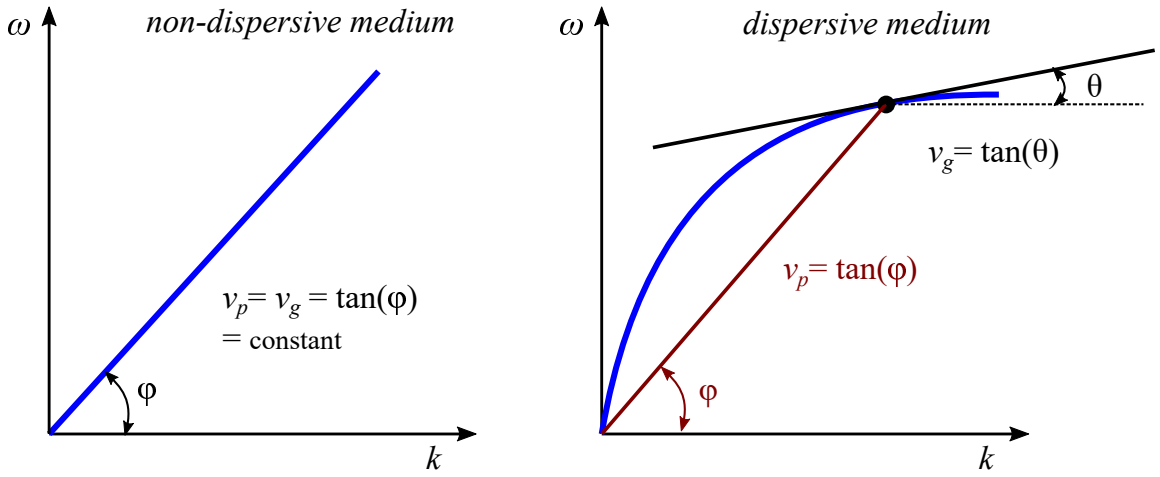

Source: elaborated by the author.

2.3 LONGITUDINAL WAVES IN RODS

2.3.1 The wave equation

Consider axial stress in a long, slender and supported rod as shown in figure 12(a) and assuming that lateral inertia effects associated with lateral contraction-expansion (or Poisson's effects) can be neglected. The coordinate x refers to cross-section of the rod and longitudinal displacement of that section is represented by $u(x,t)$. The body force $q(x,t)$ per unit volume is also considered and σ is the axial stress acting on a differential element of the rod. The free body diagram of that rod element of length dx is presented in figure 12 (b).

Using Newton's Second law, the equation of longitudinal motion for an element is given by (GRAFF, 1991)

$$-\sigma S + (\sigma + \frac{\partial \sigma}{\partial x} dx)S + q(x,t)Sdx = \rho S dx \frac{\partial^2 u}{\partial t^2} \tag{16}$$

where ρ is the material density and S is the cross-section area of the rod.

Equation (16) results in

$$\frac{\partial \sigma}{\partial x} + q(x,t) = \rho \frac{\partial^2 u}{\partial t^2} \tag{17}$$

Figure 12 - Illustration of a thin rod: (a) coordinate x and displacement $u(x,t)$ of a section of rod; (b) free body diagram of a rod element.

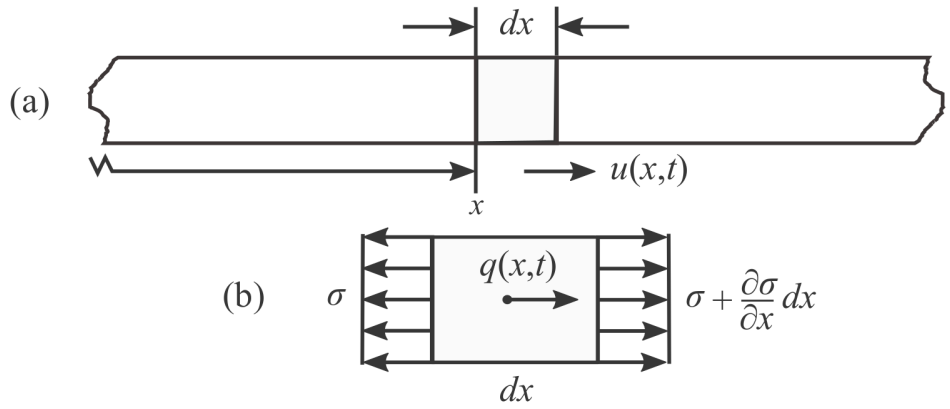

Source: elaborated by the author.

Considering an elastic behavior and applying the Hooke's law

$$\sigma = E\varepsilon \tag{18}$$

where E is Young's modulus and ε is the axial strain given by

$$\varepsilon = \frac{\partial u}{\partial x} \tag{19}$$

Substituting equation (18) and (19) into equation (17) and assuming a homogeneous rod (E and ρ not vary with x) is obtained

$$E\frac{\partial^2 u}{\partial x^2} + q(x,t) = \rho\frac{\partial^2 u}{\partial t^2} \tag{20}$$

Finally, in the absence of body forces the equation (20) reduces to

$$E\frac{\partial^2 u}{\partial x^2} = \rho\frac{\partial^2 u}{\partial t^2} \tag{21}$$

or

$$\frac{\partial^2 u}{\partial x^2} = \frac{1}{v_p^2}\frac{\partial^2 u}{\partial t^2} \tag{22}$$

where

$$v_p = \sqrt{\frac{E}{\rho}} \tag{23}$$

is the phase velocity of the longitudinal waves in a uniform rod.

Equation (22) is the *wave equation* for a rod. Note that the phase velocity is independent of frequency and because of this a rod is non-dispersive medium. In this case, the group velocity is equal to the phase velocity according to described in previous sections of this work.

Considering the free-wave propagation and assuming a time harmonic motion

$$u(x,t) = u(x)e^{j\omega t} \tag{24}$$

Replacing the equation (24) into equation (22) results in the following second-order ordinary differential equation

$$\frac{\partial^2 u(x)}{\partial x^2} + k^2 u(x) = 0 \tag{25}$$

where $k = \dfrac{\omega}{v_p}$ is the wavenumber and its solution is given by

$$u(x) = A_R e^{-jkx} + A_L e^{jkx} \tag{26}$$

In this case, the general solution of equation (22) is shown below

$$u(x,t) = (A_R e^{-jkx} + A_L e^{jkx})e^{j\omega t} \tag{27}$$

Note that the term $A_R e^{-jkx}$ represents a right-going propagating wave with amplitude A_R and the term $A_L e^{jkx}$ represents a left-going propagating wave with amplitude A_L (BRENNAN et al., 2016).

2.3.2 Wave impedance

An important concept in this field of wave propagation is the *wave impedance* or the *mechanical impedance* of a structure. Consider a right-going propagating wave $u(x,t) = A_R e^{j(\omega t - kx)}$ in a semi-infinite rod as shown in figure 13.

Figure 13 - Forced wave propagation in a semi-infinite rod.

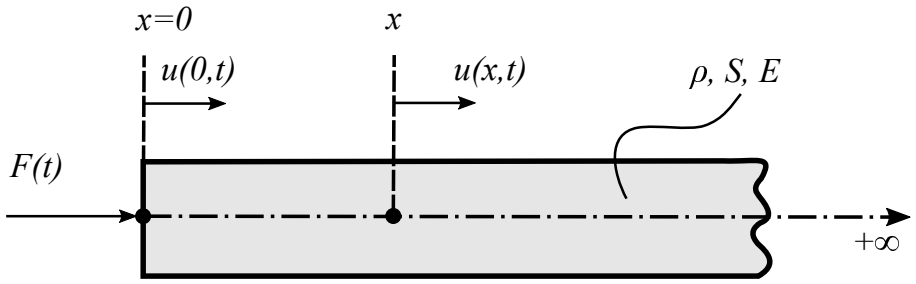

Source: elaborated by the author.

For generate such motion, a force $F(t)$ is applied on the left boundary ($x = 0$) and it is given by

$$F(t) = -SE\frac{\partial u(0,t)}{\partial x} = jkSEA_R e^{j\omega t} \tag{28}$$

and the velocity in this point of excitation can be expressed as

$$\dot{u} = \frac{\partial u(0,t)}{\partial t} = j\omega A_R e^{j\omega t} \tag{29}$$

The wave impedance Z is defined as the ratio between the applied force and the corresponding velocity at the point of excitation. In other words, wave impedance relates the velocity of the particles in a medium and the corresponding force (or stress) required to produce that velocity. Thus, it is given by (HAGEDORN; DASGUPTA, 2007)

$$Z = \frac{F(t)}{\dot{u}} = \frac{jkSEA_R e^{j\omega t}}{j\omega A_R e^{j\omega t}} = \frac{kSE}{\omega} = \rho v_p S \tag{30}$$

The impedance in the semi-infinite rod is a real quantity which does not vary with frequency and thus it can be seen as a linear viscous damper (BRENNAN et al., 2016). Similarly, it can be define the *specific impedance* Z_S as the ratio between the stress at the end of the rod and its

corresponding velocity by the following equation

$$Z_S = \rho v_p \tag{31}$$

2.3.3 Transmission, reflection and energy flux at a discontinuity

Consider a typical discontinuity between two semi-infinite rods connected in $x = 0$, where there is an abrupt change from one in respect to the other in its material properties and/or cross-section area as shown in figure 14. The parameters, ρ, S, and E are mass density, cross-section area and modulus of elasticity, respectively. The subscripts 1 and 2 refer to rod-1 and rod-2, respectively.

Figure 14 - Incident, reflected and transmitted waves at a junction between two semi-infinite rods.

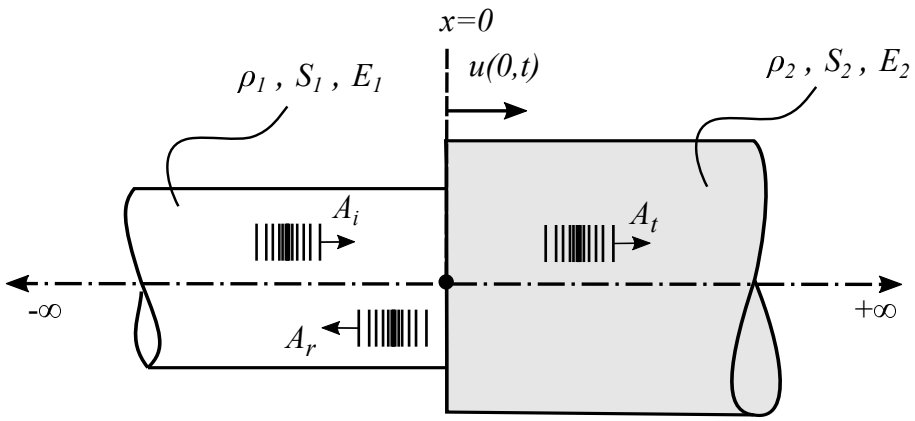

Source: elaborated by the author.

Let a positive-traveling longitudinal wave in the left side of discontinuity, when this wave achieve the discontinuity ($x = 0$) it is partly reflected back into rod-1 and partly transmitted to rod-2. Thus, the longitudinal displacement fields on either side of the discontinuity are set to given by (CREMER et al., 2005)

$$u_1(x,t) = A_i e^{j(\omega t - k_1 x)} + A_r e^{j(\omega t + k_1 x)} \tag{32}$$

$$u_2(x,t) = A_t e^{j(\omega t - k_2 x)} \tag{33}$$

where A_i, A_r and A_t are, incident, reflected and transmitted wave amplitudes, respectively. Note that the frequency ω is the same for the waves in the left and right rods, however, as the wave

velocities are different in the two semi-infinite rods (once different material is assumed for each one of them), the corresponding wave numbers are different, i.e, $k_1 \neq k_2$. At the junction ($x = 0$), there are the following requirements of displacement and force continuities (HAGEDORN; DASGUPTA, 2007; GRAFF, 1991)

$$u_1(0,t) = u_2(0,t) \tag{34}$$

and

$$S_1\sigma_1(0,t) = S_2\sigma_2(0,t) \tag{35}$$

For which the right side of the junction the force is distributed over a larger surface such the stress is reduced. The stresses intensities are determined from the wave fields and Hooke's law

$$\sigma_1(0,t) = E_1\frac{\partial u_1(0,t)}{\partial x} = -jk_1E_1A_ie^{j\omega t} + jk_1E_1A_re^{j\omega t} = \sigma_i(0,t) + \sigma_r(0,t) \tag{36}$$

and

$$\sigma_2(0,t) = E_2\frac{\partial u_2(0,t)}{\partial x} = -jk_2E_2A_te^{j\omega t} = \sigma_t(0,t) \tag{37}$$

Substituting equations (36) and (37) into equation (35) and using the equation (34), the amplitudes of the transmitted and reflected waves are obtained by

$$A_t = \frac{2k_1E_1S_1}{k_1E_1S_1 + k_2E_2S_2}A_i = \frac{2}{1 + (Z_2/Z_1)}A_i \tag{38}$$

and

$$A_r = \frac{k_1E_1S_1 - k_2E_2S_2}{k_1E_1S_1 + k_2E_2S_2}A_i = \frac{1 - (Z_2/Z_1)}{1 + (Z_2/Z_1)}A_i \tag{39}$$

where $Z_1 = \rho_1v_1S_1$ and $Z_2 = \rho_2v_2S_2$ are wave impedances for rod-1 and rod-2, respectively.

From equations (36) to (39) the following relationships for transmitted and reflected stress intensities can be obtained (GRAFF, 1991; ROSE, 2014)

$$\sigma_t = \frac{2\rho_2v_2S_1}{\rho_1v_1S_1 + \rho_2v_2S_2}\sigma_i = \frac{2(Z_2/Z_1)(S_1/S_2)}{1 + (Z_2/Z_1)}\sigma_i \tag{40}$$

$$\sigma_r = \frac{\rho_2 v_2 S_2 - \rho_1 v_1 S_1}{\rho_2 v_2 S_2 + \rho_1 v_1 S_1}\sigma_i = \frac{(Z_2/Z_1) - 1}{(Z_2/Z_1) + 1}\sigma_i \tag{41}$$

The average power (or energy flux) transfered per cycle for a harmonic force $F(t)$ acting through a collinear particle velocity $\dot{u}$ is given by (HAGEDORN; DASGUPTA, 2007; FAHY; GARDONIO, 2007)

$$P = \frac{1}{T}\int_0^T p(t)dt = \frac{\omega}{2\pi}\int_0^{\frac{2\pi}{\omega}} F(t)\dot{u}dt \tag{42}$$

were $p(t)$ is the instantaneous power and T is the period of the harmonic motion.

Using equations (32) and (33), the component displacements in real form can be written as follows (YILDIRIM, 1994)

$$u_i(x,t) = A_i \cos(\omega t - k_1 x) \tag{43}$$

$$u_r(x,t) = A_r \cos(\omega t + k_1 x) \tag{44}$$

$$u_t(x,t) = A_t \cos(\omega t - k_2 x) \tag{45}$$

From Hooke's law (Eq. 18) and using equations (43) to (45), the component forces at the junction ($x = 0$) are given by

$$F_i(0,t) = +k_1 E_1 S_1 A_i \sin(\omega t) \tag{46}$$

$$F_r(0,t) = -k_1 E_1 S_1 A_r \sin(\omega t) \tag{47}$$

$$F_t(0,t) = +k_2 E_2 S_2 A_t \sin(\omega t) \tag{48}$$

and the component velocities (time derivative of displacements u) are

$$v_i(0,t) = -A_i\omega\sin(\omega t) \tag{49}$$

$$v_r(0,t) = -A_r\omega\sin(\omega t) \tag{50}$$

$$v_t(0,t) = -A_t\omega\sin(\omega t) \tag{51}$$

Substituting the equations of forces (46) to (48) and the equations of velocities (49) to (51) into the equation (42) we obtain as solution the average power carried by the incident, reflected, and transmitted harmonic waves, respectively

$$P_i = -\frac{1}{2}k_1E_1S_1\omega A_i^2 = -\frac{1}{2}\rho_1v_1S_1\omega^2A_i^2 \tag{52}$$

$$P_r = +\frac{1}{2}k_1E_1S_1\omega A_r^2 = +\frac{1}{2}\rho_1v_1S_1\omega^2A_r^2 \tag{53}$$

$$P_t = -\frac{1}{2}k_2E_2S_2\omega A_t^2 = -\frac{1}{2}\rho_2v_2S_2\omega^2A_t^2 \tag{54}$$

Based on these equations is possible to define the coefficients of power reflection C_{PR}, and power transmission C_{PT} as

$$C_{PR} = \frac{P_r}{P_i} = \left(\frac{A_r}{A_i}\right)^2 \tag{55}$$

$$C_{PT} = \frac{P_t}{P_i} = \frac{k_2E_2S_2}{k_1E_1S_1}\left(\frac{A_t}{A_i}\right)^2 = \frac{\rho_2v_2S_2}{\rho_1v_1S_1}\left(\frac{A_t}{A_i}\right)^2 \tag{56}$$

From the equations (55) and (56) and using equations (38) and (39) is possible to show that (HAGEDORN; DASGUPTA, 2007)

$$P_r + P_t = \left[\frac{\rho_2 v_2 S_2}{\rho_1 v_1 S_1} \left(\frac{A_t}{A_i} \right)^2 + \left(\frac{A_r}{A_i} \right)^2 \right] P_i = P_i \tag{57}$$

This last equation shows that incident average power is partially reflected and partially transmitted at the junction of the rod, and the sum of the scattered average power is equal to the incident average power, i.e., in this scattering process there is energy conservation. Also, for convenience that equation can be rewritten by

$$C_{PR} + C_{PT} = 1 \tag{58}$$

to simplify a design process of a periodic hybrid rod.

3 PROPOSED APPROACH FOR DESIGNING PERIODIC RODS

In this chapter, an approach to design periodic rods is developed using the methodology based on state vectors. This methodology has been employed and validated in the study of the coupling dynamics between piezoceramic actuators and a beam (BRENNAN et al., 1997), as well as in studies of active vibration control in unidimensional structures (BRENNAN, 1994). As a result of the present proposal, equations for wave transmission and reflection are obtained in periodic rods written explicitly in terms of physical and geometrical structural properties. The approach considers a finite number of cells embedded in an originally homogeneous rod. The transfer matrix eigenvalue problem for this new structure is solved and, finally, it is possible to obtain the dispersion curves from the roots of an analytical equation, which is regarded as an important simplification in the process of designing this kind of structures.

3.1 METHODOLOGY

Initially, the model consider a hybrid rod with a single cell connected to two semi-infinite rods (parts b with cross-sectional area S_b) as shown in figure 15. The unit cell consists of two segments a and c with lengths L_a and L_c and cross-sectional area S_a and S_c, respectively. Points 1 to 3 indicate the location of each junction.

Figure 15 - Hybrid rod composed by a single cell connected to two semi-infinite rods.

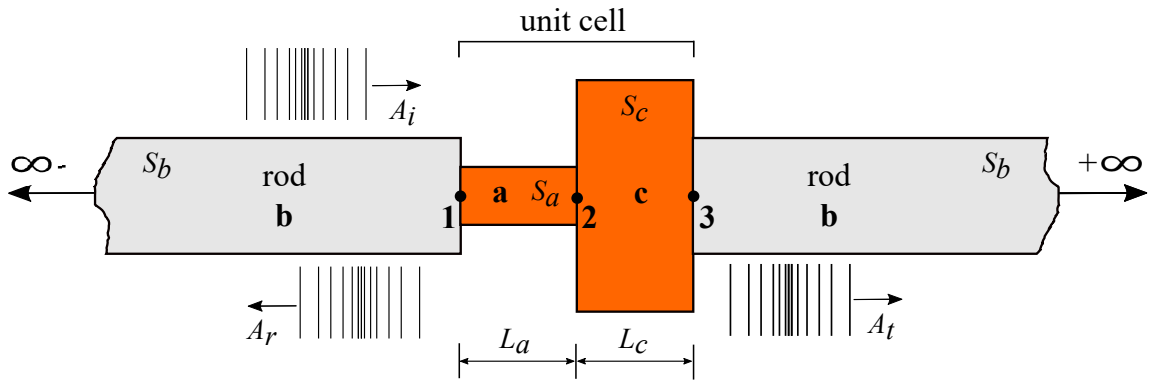

Source: elaborated by the author.

The relationship between a state vector and the longitudinal waves vector is given by (BRENNAN et al., 1997; BRENNAN, 1994)

$$\mathbf{h}(\omega) = \mathbf{H}(\omega)\mathbf{a}(\omega) \tag{59}$$

The *state vector* $\mathbf{h}(\omega)$, the *transformation matrix* $\mathbf{H}(\omega)$ and the *vector of wave amplitudes* $\mathbf{a}(\omega)$ are given by

$$\mathbf{h}(\omega) = \begin{Bmatrix} u \\ F \end{Bmatrix} \qquad \mathbf{H}(\omega) = \begin{bmatrix} 1 & 1 \\ jkES & -jkES \end{bmatrix} \qquad \mathbf{a}(\omega) = \begin{Bmatrix} A_L \\ A_R \end{Bmatrix} \tag{60}$$

where u is axial displacement, F is axial force, j is $\sqrt{-1}$, E is Young's modulus, S is the cross-sectional area, A_L and A_R are left and right going longitudinal wave amplitudes as previously defined. For simplify the notation in this text, it is considered $\mathbf{h}(\omega) = \mathbf{h}$, $\mathbf{H}(\omega) = \mathbf{H}$ and $\mathbf{a}(\omega) = \mathbf{a}$.

The relationship between the wave vectors $\mathbf{a}_R$ and $\mathbf{a}_L$ is given by

$$\mathbf{a}_R = \mathbf{T}\mathbf{a}_L \tag{61}$$

where subscripts L and R denote the left and right hand segments and $\mathbf{T}$ is the *spatial transformation matrix* given by

$$\mathbf{T} = \begin{bmatrix} e^{jkL} & 0 \\ 0 & e^{-jkL} \end{bmatrix} \tag{62}$$

where L is the length of segment. The force balance and continuity of displacement at the junctions can be applied to give the relationships between the state vectors at the junctions

$$\mathbf{h}_{1b} = \mathbf{h}_{1a} \tag{63}$$

$$\mathbf{h}_{2a} = \mathbf{h}_{2c} \tag{64}$$

$$\mathbf{h}_{3c} = \mathbf{h}_{3b} \tag{65}$$

where the subscripts b denotes the sections of the homogeneous parts of the rod (before and after of the periodic part), a-c are first and second parts of the rod cell and 1-3 denote the location of junctions.

Equations (63) to (65) can be transformed into wave-mode coordinates using equation (59) such that

$$\mathbf{H}_b\mathbf{a}_{1b} = \mathbf{H}_a\mathbf{a}_{1a} \tag{66}$$

$$\mathbf{H}_a\mathbf{a}_{2a} = \mathbf{H}_c\mathbf{a}_{2c} \tag{67}$$

$$\mathbf{H}_c\mathbf{a}_{3c} = \mathbf{H}_b\mathbf{a}_{3b} \tag{68}$$

Using the equation (61) it is possible to write

$$\mathbf{a}_{2a} = \mathbf{T}_a\mathbf{a}_{1a} \tag{69}$$

$$\mathbf{a}_{3c} = \mathbf{T}_c\mathbf{a}_{2c} \tag{70}$$

From equations (66) to (70) the following relation can be obtained

$$\mathbf{H}_b\mathbf{a}_{3b} = (\mathbf{H}_c\mathbf{T}_c\mathbf{H}_c^{-1}\mathbf{H}_a\mathbf{T}_a\mathbf{H}_a^{-1})\mathbf{H}_b\mathbf{a}_{1b} \tag{71}$$

which can be rewritten as

$$\mathbf{H}_b\mathbf{a}_{3b} = \tilde{\mathbf{T}}_{cell}\mathbf{H}_b\mathbf{a}_{1b} \tag{72}$$

where

$$\tilde{\mathbf{T}}_{cell} = \mathbf{H}_c \mathbf{T}_c \mathbf{H}_c^{-1} \mathbf{H}_a \mathbf{T}_a \mathbf{H}_a^{-1} \tag{73}$$

Based on equation (72) it is possible to note the periodic part of this proposed hybrid rod is represented by the transfer matrix of that single cell (Eq. 73). In this case, a hybrid rod with N cells as illustrated in figure 16 can be defined by the following relation

$$\mathbf{H}_b \mathbf{a}_{3b} = \tilde{\mathbf{T}}_G \mathbf{H}_b \mathbf{a}_{1b} \tag{74}$$

where the global transfer matrix $\tilde{\mathbf{T}}_G$ for a periodic structure composed by N cells can be obtained by

$$\tilde{\mathbf{T}}_G = (\mathbf{H}_c \mathbf{T}_c \mathbf{H}_c^{-1} \mathbf{H}_a \mathbf{T}_a \mathbf{H}_a^{-1})_N (\mathbf{H}_c \mathbf{T}_c \mathbf{H}_c^{-1} \mathbf{H}_a \mathbf{T}_a \mathbf{H}_a^{-1})_{N-1} \ldots (\mathbf{H}_c \mathbf{T}_c \mathbf{H}_c^{-1} \mathbf{H}_a \mathbf{T}_a \mathbf{H}_a^{-1})_1 \tag{75}$$

or, similarly

$$\tilde{\mathbf{T}}_G = (\tilde{\mathbf{T}}_{cell})^N \tag{76}$$

Figure 16 - Hybrid rod with N periodic cells.

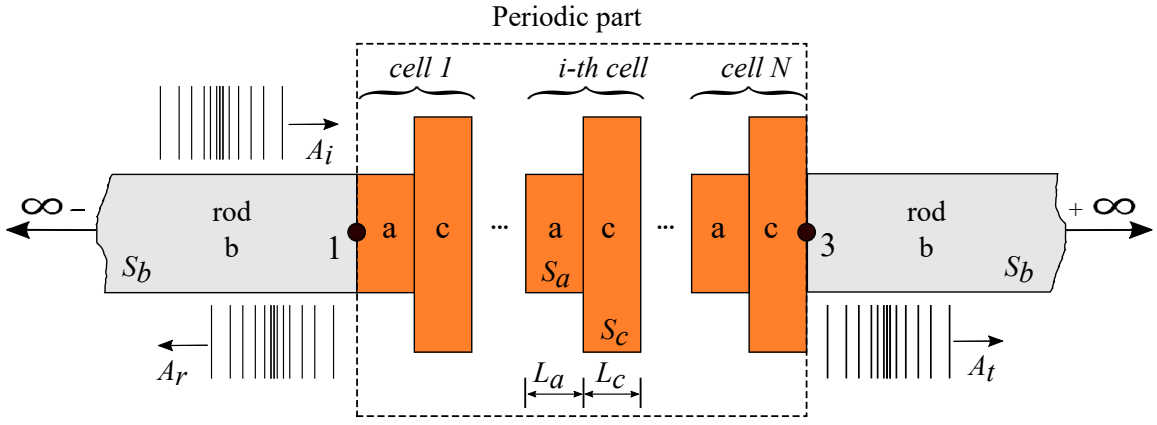

Source: elaborated by the author.

Equation (74) can be rearranged in terms of **incoming** and **outgoing** waves. The periodic structure can therefore be represented by the block diagram shown in figure 17.

Figure 17 - Block diagram of a periodic structure as incoming and outgoing waves.

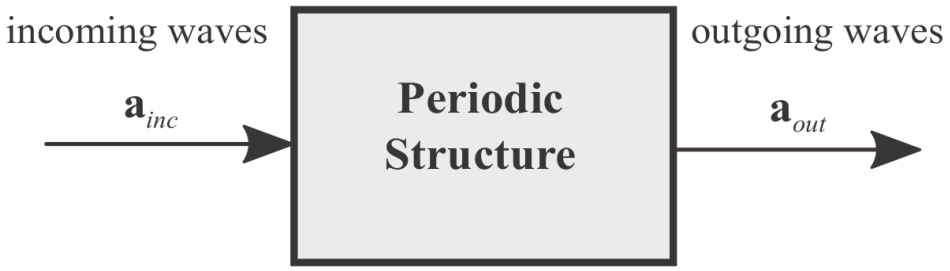

Source: elaborated by the author.

The expression relating the waves is a classical notation from the literature such that

$$\mathbf{a}_{out} = -\gamma^{-1}\mu\mathbf{a}_{inc} \tag{77}$$

where the wave vectors are given by

$$\mathbf{a}_{inc} = \left\{ \begin{array}{c} A_{(3b)L} \\ A_{(1b)R} \end{array} \right\} = \left\{ \begin{array}{c} 0 \\ A_i \end{array} \right\} \tag{78}$$

and

$$\mathbf{a}_{out} = \left\{ \begin{array}{c} A_{(1b)L} \\ A_{(3b)R} \end{array} \right\} = \left\{ \begin{array}{c} A_r \\ A_t \end{array} \right\} \tag{79}$$

Note that the term $A_{(3b)L} = 0$, i.e., is assumed that there are no incident waves from the right side of the structure, according to previously presented in this text (see section 1.1).

The matrices μ and γ are given by

$$\mu = [(\mathbf{H}_b)_1 \mid (-\tilde{\mathbf{H}})_2] \tag{80}$$

and

$$\gamma = [(-\tilde{\mathbf{H}})_1 \mid (\mathbf{H}_b)_2] \tag{81}$$

where $\tilde{\mathbf{H}} = \tilde{\mathbf{T}}_G \mathbf{H}_b$ and the subscripts 1?2 denote the columns of the respective matrices given in the brackets.

3.2 EQUATION FOR WAVE TRANSMISSION

After some mathematical manipulations (see details in appendix A), from equation (77) we can obtain the following relationship for transmitted A_t and incident A_i amplitudes waves

$$\frac{A_t}{A_i} = \frac{j2}{\eta(\Omega)}(\alpha^2 + \beta^2 + \alpha\beta b(\Omega)) \tag{82}$$

where

$$\begin{aligned}\eta(\Omega) = \alpha[(-S_{ab}\sqrt{E_{ab}\rho_{ab}} - \frac{1}{S_{ab}\sqrt{E_{ab}\rho_{ab}}})\sin(\pi\Omega)\cos(\pi\Omega L_{ca}\sqrt{\frac{\rho_{ca}}{E_{ca}}}) + \\ (-S_{cb}\sqrt{E_{cb}\rho_{cb}} - \frac{1}{S_{cb}\sqrt{E_{cb}\rho_{cb}}})\cos(\pi\Omega)\sin(\pi\Omega L_{ca}\sqrt{\frac{\rho_{ca}}{E_{ca}}})] + j[-\alpha b(\Omega) - 2\beta]\end{aligned} \tag{83}$$

$$\begin{aligned}b(\Omega) = -2\cos(\pi\Omega)\cos(\pi\Omega L_{ca}\sqrt{\frac{\rho_{ca}}{E_{ca}}}) + (S_{ca}\sqrt{E_{ca}\rho_{ca}} + \frac{1}{S_{ca}\sqrt{E_{ca}\rho_{ca}}})\times \\ \times \sin(\pi\Omega)\sin(\pi\Omega L_{ca}\sqrt{\frac{\rho_{ca}}{E_{ca}}})\end{aligned} \tag{84}$$

$$\alpha = \frac{\Lambda_1^N - \Lambda_2^N}{\Lambda_1 - \Lambda_2}, \quad \beta = \frac{\Lambda_2\Lambda_1^N - \Lambda_1\Lambda_2^N}{\Lambda_1 - \Lambda_2} \tag{85}$$

N is the number of cells and $\Lambda_{1,2}$ are the eigenvalues obtained from $\tilde{\mathbf{T}}_{cell}$ matrix (see details in section 3.4).

$$L_{ca} = \frac{L_c}{L_a} \tag{86}$$

$$S_{ab} = \frac{S_a}{S_b} \qquad S_{cb} = \frac{S_c}{S_b} \qquad S_{ca} = \frac{S_c}{S_a} \tag{87}$$

$$E_{ab} = \frac{E_a}{E_b} \qquad E_{cb} = \frac{E_c}{E_b} \qquad E_{ca} = \frac{E_c}{E_a} \tag{88}$$

$$\rho_{ab} = \frac{\rho_a}{\rho_b} \qquad \rho_{cb} = \frac{\rho_c}{\rho_b} \qquad \rho_{ca} = \frac{\rho_c}{\rho_a} \tag{89}$$

are ratios of geometric and physical parameters and

$$\Omega = \frac{\omega L_a}{\pi v_a} \tag{90}$$

is non-dimensional frequency. From the equations (87) to (89) it is easy to show that

$$S_{cb} = S_{ab} S_{ca} \tag{91}$$

$$E_{cb} = E_{ab} E_{ca} \tag{92}$$

$$\rho_{cb} = \rho_{ab} \rho_{ca} \tag{93}$$

For clarity, equation (82) is a new proposition of this work to study the hybrid rod defined herein . Based on this relation and using the very convenient physical parameters normalization (Eqs. 86 to 89) it is possible to design a hybrid rod to satisfy a project engineering requirements.

3.3 EQUATION FOR WAVE REFLECTION

The proposed formulation also allows to study a relation for the reflected (A_r) and incident (A_i) waves amplitudes as shown in appendix A. According to the results (section 4.1.2), this is an equivalent way for analysing the vibration suppression problem involving this kind of hybrid rods.

$$\begin{aligned}\frac{A_r}{A_i} = \{-\alpha[(-S_{ab}\sqrt{E_{ab}\rho_{ab}} + \frac{1}{S_{ab}\sqrt{E_{ab}\rho_{ab}}})\sin(\pi\Omega)\cos(\pi\Omega L_{ca}\sqrt{\frac{\rho_{ca}}{E_{ca}}})+ \\ (-S_{cb}\sqrt{E_{cb}\rho_{cb}} + \frac{1}{S_{cb}\sqrt{E_{cb}\rho_{cb}}})\sin(\pi\Omega L_{ca}\sqrt{\frac{\rho_{ca}}{E_{ca}}})\cos(\pi\Omega)]- \\ j\alpha[(S_{ca}\sqrt{E_{ca}\rho_{ca}} - \frac{1}{S_{ca}\sqrt{E_{ca}\rho_{ca}}})\sin(\pi\Omega)\sin(\pi\Omega L_{ca}\sqrt{\frac{\rho_{ca}}{E_{ca}}})]\}/\eta\end{aligned} \tag{94}$$

3.4 TRANSFER MATRIX EIGENVALUE ANALYSIS

Equation (72) can be rewritten as

$$\left\{ \begin{array}{c} u_R \\ F_R \end{array} \right\} = \tilde{\mathbf{T}}_{cell} \left\{ \begin{array}{c} u_L \\ F_L \end{array} \right\} \tag{95}$$

The periodic condition (given by equation 1) for the displacements and forces in a section implies to the following equation (BRILLOUIN, 1953)

$$\left\{ \begin{array}{c} u_R \\ F_R \end{array} \right\} = \Lambda \left\{ \begin{array}{c} u_L \\ F_L \end{array} \right\} \tag{96}$$

From equations (95) and (96) the following eigenvalue problem is defined

$$(\tilde{\mathbf{T}}_{cell} - \Lambda\mathbf{I}) \left\{ \begin{array}{c} u_L \\ F_L \end{array} \right\} = \mathbf{0} \tag{97}$$

where $\mathbf{I}$ is the identity matrix and Λ is the eigenvalue which depends on the frequency.

The nontrivial solution of this equation requires to solve $det(\tilde{\mathbf{T}}_{cell} - \Lambda\mathbf{I}) = 0$. In this case

the following equation is defined (see details in appendix B)

$$\Lambda^2 + b(\Omega)\Lambda + 1 = 0 \tag{98}$$

where $b(\Omega)$ is give by equation (84) and $det()$ indicates the determinant function.

Therefore, the roots of the equation (98) are the eigenvalues of the matrix $\mathbf{T}_{cell}$. Similar results for this equation can be found in reference (NIELSEN; SOROKIN, 2015). Although these authors consider a different formulation it is possible to use their results to verify the eigenvalues obtained from this proposed approach.

4 NUMERICAL SIMULATIONS

In this chapter, the results for the numerical simulations using the proposed transmission and reflection relations (equations 82 and 94), respectively, are presented. Structures with geometrical periodicity are considered in order to evaluate the responses of transmission, reflection, and energy flow of waves that propagate longitudinally. Furthermore, the locations and shapes of the stop bands are discussed, and the analysis of the dispersion curves, obtained by the eigenvalues and propagation constants calculated from the equations (98) and (2), respectively, is carried out.

4.1 STRUCTURE WITH GEOMETRICAL PERIODICITY

Consider the structure with geometrical periodicity illustrated in figure 18. In this case, the values of the physical properties (modulus of elasticity and density) are considered the same for the whole hybrid structure. The influence of the number of cells N, cross-sectional area ratio S_{ca}, and length ratio L_{ca} related to the cells composing parts, is evaluated on the responses of wave transmission and reflection, as well as on the stop bands formation and energy flow. The results are presented through curves of transmission and reflection defined in terms of frequency and the geometrical parameters of the periodic structure.

Figure 18 - Structure with geometric periodicity.

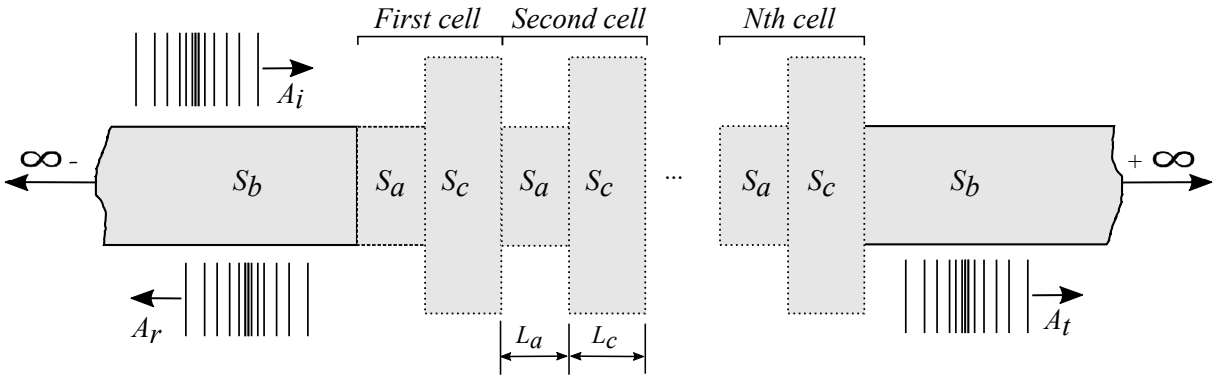

Source: elaborated by the author.

Figure 19 shows the curve obtained for the wave transmission through a periodic structure whose parameters are: $N = 3$, $L_{ca} = 1$, $S_{ca} = S_{cb} = 5$, $S_{ab} = 1$, $\rho_{cb} = \rho_{ca} = \rho_{ab} = 1$ and $E_{cb} = E_{ca} = E_{ab} = 1$. This curve results from the amplitude ratio of transmitted and incident waves, as defined by equation (82). The stop bands is clearly observed, that is, the frequency bands in which the transmitted waves are significantly attenuated. On the other hand, for the same structure, figure 20 shows the curve for reflection, that is, the amplitude ratio of reflected and incident waves, as defined by equation (94). Also, as expected, the existence of frequency bands in which reflection increases towards the unity is observed. Note that, for both curves, the stop bands arise periodically, presenting multiple repetitions of integer numbers of the non-dimensional frequency Ω. Depending on the values of L_{ca}, groups of stop bands arise within a frequency band, as shown in figure 21. Note that there are five groups of stop bands (*SB*) in the frequency range considered, each one containing three stop bands. For simplicity and clarity of understanding, in the next sections only the first group of stop bands will be presented in the results. Nevertheless, the same analysis can be applied to the remaining cases since the response has a periodic behavior.

Figure 19 - Transmission for $N = 3$, $L_{ca} = 1$, $S_{ca} = 5$, $S_{cb} = 5$, $S_{ab} = 1$, $\rho_{cb} = \rho_{ca} = \rho_{ab} = 1$ and $E_{cb} = E_{ca} = E_{ab} = 1$.

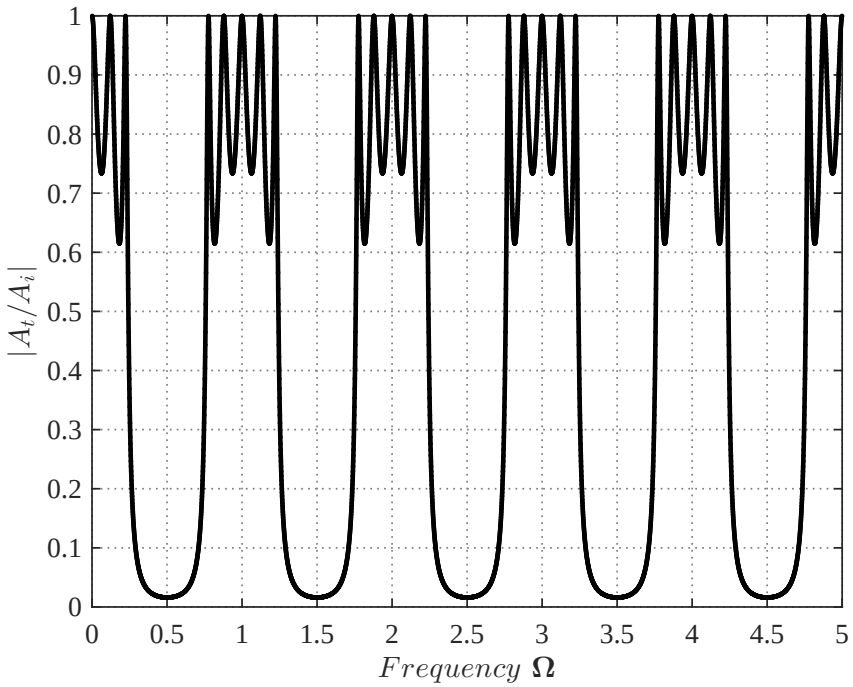

Source: elaborated by the author.

Figure 20 - Reflection for $N = 3$, $L_{ca} = 1$, $S_{ca} = 5$, $S_{cb} = 5$, $S_{ab} = 1$, $\rho_{cb} = \rho_{ca} = \rho_{ab} = 1$ and $E_{cb} = E_{ca} = E_{ab} = 1$.

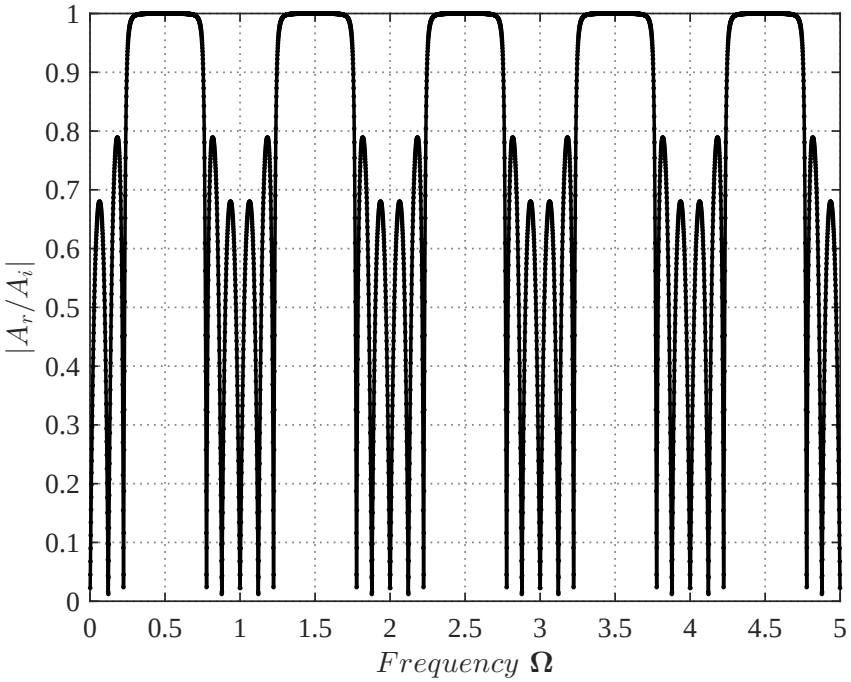

Source: elaborated by the author.

Figure 21 - Transmission for $N = 3$, $L_{ca} = 3$, $S_{ca} = 5$, $S_{cb} = 5$, $S_{ab} = 1$, $\rho_{cb} = \rho_{ca} = \rho_{ab} = 1$ and $E_{cb} = E_{ca} = E_{ab} = 1$.

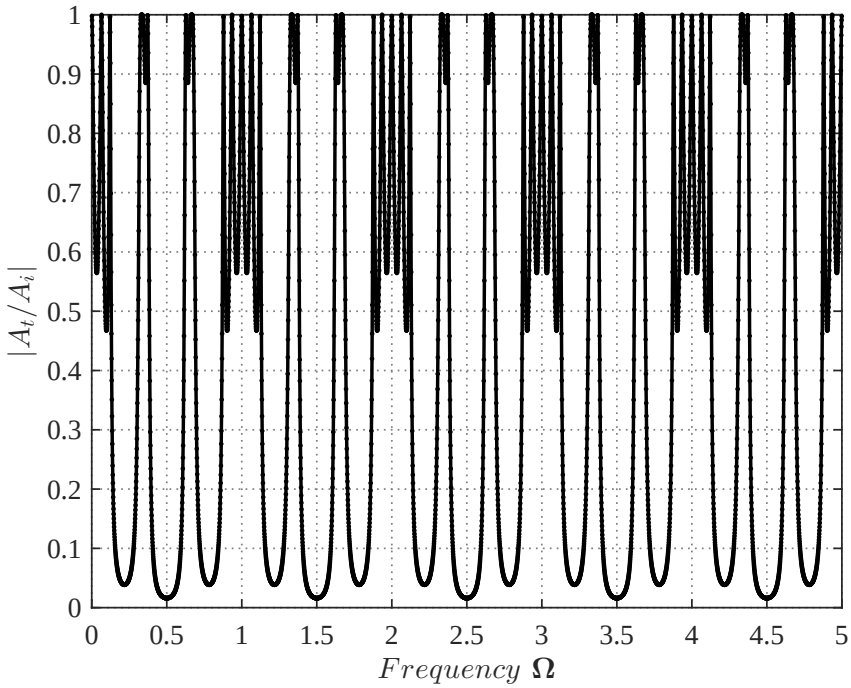

Source: elaborated by the author.

4.1.1 Analysis of waves transmission

Figure 22 shows the results obtained considering different numbers of cells for the periodic structures. The remaining values of the physical and geometrical parameters are considered fixed and are described in the titles of each figure in this text. To better visualize the results, figure 23 shows a close-up of figure 22. It can be seen that the attenuation increases substantially as the number of cells changes from $N = 1$ to $N = 4$. From four cells on, no significant attenuation is observed. On the other hand, the increase in number of cells does not cause the stop band width to change significantly.

Figure 22 - Transmission for different number of cells considering $L_{ca} = 1$, $S_{ca} = 5$, $S_{cb} = 5$, $S_{ab} = 1$, $\rho_{cb} = \rho_{ca} = \rho_{ab} = 1$ and $E_{cb} = E_{ca} = E_{ab} = 1$.

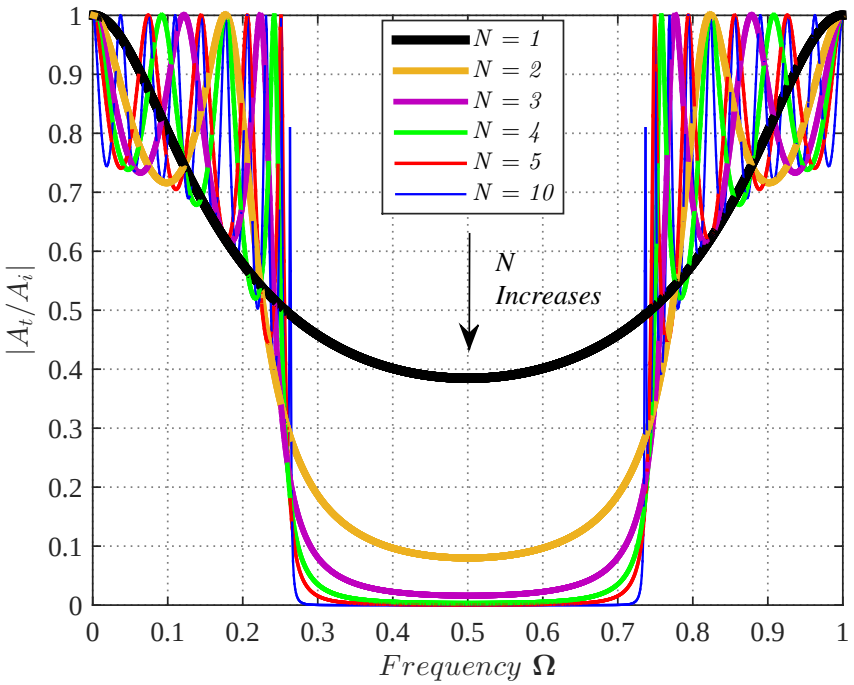

Source: elaborated by the author.

Figure 23 - Zoom in stop band of figure 22 for different number of cells considering $L_{ca} = 1$, $S_{ca} = 5$, $S_{cb} = 5$, $S_{ab} = 1$, $\rho_{cb} = \rho_{ca} = \rho_{ab} = 1$ and $E_{cb} = E_{ca} = E_{ab} = 1$.

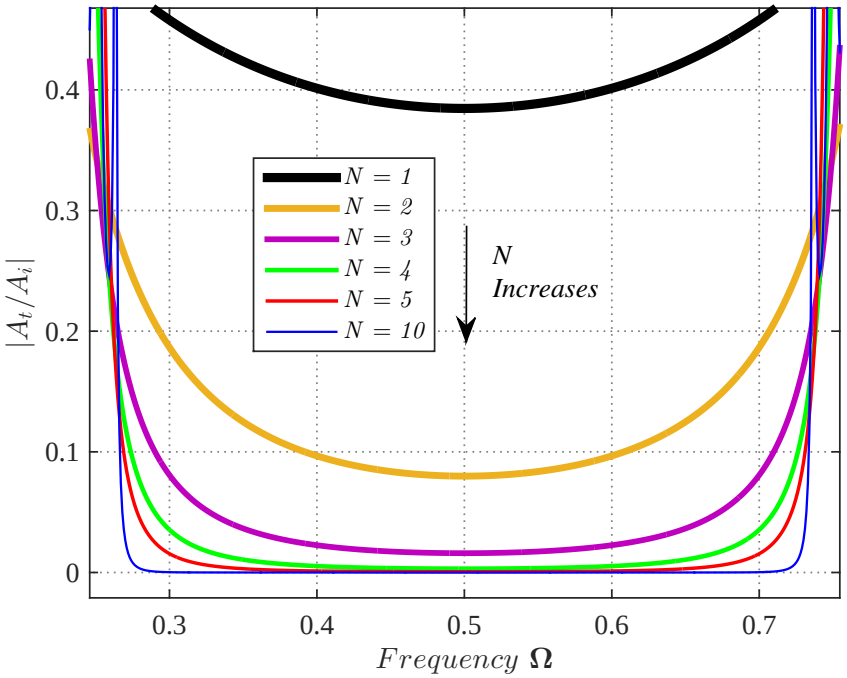

Source: elaborated by the author.

The minimum values of the transmission curves of figure 22, within the stop bands, are calculated and shown in figure 24 for different numbers of cells and S_{ca}. It can be seen that for $S_{ca} = 1$ the structure becomes a homogeneous rod (non-periodic), and there is no stop band. Therefore, the transmitted wave's amplitude is equal to the one from the incident wave. For values of S_{ca} different from one there are stop bands, and thus an attenuation of the transmitted wave is observed. Note that if the number of cells N and the area ratio S_{ca} increase the attenuation level of the transmitted waves increase too. It is important to point out that, for the cases in which the project cannot assume certain values of S_{ca} (due to space limitations, for instance) to attain the desired attenuation, lower values of S_{ca} alongside a higher number of cells can be used as an alternative. For example, if a transmission value of 0.03 is desired, a structure with $N = 6$ and $S_{ca} = 2$ can be used instead of choosing $N = 3$ and $S_{ca} = 4$ (see figure 24). Therefore, this is a very practical process when designing such structures.

Figure 24 - Minimum values of the transmission for different values of S_{ca} and number of cells considering $L_{ca} = 1$, $S_{ab} = 1$, $\rho_{cb} = \rho_{ca} = \rho_{ab} = 1$ and $E_{cb} = E_{ca} = E_{ab} = 1$.

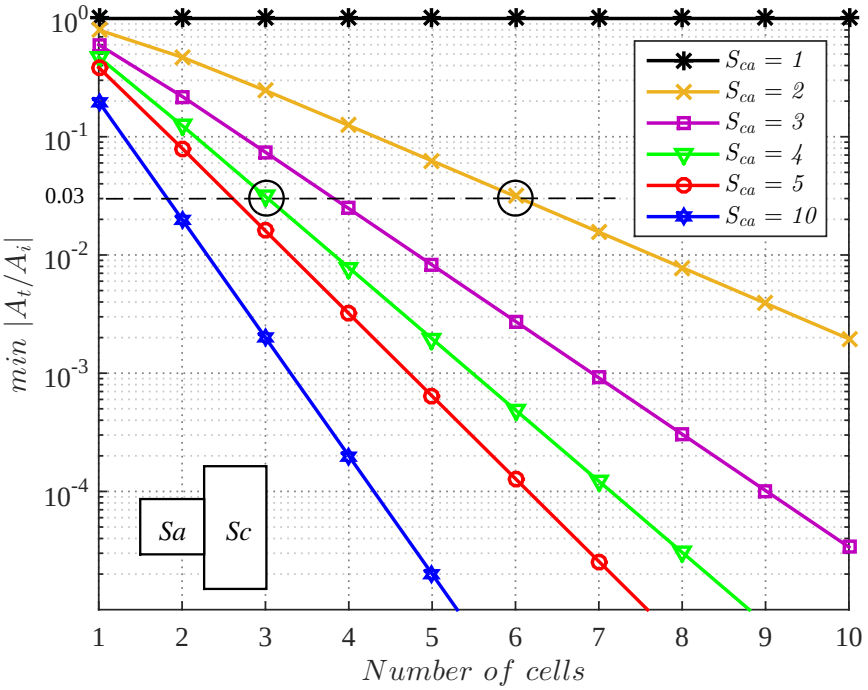

Source: elaborated by the author.

Unlike the number of cells, the geometrical parameter S_{ca} causes an important effect on the stop band widths. To evaluate such effect, these frequency bandwidths are calculated for different values of S_{ca} and an attenuation reference line of $-3\ dB$[1] is considered. The difference between the two points of intersection with the transmission curve is calculated, as shown in figure 25. The results obtained for the bandwidths (BW) are shown in figure 26. In this figure, a significant change in the bandwidth can be seen as S_{ca} increases or decreases. Note that the bandwidth has a symmetrical behavior for inverse values of S_{ca}, i.e., the same bandwidth is obtained for S_{ca} or $1/S_{ca}$. Moreover, as the number of cells increases, a slight bandwidth reduction is observed since an increase in its value is followed by an increase in the amplitude attenuation of the stop bands, as shown in figures 22 and 24.

[1] This reference represents the bandwidth at $1/\sqrt{2}$ since $20\log_{10}(1/\sqrt{2}) \approx -3\ dB$.

Figure 25 - Transmission and bandwidth for different values of S_{ca} considering $N = 3$, $L_{ca} = 1$, $S_{ab} = 1$, $\rho_{cb} = \rho_{ca} = \rho_{ab} = 1$ and $E_{cb} = E_{ca} = E_{ab} = 1$.

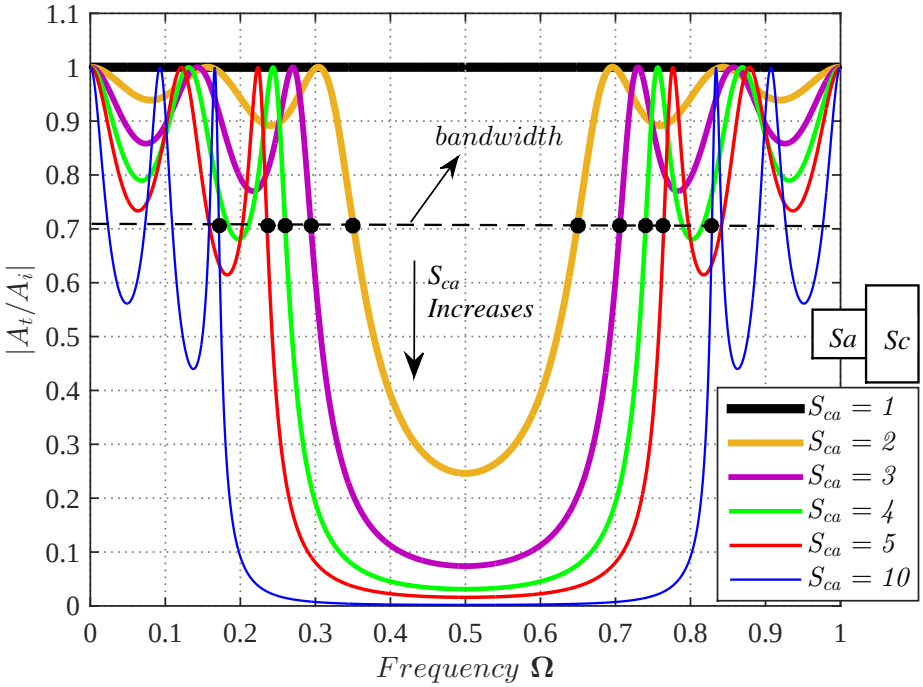

Source: elaborated by the author.

Figure 26 - Bandwidth for different values of S_{ca} and number of cells considering $L_{ca} = 1$, $S_{ab} = 1$, $\rho_{cb} = \rho_{ca} = \rho_{ab} = 1$ and $E_{cb} = E_{ca} = E_{ab} = 1$.

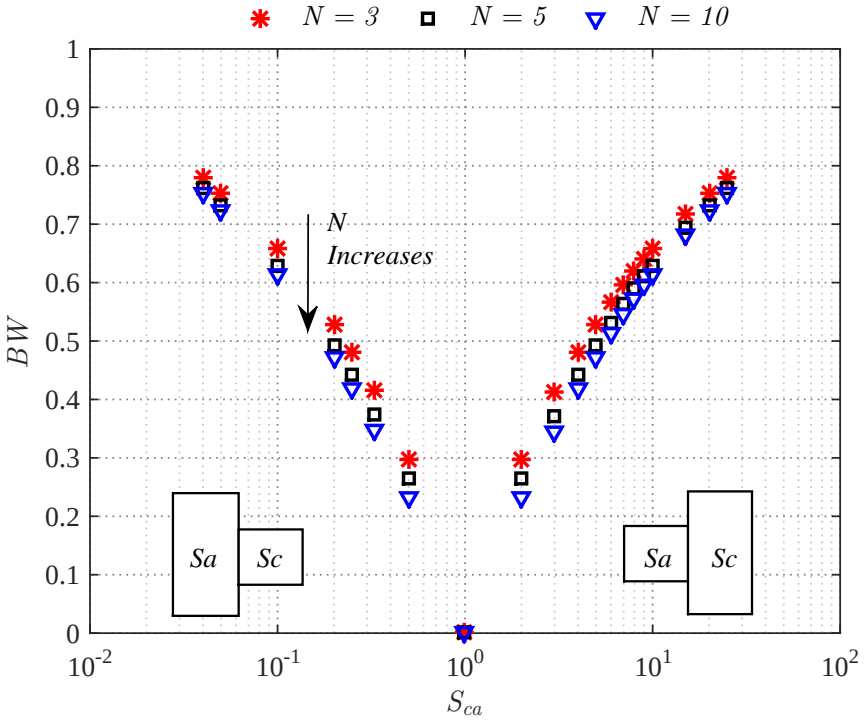

Source: elaborated by the author.

Figure 27 shows the effect of the geometrical parameter L_{ca} on the stop bands formation for integer values of this parameter. It can be seen that the stop bands arise within the frequency band $0 \leqslant \Omega \leqslant 1$, and the number of unities is equal to the values of L_{ca}; that is, if $L_{ca} = 1$ there is only 1 stop band, if $L_{ca} = 2$ there are 2 stop bands, and so on. On the other hand, figure 28 shows the stop bands formation for values of L_{ca} lower than the unity. In this case, it can be seen that they do not arise within a unit non-dimensional frequency band, but rather within a frequency band whose maximum value is the inverse of L_{ca}. Also, it can be seen that the number of stop bands is the inverse of L_{ca}. For example, if $L_{ca} = 1/2$ there are 2 stop bands that are within the frequency band $0 \leqslant \Omega \leqslant 2$; if $L_{ca} = 1/4$ there are 4 stop bands that are within the frequency band $0 \leqslant \Omega \leqslant 4$, and so on.

Figure 27 - Stop bands for different values of $L_{ca} \geqslant 1$ considering $N = 3$, $S_{ca} = 5$, $S_{cb} = 5$, $S_{ab} = 1$, $\rho_{cb} = \rho_{ca} = \rho_{ab} = 1$ and $E_{cb} = E_{ca} = E_{ab} = 1$.

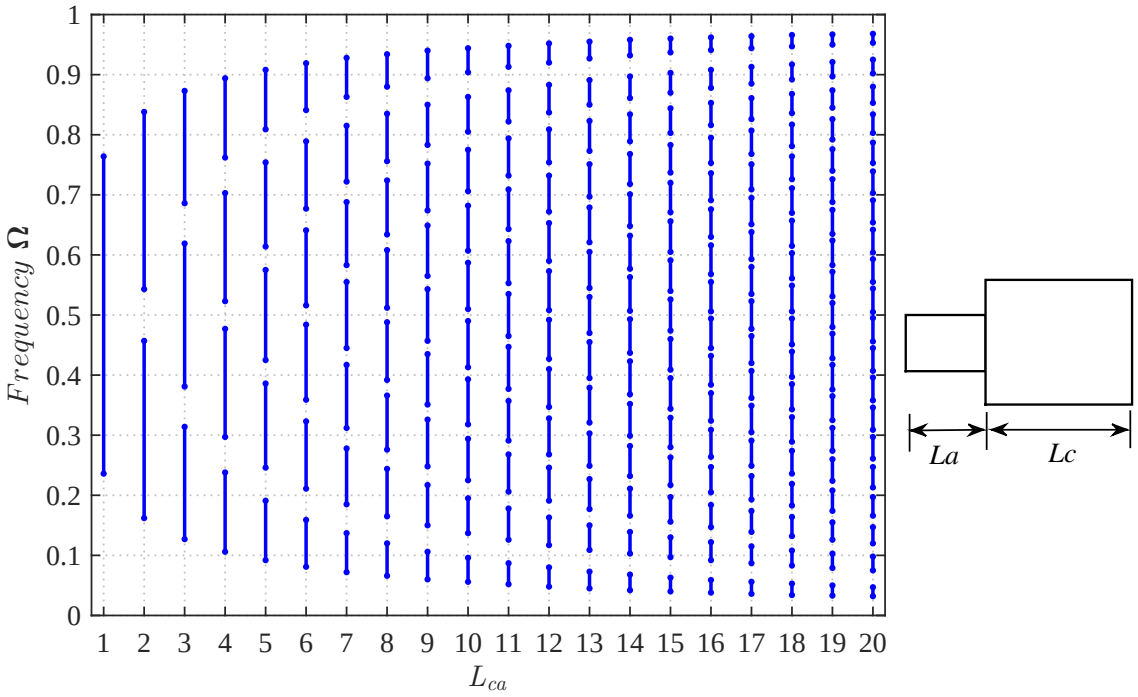

Source: elaborated by the author.

Figure 28 - Stop bands for different values of $L_{ca} < 1$ considering $N = 3$, $S_{ca} = 5$, $S_{cb} = 5$, $S_{ab} = 1$, $\rho_{cb} = \rho_{ca} = \rho_{ab} = 1$ and $E_{cb} = E_{ca} = E_{ab} = 1$.

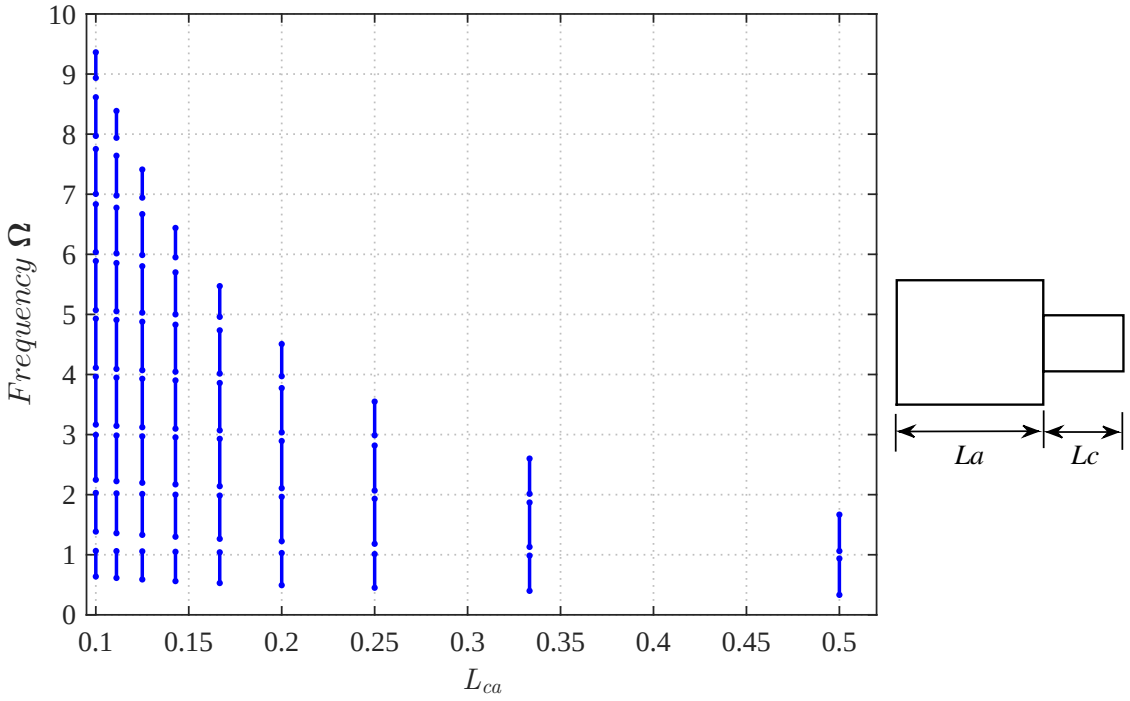

Source: elaborated by the author.

The transmission curve for $L_{ca} = 3$ is shown in figure 29. It can be seen that there is a group consisting of three stop bands within the frequency band $0 < \Omega < 1$. In addition, the stop band widths for different values of S_{ca} are shown in figure 30. One notices that the width of the first and the third stop bands are the same, but both are narrower than the second one.

The transmission curve for $L_{ca} = 1/3$ is shown in figure 31. It can be seen that, in this case, there is a group consisting of three stop bands within the frequency band $0 \leq \Omega \leq 3$. Figure 32, in turn, shows the stop band widths for different values of S_{ca}. One notices the same characteristic on these widths, similar to the shape for $L_{ca} = 3$.

Figure 29 - Transmission and bandwidth considering $N = 3$ cells, $L_{ca} = 3$, $S_{ca} = 5$, $S_{cb} = 5$, $S_{ab} = 1$, $\rho_{cb} = \rho_{ca} = \rho_{ab} = 1$ and $E_{cb} = E_{ca} = E_{ab} = 1$.

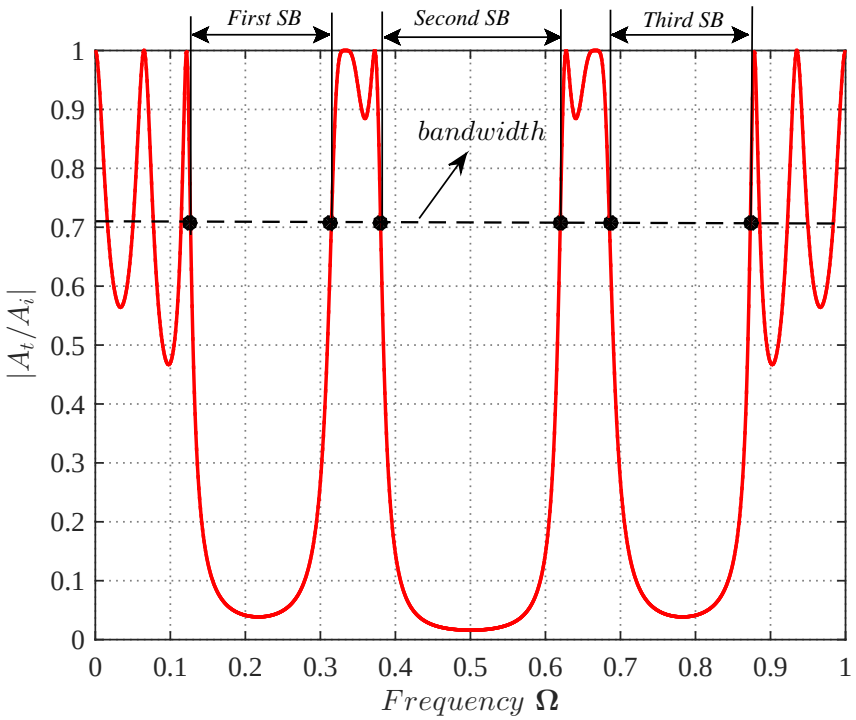

Source: elaborated by the author.

Figure 30 - Bandwidths for different values of S_{ca} considering $N = 3$, $L_{ca} = 3$, $S_{ab} = 1$, $\rho_{cb} = \rho_{ca} = \rho_{ab} = 1$ and $E_{cb} = E_{ca} = E_{ab} = 1$.

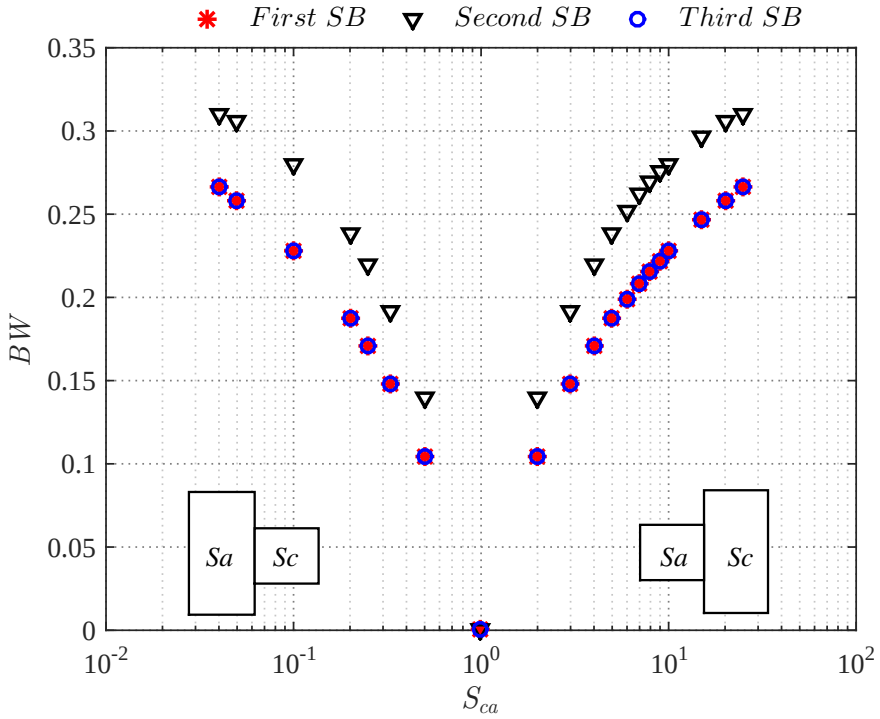

Source: elaborated by the author.

Figure 31 - Transmission and bandwidth considering $N = 3$, $L_{ca} = 1/3$, $S_{ca} = 5$, $S_{cb} = 5$, $S_{ab} = 1$, $\rho_{cb} = \rho_{ca} = \rho_{ab} = 1$ and $E_{cb} = E_{ca} = E_{ab} = 1$.

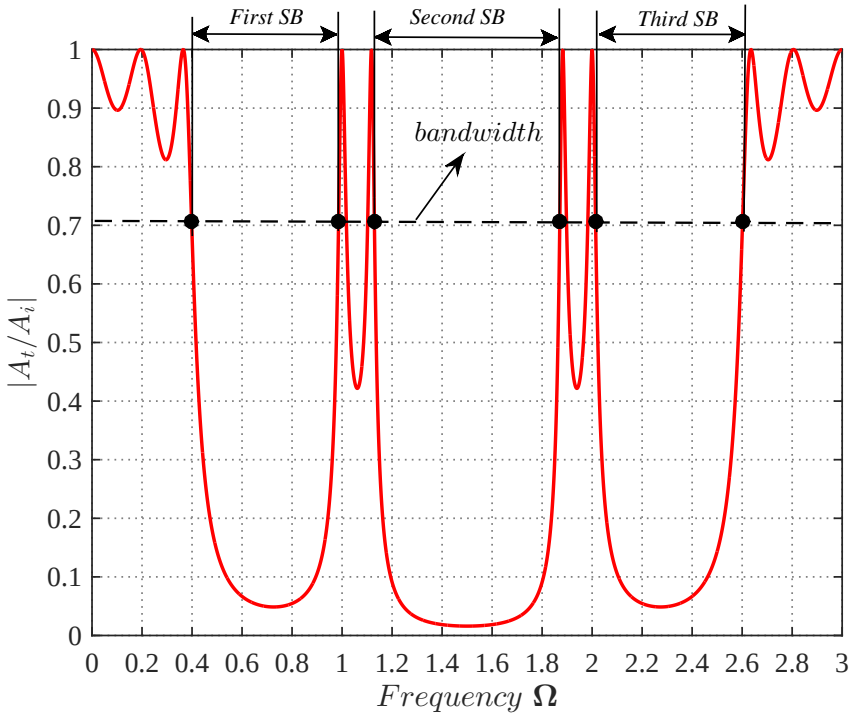

Source: elaborated by the author.

Figure 32 - Bandwidths for different values of S_{ca} considering $N = 3$, $L_{ca} = 1/3$, $S_{ab} = 1$, $\rho_{cb} = \rho_{ca} = \rho_{ab} = 1$ and $E_{cb} = E_{ca} = E_{ab} = 1$.

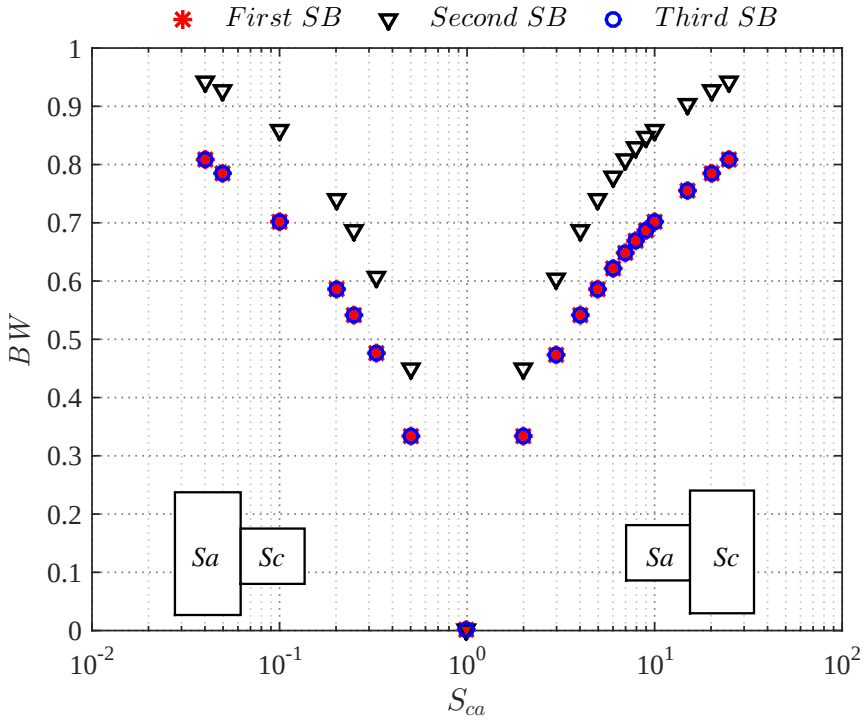

Source: elaborated by the author.

4.1.2 Analysis of the wave reflection

The numerical results obtained for the reflection of longitudinal waves are presented in this section. Figure 33 shows the reflection curves for periodic structures using different numbers of cells. The remaining values of the physical and geometrical parameters are fixed, as indicated in the figures. To better visualize the results, figure 34 shows a close-up of figure 33. It can be clearly seen that the amplitude of reflected waves increases significantly as the number of cells in the structure changes from $N = 1$ to $N = 3$. From three cells on there exists already a frequency range in which full reflection of the incident wave occurs. On the other hand, the increase in number of cells does not cause any significant change in stop band widths.

Figure 33 - Reflection for different number of cells considering $L_{ca} = 1$, $S_{ca} = 5$, $S_{cb} = 5$, $S_{ab} = 1$, $\rho_{cb} = \rho_{ca} = \rho_{ab} = 1$ and $E_{cb} = E_{ca} = E_{ab} = 1$.

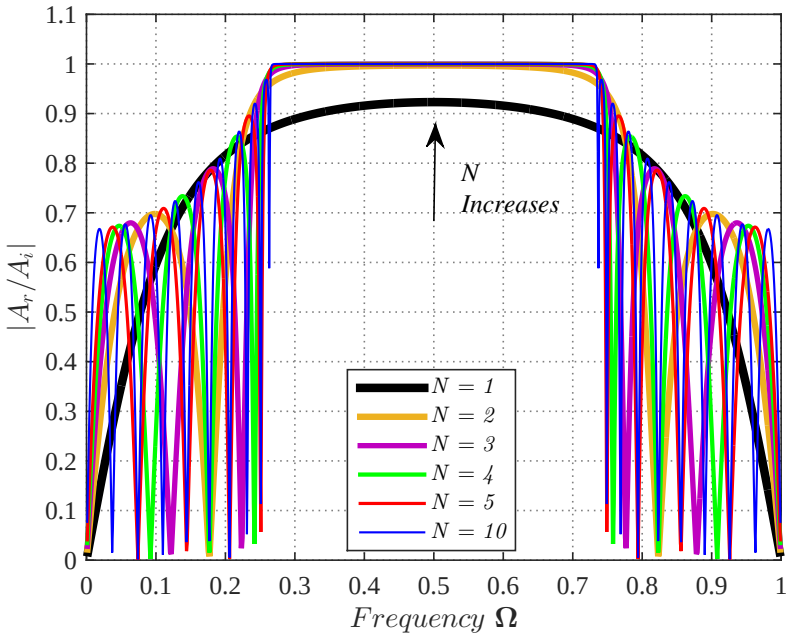

Source: elaborated by the author.

Figure 34 - Zoom in stop band of figure 33 for different number of cells considering $L_{ca} = 1$, $S_{ca} = 5$, $S_{cb} = 5$, $S_{ab} = 1$, $\rho_{cb} = \rho_{ca} = \rho_{ab} = 1$ and $E_{cb} = E_{ca} = E_{ab} = 1$.

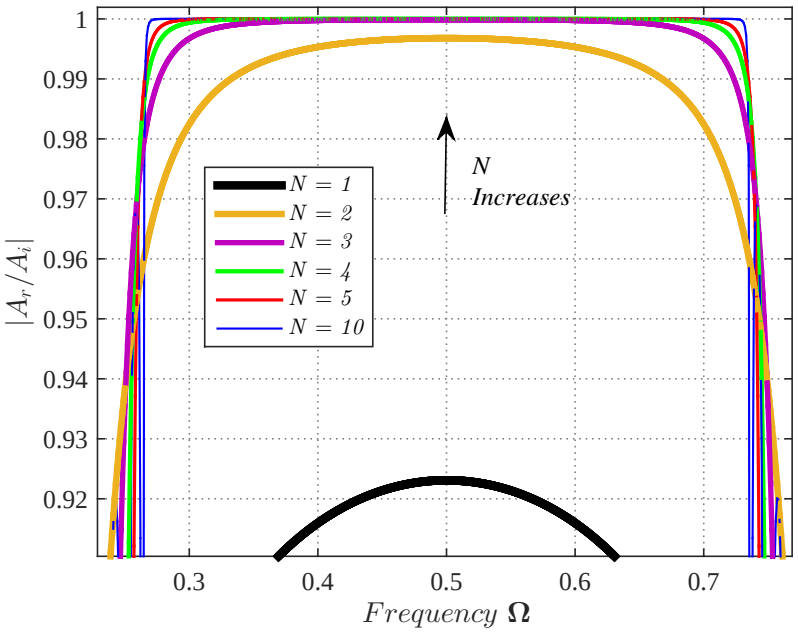

Source: elaborated by the author.

The maximum values of the reflection curves of figure 33, within the stop bands, are calculated and shown in figure 35 for different numbers of cells and cross-sectional area ratios $S_{ca} = 1$. It can be seen that, for $S_{ca} = 1$, the structure becomes a homogeneous rod (non-periodic) and, therefore, since there is no stop band, the amplitude of the reflected wave is zero. As for the values of S_{ca} that are different from the unity, there exist stop bands and, therefore, reflection of the incident wave is observed. Note that the ratio S_{ca} and the number of cells N cause an increase in the reflection as these values get higher. It is important to point out that, for specific cases in which the project cannot assume values of S_{ca} in order to guarantee the desired level of reflection, it is possible to reach such level by applying lower values of S_{ca} alongside a higher number of cells, as previously observed for the transmission curves. This observation is presented in section 4.1.1 for the transmission analysis.

Like transmission, it can also be seen that, for reflection, the geometrical parameter S_{ca} causes an important effect on the stop band widths. To evaluate such effect, similarly to the transmission analysis, these frequency bandwidths are calculated for different values of S_{ca} and amplitude ratio of $1/\sqrt{2}$, as indicated by the black circles on this reference line (Fig. 36). The results obtained for the bandwidths (BW) are shown in figure 37. Note that the bandwidths are the same for reflection and transmission. Moreover, figures 38 and 39 show both the reflection and transmission curves for $L_{ca} = 1$ and $L_{ca} = 1/3$, respectively, in which one can clearly note that their intersection occurs at $1/\sqrt{2}$. This fact shall be discussed in the next section.

Figure 35 - Maximum values of the reflection for different values of S_{ca} and number of cells considering $L_{ca} = 1$, $S_{ab} = 1$, $\rho_{cb} = \rho_{ca} = \rho_{ab} = 1$ and $E_{cb} = E_{ca} = E_{ab} = 1$.

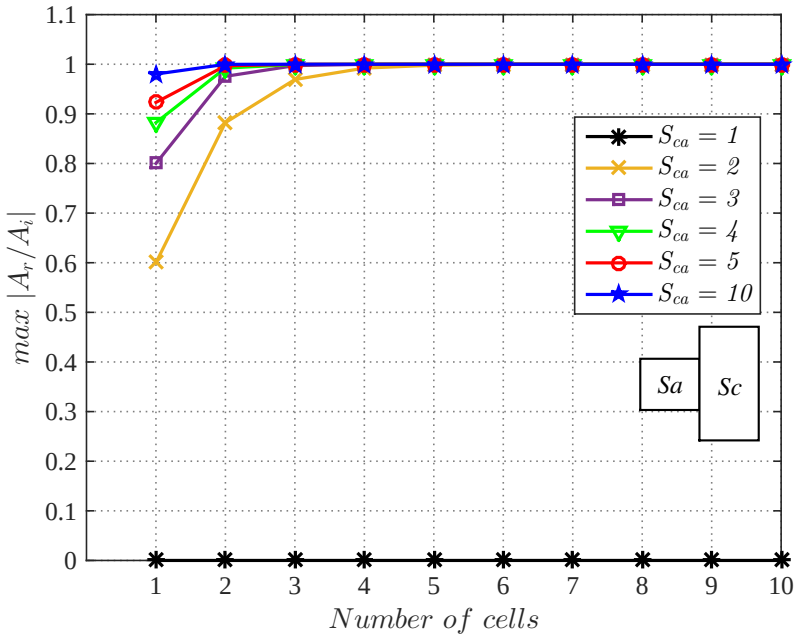

Source: elaborated by the author.

Figure 36 - Reflection and bandwidth for different values of S_{ca} considering $N = 3$, $L_{ca} = 1$, $S_{ab} = 1$, $\rho_{cb} = \rho_{ca} = \rho_{ab} = 1$ and $E_{cb} = E_{ca} = E_{ab} = 1$.

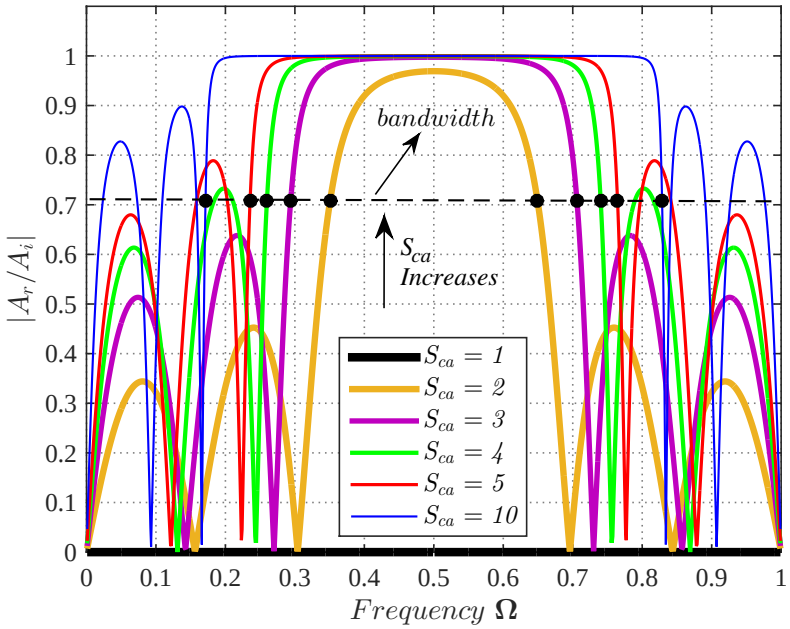

Source: elaborated by the author.

Figure 37 - Bandwidths for different values of S_{ca} considering $N = 3$, $L_{ca} = 1$, $S_{ab} = 1$, $\rho_{cb} = \rho_{ca} = \rho_{ab} = 1$ and $E_{cb} = E_{ca} = E_{ab} = 1$.

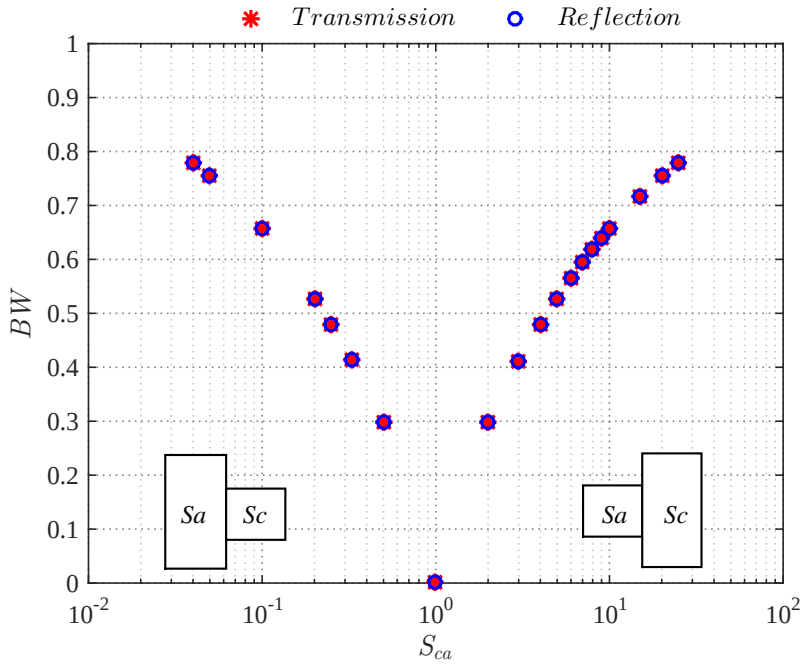

Source: elaborated by the author.

Figure 38 - Transmission, reflection and bandwidth considering $N = 3$, $L_{ca} = 1$, $S_{ca} = 5$, $S_{cb} = 5$, $S_{ab} = 1$, $\rho_{cb} = \rho_{ca} = \rho_{ab} = 1$ and $E_{cb} = E_{ca} = E_{ab} = 1$.

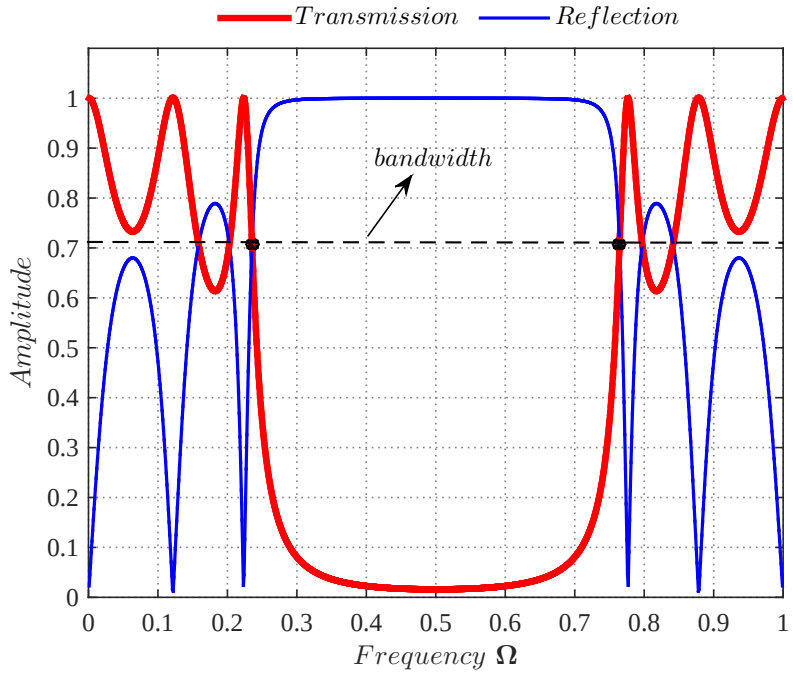

Source: elaborated by the author.

Figure 39 - Transmission, reflection and bandwidth considering $N = 3$, $L_{ca} = 1/3$, $S_{ca} = 5$, $S_{cb} = 5$, $S_{ab} = 1$, $\rho_{cb} = \rho_{ca} = \rho_{ab} = 1$ and $E_{cb} = E_{ca} = E_{ab} = 1$.

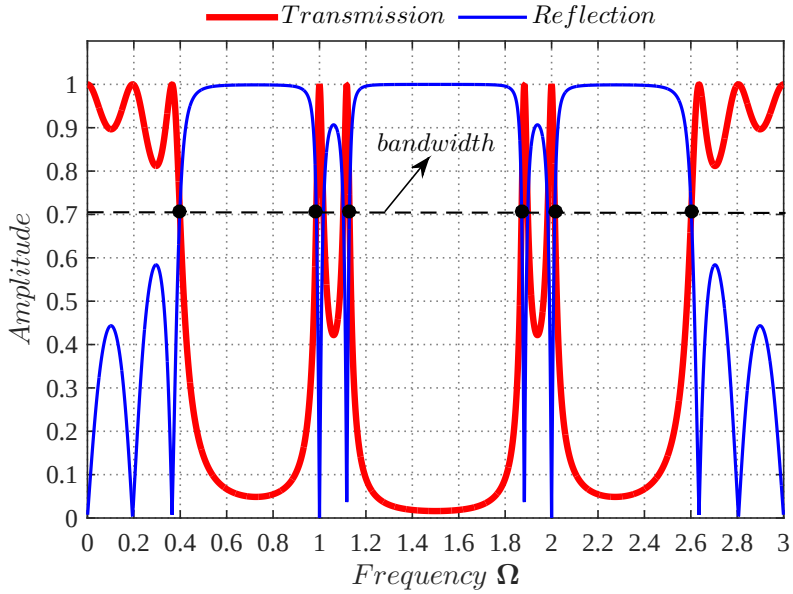

Source: elaborated by the author.

4.1.3 Power transmission and reflection

The numerical results obtained for the mean power analysis of transmitted and reflected waves in periodic rods are presented in this section. The main goal is to verify power distribution and energy conservation during the process of wave dispersion, as presented in section 2.3.3. Figure 40 shows the coefficients of transmitted power C_{PT} and reflected power C_{PR}, respectively, for the periodic structure whose configuration is defined in its title. In this figure, it can be seen that the curves intersect at $C_{PT} = C_{PR} = 0.5$, that is, the point where the incident power is equally divided into transmitted and reflected power. Note that, for $C_{PT} = 0.5$, the corresponding transmission value is equal to $1/\sqrt{2}$, which therefore means that the intersection of both transmission and reflection curves (see figures 38 and 39) occurs when the energy flow of transmitted and reflected waves is the same. Figure 42, in turn, shows that the sum of transmission and reflection powers is equal to the incident power, that is, the energy flow is conserved, as expected by equation (58).

Figure 40 - Coefficients of transmission and reflection power for $N = 3$, $L_{ca} = 1$, $S_{ca} = 5$, $S_{cb} = 5$, $S_{ab} = 1$, $\rho_{cb} = \rho_{ca} = \rho_{ab} = 1$ and $E_{cb} = E_{ca} = E_{ab} = 1$.

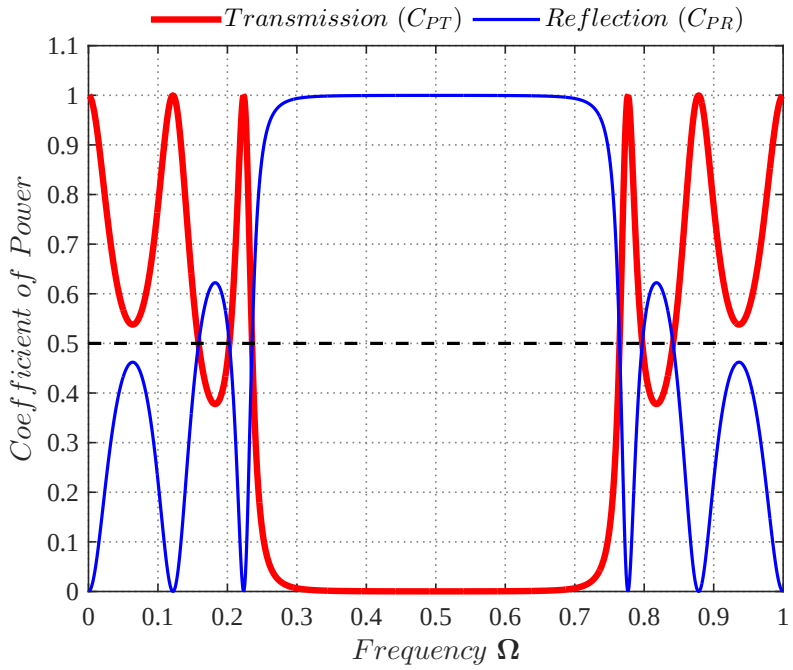

Source: elaborated by the author.

Figure 41 - Coefficients of transmission power versus transmission for different values of cells considering $L_{ca} = 1$, $S_{ca} = 5$, $S_{cb} = 5$, $S_{ab} = 1$, $\rho_{cb} = \rho_{ca} = \rho_{ab} = 1$ and $E_{cb} = E_{ca} = E_{ab} = 1$.

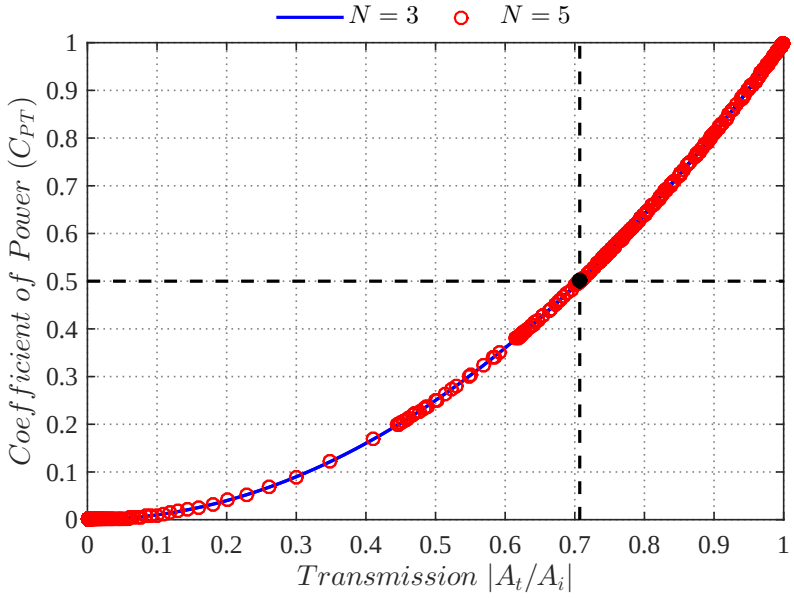

Source: elaborated by the author.

Figure 42 - Coefficient of total power considering $N = 3$, $L_{ca} = 1/3$, $S_{ca} = 5$, $S_{cb} = 5$, $S_{ab} = 1$, $\rho_{cb} = \rho_{ca} = \rho_{ab} = 1$ and $E_{cb} = E_{ca} = E_{ab} = 1$.

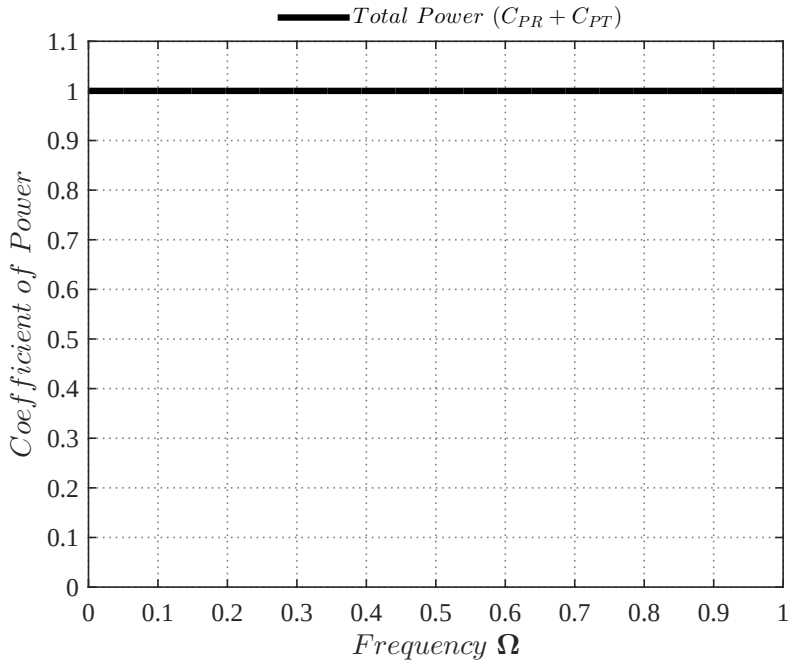

Source: elaborated by the author.

4.1.4 Analysis of dispersion

As discussed in section 2.1.2, the dispersion curves can be used to predict in which frequency bands the stop bands arise. These curves can be analyzed using the eigenvalues from the unit cell's transfer matrix (which are the roots of Eq. 98), or using the propagation constants obtained through the Bloch parameters ψ. Figures 43 and 44 show the dispersion curves using the eigenvalues obtained for the structures whose results of transmission and reflection are shown in figures 38 and 39. Note that the stop bands exist for values of $|\Lambda| \neq 1$, and are located in the corresponding frequency bands observed in the transmission and reflection curves. It is important to point out that similar results for this kind of analysis were obtained and discussed in greater detail in the reference (NIELSEN; SOROKIN, 2015).

Figure 43 - Eigenvalues considering $N = 3$, $L_{ca} = 1$, $S_{ca} = 5$, $S_{cb} = 5$, $S_{ab} = 1$, $\rho_{cb} = \rho_{ca} = \rho_{ab} = 1$ and $E_{cb} = E_{ca} = E_{ab} = 1$.

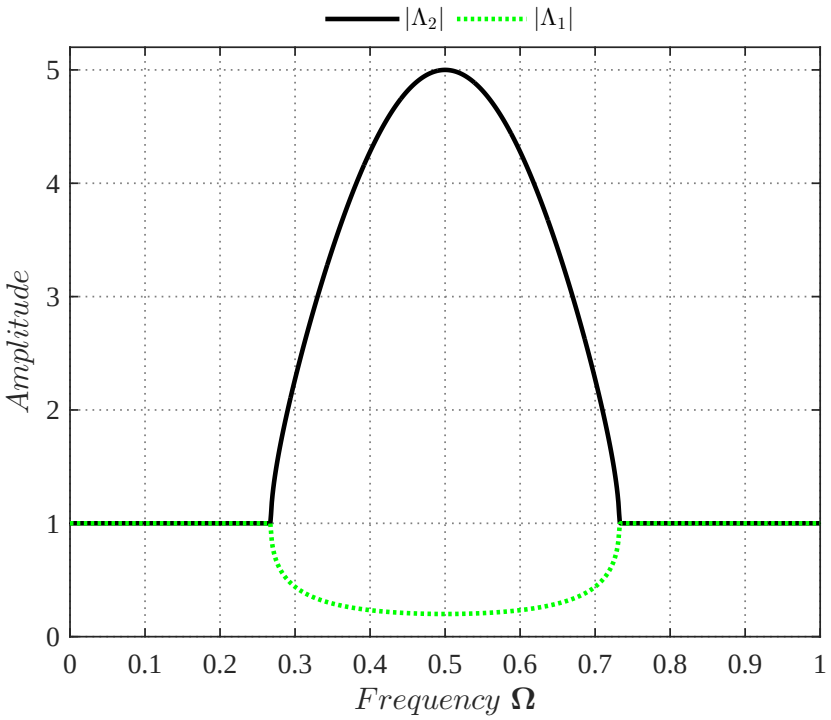

Source: elaborated by the author.

Figure 44 - Eigenvalues considering $N = 3$, $L_{ca} = 1/3$, $S_{ca} = 5$, $S_{cb} = 5$, $S_{ab} = 1$, $\rho_{cb} = \rho_{ca} = \rho_{ab} = 1$ and $E_{cb} = E_{ca} = E_{ab} = 1$.

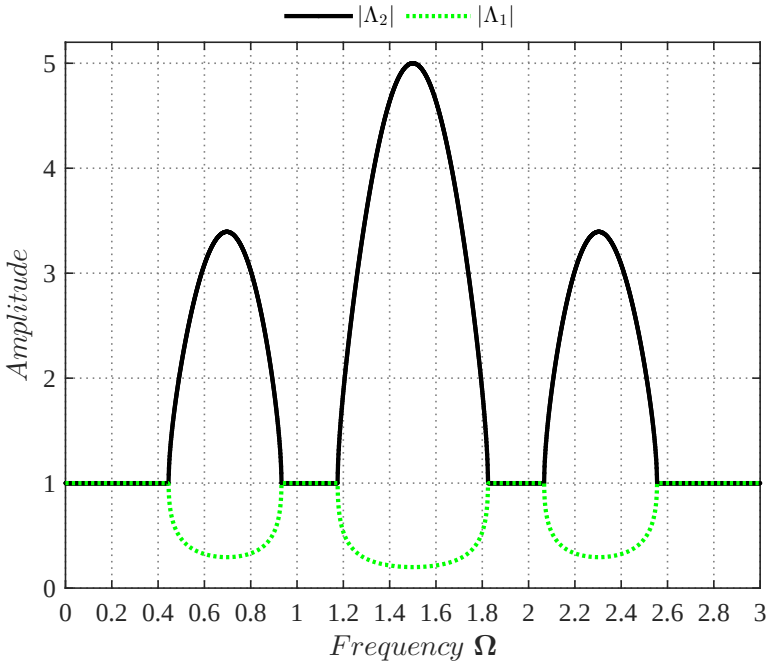

Source: elaborated by the author.

Likewise, figures 45 and 46 show the dispersion curves, but now using the propagation

constants. It can be seen that the stop bands are located in those frequency bands where the values of ψ have a real part (attenuation factor) and an imaginary part (phase factor) with values that are constant and equal to π or 0. On the other hand, for values of ψ with only an imaginary part, the wave propagation occurs without attenuation, thus defining the pass band.

Figure 45 - Propagation constants considering $N = 3$, $L_{ca} = 1$, $S_{ca} = 5$, $S_{cb} = 5$, $S_{ab} = 1$, $\rho_{cb} = \rho_{ca} = \rho_{ab} = 1$ and $E_{cb} = E_{ca} = E_{ab} = 1$.

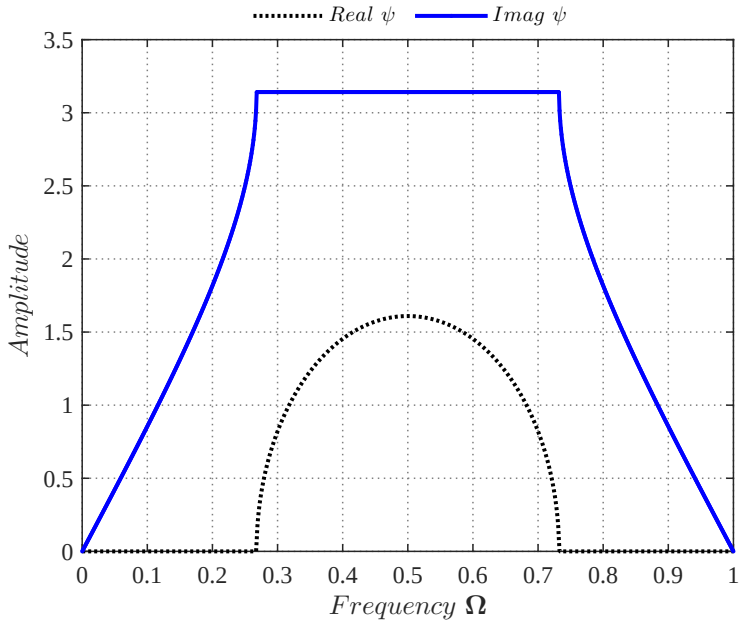

Source: elaborated by the author.

Figure 46 - Propagation constants considering $N = 3$, $L_{ca} = 1/3$, $S_{ca} = 5$, $S_{cb} = 5$, $S_{ab} = 1$, $\rho_{cb} = \rho_{ca} = \rho_{ab} = 1$ and $E_{cb} = E_{ca} = E_{ab} = 1$.

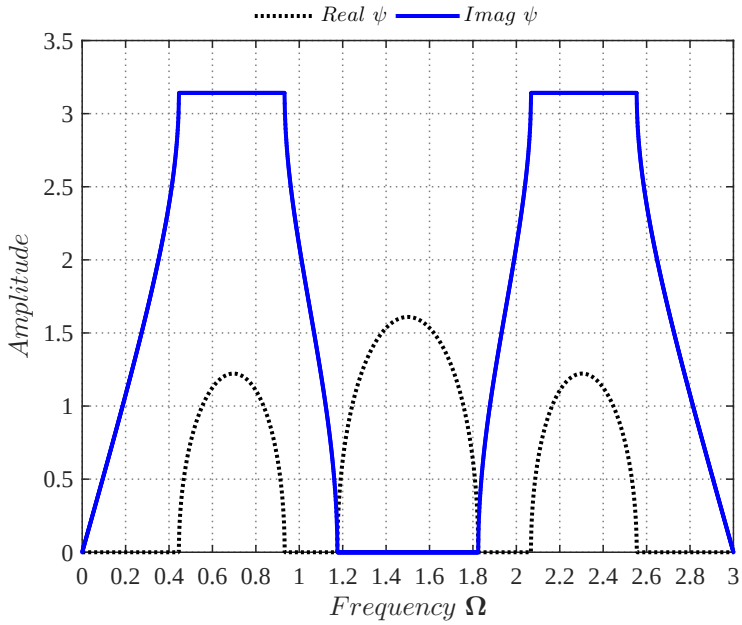

Source: elaborated by the author.

5 PRACTICAL ASPECTS OF PERIODIC RODS DESIGN

In this chapter, practical aspects of periodic rod design are discussed. When designing structures, engineers must meet certain requirements, such as frequency band, attenuation amplitudes at vibration levels, as well as geometric constraints, for example. Therefore, for clarity of understanding, practical details and a hypothetical condition of a vibration problem are presented as follows. For practical purposes, quantities that involve states (displacement, velocity and acceleration) are usually used instead of wave amplitudes. The following results are thus converted from wave amplitudes to a displacement relation between the right and left sides, u_R and u_L, respectively, of the periodic part (see figure 47). From equations (59) and (60), it follows that

$$u_L = A_r + A_i \tag{99}$$

and

$$u_R = A_t \tag{100}$$

The relationship between equations (100) and (99) results in the transmission written in terms of displacements,

$$\frac{u_R}{u_L} = \frac{\dfrac{A_t}{A_i}}{\dfrac{A_r}{A_i} + 1} \tag{101}$$

Practical engineering problems involve finite structures, it is thus also necessary to adapt the model developed in this thesis (infinite periodic rod) such that it represents a finite periodic rod. For this purpose, it must be considered that the cross-sectional area of the homogeneous rod S_b assumes a lower value in relation to the other cross-sectional areas, as illustrated in figure 47. Therefore, in the simulations presented in section 5.2, the following values are considered: $S_{ab} = 1000$ and $S_{cb} = 1000 \times S_{ca}$.

Figure 47 - Illustration of the approximation considered from the infinite model (theoretical) to the finite model (real), in which the cross-sectional area S_b tends to zero.

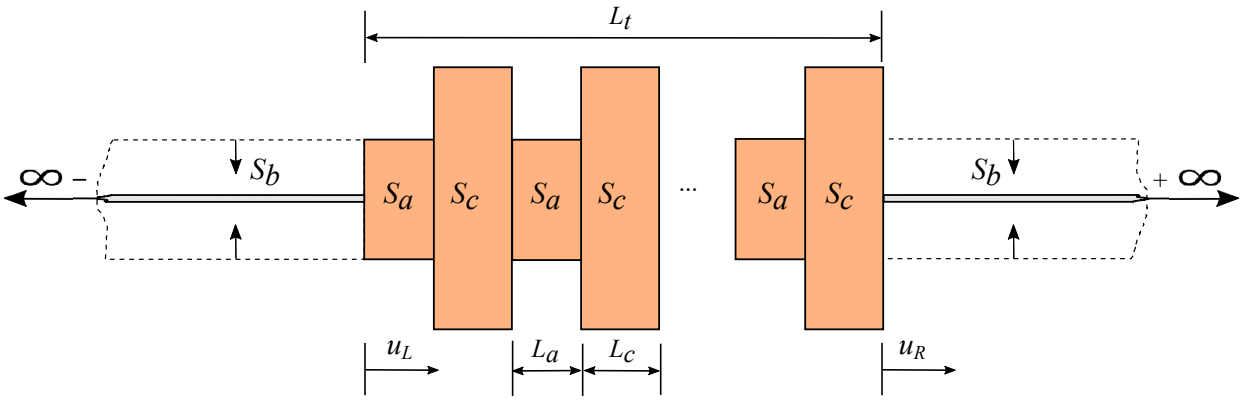

Source: elaborated by the author.

5.1 HYPOTHETICAL REQUIREMENTS OF A PRACTICAL PROBLEM

Consider the practical vibration problem in which the goal is to design a rod with only geometrical periodicity, where the material is the same for the whole structure, to meet the following requirements:

1. Stop band located around 3000 Hz (central frequency);
2. Minimum bandwidth (BW) of 1000 Hz;
3. Maximum area ratio of $S_{ca} = 2$ due to a hypothetical space constraint for the structure;
4. Minimum attenuation of 80%, that is, maximum transmission of 0.2;
5. Total length of the rod L_t smaller or equal to 1000 mm.

5.2 CANDIDATE SOLUTIONS

In this section, three candidate solutions for the design of the periodic rod corresponding to the requirements from section 5.1 are presented. To better illustrate this process, initially, the first two solutions do not meet all requirements. On the other hand, a discussion of how to interpret the results is carried out and, in this case, how to choose the appropriate material for the project as well.

5.2.1 Steel material

Initially, suppose that the steel ($E = 210\ Gpa$ and $\rho = 7800\ kg/m^3$) is the material available for manufacturing the periodic rod. From the results obtained in this work (section 4.1.1),

requirements 1, 2 and 3 (location, bandwidth and area ratio) are met for values of $L_a = 430$ *mm*, $S_{ca} = 2$ and $N = 1$ in the condition that $L_{ca} = 1$, as seen in figure 48. Note that, for $L_{ca} = 3$ and $L_{ca} = 5$, requirement 1 is met, but requirements 2 and 5 are not, since for these two conditions of L_{ca} the lengths of a single cell are 1720 *mm* and 2580 *mm*, respectively, and thus higher than the maximum L_t required.

To evaluate requirement 4 (attenuation level), the effects of the number of cells are evaluated, as shown in figure 49. Note that the requirement is met when N=3. However, for such number of cells the condition related to the total length of the periodic rod is not: $L_t = N \times L_{cell} = N \times (L_a + L_c) = 3 \times (432 + 432) = 3 \times (864) = 2592\ mm > 1000$.

Conclusion for the steel:: requirements 1, 2, 3 and 4 are met, but requirement 5 is not. Therefore, the material must be changed.

Figure 48 - Stop bands for different values of L_{ca} considering $L_a = 432$ *mm* (steel case) or $L_a = 421,9$ *mm* (aluminum case) or $L_a = 135$ *mm* (nylon case), $N = 1$, $S_{ca} = 2$, $S_{ab} = 1000$ and $S_{cb} = 2000$.

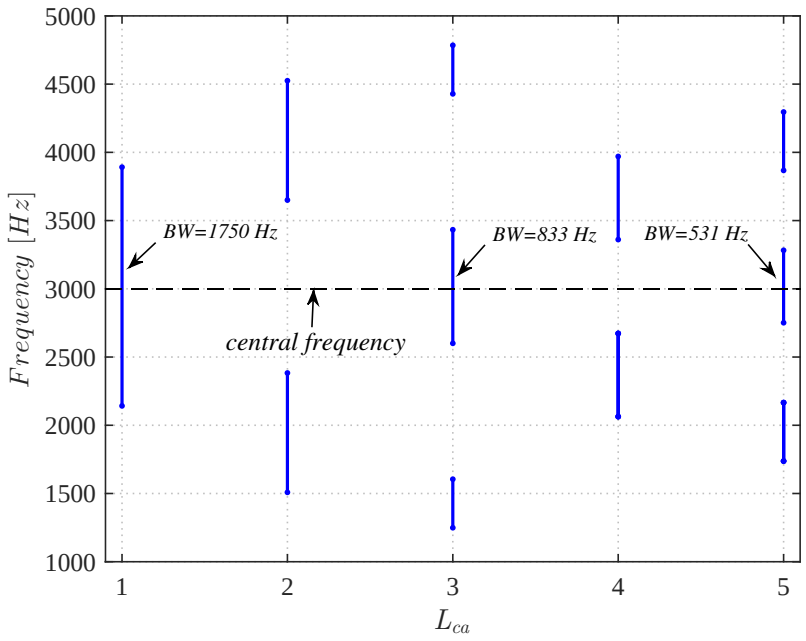

Source: elaborated by the author.

By inspection of equation (90), for the same value of L_a, lower values for the propagation speed v_a (lower E/ρ) result in lower values for the dimensional frequency ω and, as a consequence, the stop bands are located in lower frequencies. On the other hand, lower values of L_a cause the stop bands to arise in higher frequencies. Therefore, an alternative to meet the requirements imposed is to use a material whose propagation speed is lower than the one of steel, which renders possible the reduction of length L_a.

Figure 49 - Transmission for different values of N considering $L_a = 432\ mm$ (steel case) or $L_a = 421,9\ mm$ (aluminum case) or $L_a = 135\ mm$ (nylon case), $L_{ca} = 1$ and $S_{ca} = 2$, $S_{ab} = 1000$ and $S_{cb} = 2000$.

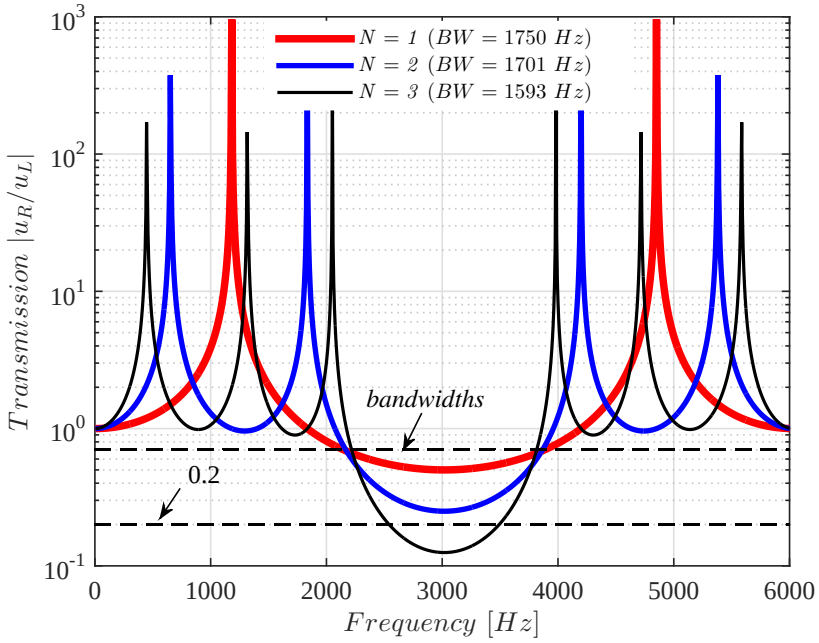

Source: elaborated by the author.

5.2.2 Aluminum material

Consider the aluminum ($E = 70\ Gpa$ and $\rho = 2700\ kg/m^3$) as the candidate material for manufacturing the periodic rod. Repeating all the simulations for this material, for $L_a = 421,9\ mm$, and keeping the values of N, S_{ca} and L_{ca}, equivalent results are obtained, as shown in figures 48 and 49. Thus, for this case, requirements 1, 2, 3 and 4 are also met, but requirement 5 is not: $L_t = N \times L_{cell} = N \times (L_a + L_c) = 3 \times (421,9 + 421,9) = 3 \times (843,8) = 2531,4\ mm >$ 1000. Note that the aluminum's wave propagation speed $\sqrt{E_{Al}/\rho_{Al}} \approx 5091\ m/s$ is close to the one of steel $\sqrt{E_{steel}/\rho_{steel}} \approx 5188\ m/s$, which does not allow a considerable reduction in length L_a.

Conclusion for the aluminum: requirements 1, 2, 3 and 4 are met, but requirement 5 is not. Therefore, the material must be changed.

5.2.3 Nylon material

In the case of Nylon ($E = 3\ Gpa$ and $\rho = 1130\ kg/m^3$), the propagation speed is around $\sqrt{E_{ny}/\rho_{ny}} \approx 1630\ m/s$, which is quite different from those of steel and aluminum. Therefore, a considerable reduction in length L_a is expected in relation to the two previous cases. Repeating the analysis for this material, for $L_a = 135\ mm$, and keeping the values of N, S_{ca} and L_{ca}, equiv-

alent results to those shown in figures 48 and 49 are obtained. For this case, the requirement of total length of the rod is met, since $L_t = N \times L_{cell} = N \times (L_a + L_c) = 3 \times (135 + 135) = 3 \times (270) = 810\ mm < 1000\ mm$.

Conclusion for the nylon: all requirements are met.

Therefore, considering a cylindrical periodic rod with a segment diameter c of 50 *mm*, the full design is given as follows:

- Number of cells, $N = 3$;
- Area ratio, $S_{ca} = 2$;
- Segments length ratio, $L_{ca} = 1$;
- Segment diameter c, $d_c = 50,0\ mm$;
- Segment diameter a, $d_a = (\sqrt{1/S_{ca}}) \times d_c = 35,4\ mm$;
- Segment length a, $L_a = 135,0\ mm$;
- Segment length c $L_c = 135,0\ mm$;
- Total length of the periodic rod, $L_t = 810,0\ mm$.

Figure 50 shows a periodic rod whose dimensions are specified above. Therefore, to validate the design approach proposed in this work, the experimental results for the periodic rod defined are presented in the next section.

Figure 50 - Illustration of a cylindrical periodic rod whose dimensions are obtained using nylon as material.

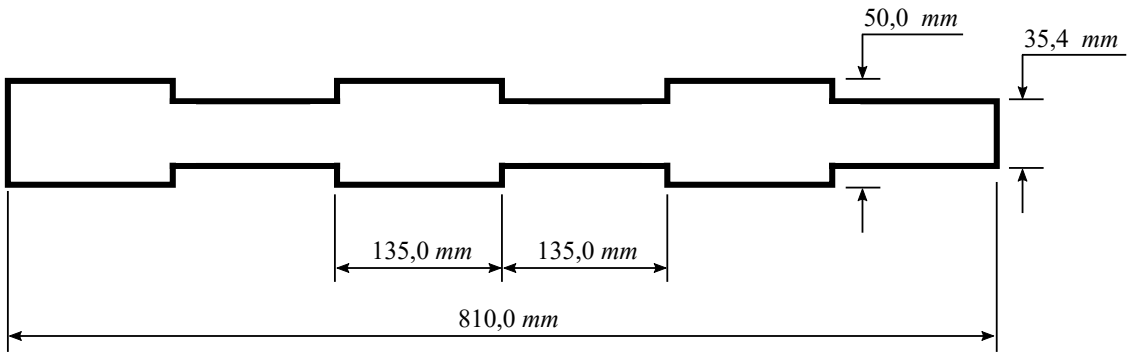

Source: elaborated by the author.

5.3 EXPERIMENTAL VALIDATION

In this section, the transmission is obtained experimentally in terms of acceleration measured at the ends of a cylindrical periodic rod made of nylon whose specifications are listed in section 5.2.3 and illustrated by figure 50. Furthermore, the theoretical and experimental results are compared to validate the methodology proposed in this thesis.

5.3.1 Experimental setup for stop band analysis

The experimental setup is illustrated in figure 51. In this figure can be seen a right hand side higher diameter part which is used to fix the accelerometer and avoid to damage it with the impact hammer. The equipments used consists of: two uniaxial accelerometers (PCB 352A25 miniature), an impact hammer (PCB 086C04), acquisition system (LMS SCADAS Mobile, 8 channels), and a computer (DELL Intel(R) Core(TM) i7-2600, CPU 3.4 GHz, 16GB RAM). The periodic rod is hung by elastic bands to simulate the free-free condition, as shown in figure 52 and, in addition, it is excited by an impact force at the end whose diameter is the smallest. Then, the vibrations are measured by two accelerometers fixed at both ends of the rod. The measurements are obtained and post-processed using the software LMS Test.Lab Impact Testing version 14A with the following acquisition settings: 6400 Hz of bandwidth, 8192 spectral lines, 1,28 acquisition time and 0,78125 of resolution.

Figure 51 - Schematic of experimental setup showing the periodic rod, accelerometers, impact hammer, acquisition system and computer.

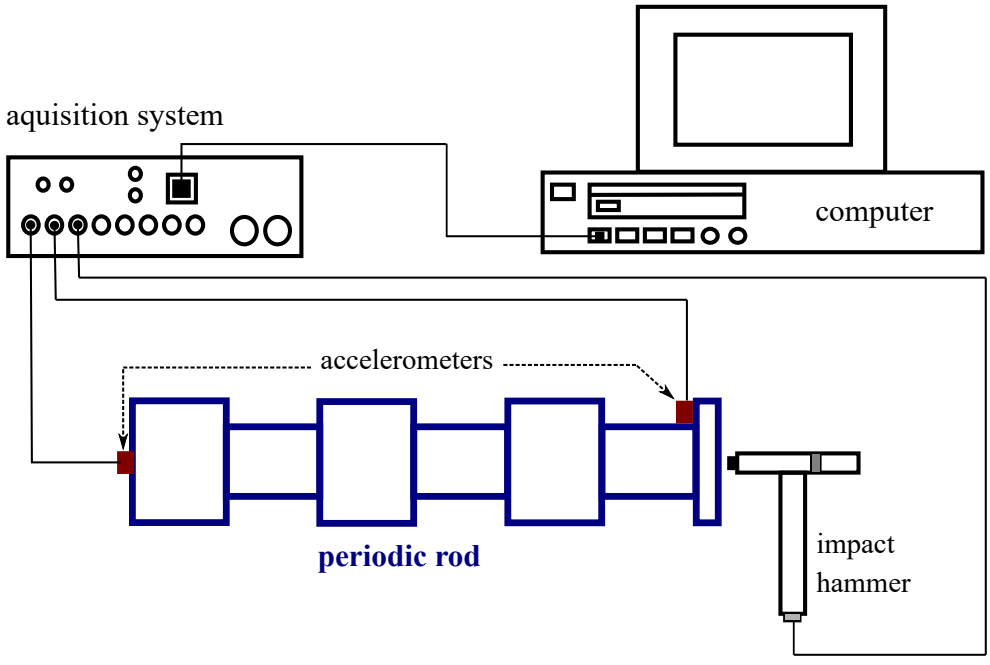

Source: elaborated by the author.

Figure 52 - Periodic rod suspended.

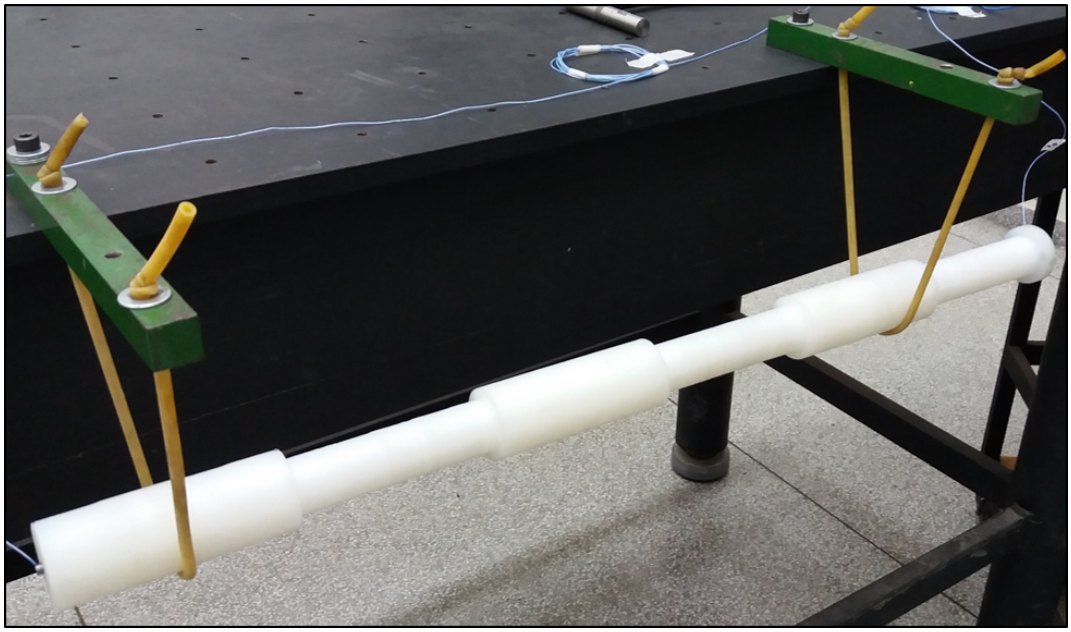

Source: elaborated by the author.

5.3.2 Results and discussions

To represent the manufactured structure, three measurements of diameter were made on each cell in order to obtain mean values for the diameters d_a and d_c. Then, a value of $1,82$ was obtained for the area ratio S_{ca}. To include structural damping in the theoretical model, a commonly used strategy in the literature was adapted (the use of a complex modulus of elasticity), and afterwards $E_{ca} = E_{ca}(1 + j\xi)$ was considered, where ξ is equivalent to the damping factor. The theoretical and experimental responses for the vibration transmission are shown in figure 53. The result from the experimental test shows that the stop band arises between 2311 and 3782 Hz ($BW = 1471$ Hz) and, for a damping factor equal to $\xi = 0,08$, obtained by arbitrary choice to visually match the curves, the theoretical model predicts a stop band between 2305 and 3766 Hz ($BW = 1461$ Hz). In addition, despite a reduction in the stop bands' bandwidth caused by the dimensional variations observed in the periodic rod, it can be seen that all of the design requirements specified in section 5.1 are met.

Figure 53 - Comparison between experimental and theoretical results.

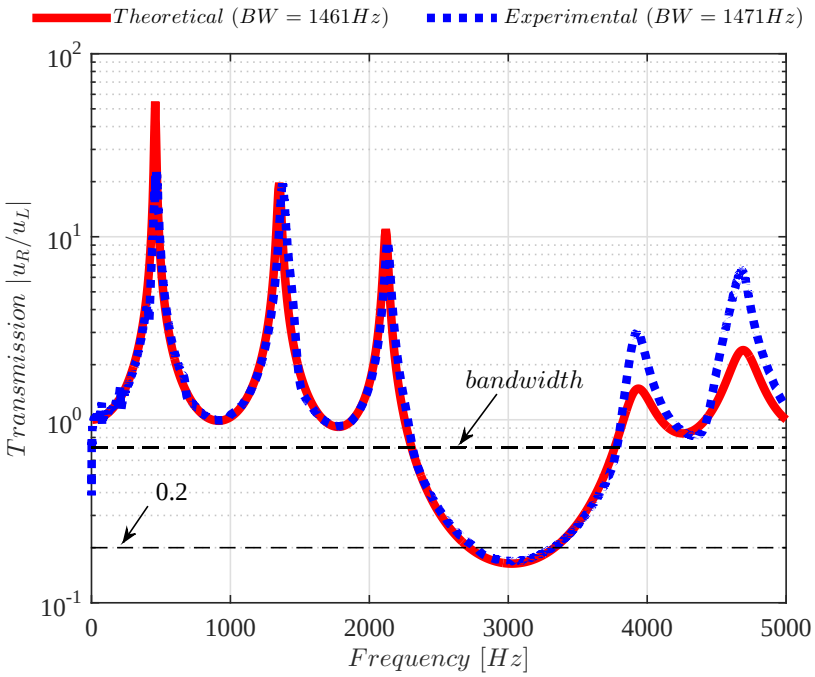

Source: elaborated by the author.

6 CONCLUSIONS

This work has presented an alternative approach to design periodic rod structures. Different analysis techniques concerning this kind of structure have been developed in the literature. In general, they discuss how to find the stop bands for a definite structure geometry. However, the practical problem in engineering is, rather, to define a structure that results in vibration attenuation in certain frequency bands of interest. In addition, analysts must understand other requirements, such as dimensions and types of materials. Therefore, the present work introduces a contribution based on this context.

According to the alternative method for designing periodic rods presented in this work, as well as to the theoretical and experimental results obtained, one can conclude that:

- it is possible to model a periodic infinite hybrid rod by connecting a finite periodic structure between two semi-infinite rods. To do so, the methodology that relates state vectors and wave amplitudes – already known in the literature – is employed;
- it is possible to obtain physical-mathematical scalar relations for the transmission and reflection of waves that propagate in periodic structures. These equations are important tools for the design and analysis of such structures, since they are written in terms of physical properties and geometrical structural parameters;
- the simulations performed indicate that when designing a periodic rod as shown herein, 3 to 4 cells can be used such that the attenuation levels attained represent what is obtained for a periodic structure in its entire extent. Other geometrical and material combinations can provide different results;
- the geometrical parameters of the periodic structure (length ratio L_{ca}, area ratio S_{ca} and number of cells N) have an important influence on stop bands formation, as well as on their characteristics, such as: location in the frequency spectrum, bandwidth and attenuation levels;
- from the analytical formulation it is possible to find a second-order polynomial equation for the transfer matrix eigenvalues similar to the results in the literature (as shown in section 3.4). From this equation the parameters α and β were defined, which constitute the expressions for transmission and reflection. These equations developed can thus be used independently since both lead to the same conclusion (stops bands location and bandwidth in the frequency spectrum, as well as attenuation levels)

- the transmission and reflection curves intersect at the amplitude of $1/\sqrt{2}$, and it occurs when the energy flows of transmitted and reflected waves are the same ($C_{PT} = C_{PR} = 0,5$). Also, for this amplitude value, the stop bands bandwidths for transmission and reflection are equal. Furthermore, it has been shown that in the process of wave dispersion in non-dissipative periodic rods, there exists energy flow conservation, that is, the energy from the incident wave is partially divided into reflected and transmitted energies;

- to represent a finite periodic rod, the homogeneous rod's cross-sectional S_b tending to zero must considered in the model developed (infinite periodic rod). Besides, the results obtained in terms of wave amplitude can be easily converted into uniaxial displacements. This strategy is the key to apply the proposed formulation to real engineering problems, since the structures are finite.

Also, practical details for defining a structure that meets hypothetical requirements of a vibration suppression problem are presented in this work. For this case, to illustrate the design technique's application, three candidate solutions are presented for the design of the periodic rod based on the desired requirements, and it has been shown that one of them meets such requirements. Moreover, the material adopted has demonstrated to have an important influence on the stop bands location, that is, materials whose wave propagation speed is lower cause the stop bands to arise in lower frequencies. Additionally, on the other hand, smaller lengths L_a cause the stop bands to arise in higher frequencies.

To verify the proposed formulation, a periodic rod has been designed applying the methodology developed in this work. Experimental tests have been carried out to verify the stop bands predicted by the formulation. Using a nylon rod with 3 cells and 0,81 meters in length, the stop band was identified between 2311 and 3782 Hz, which is consistent with the computer simulations. Also, it has been considered an non-dimensional ratio to include structural damping through the complex modulus of elasticity. A value of $\eta = 0,08$ has been chosen by exhaustive search (arbitrary choices) to represent the dynamics of the first three modes with the visual similarity criterion between the curves.

Finally, it must be stressed that the formulation developed seems favorable to its application in this kind of structure, especially because the equations are scalar and, thereby, no solutions for matrix systems equations are required, as seen in formulations using finite elements methods and spectrum elements. Furthermore, compared to the classic parametrization by impedance ratio, the parametrization of equations by physical and non-dimensional geometrical properties broadens the understanding of the designer. In addition, vibration suppression using this approach is more appropriate to big structures when metallic materials are employed (owing to their high wave propagation speed). On the other hand, the use of materials whose wave propagation speed is low may make feasible the design of small structures with vibration suppression in low frequencies.

6.1 FUTURE WORK SUGGESTIONS

In developing this thesis, complementary development opportunities have been identified, which can also be helpful to design periodic structures. Therefore, some suggestions are presented as follows:

- to develop the design graphics (figures 24, 26 and 27) for cells of material periodicity, mixed (geometry and material), among other variations;
- to adapt the methodology proposed in this thesis to the design of periodic beam structures, as well as make use of combined solutions of longitudinal, flexural and shear waves propagation;
- to discuss the use of this formulation on the design of truss structures, seeking the inclusion of rods with periodic cells in strategical positions;
- to evaluate applications of suppression of noise caused by propagation in solid medium in this kind of structures;
- to seek strategies to include damping in the formulation developed in order to adjust each mode of interest.

REFERENCES

ANDREESCU, T. **Essential linear algebra with aplications**: a problem - solving approach. [S.l.]: Birkhauser, 2014.

ASIRI, S. Vibration attenuation of automotive vehicle engine using periodic mounts. **International Journal of Vehicle Noise and Vibration**, v. 3, n. 3, p. 302 – 315, 2007.

ASIRI, S.; BAZ, A.; PINES, D. Periodic struts for gearbox support system. **Journal of Vibration and Control**, v. 11, n. 6, p. 709–721, 2005.

BRENNAN, M. J. **Active control of waves on one-dimensional structures**. Thesis (PhD) — Faculty of Enginnering and Applied Science, University of Southampton, Southampton, 1994.

BRENNAN, M. J.; ELLIOTT, S. J.; PINNINGTON, R. J. The dynamic coupling between piezoceramic actuators and a beam. **Acoustical Society of America**, v. 102, n. 4, p. 1931–1942, 1997.

BRENNAN, M. J.; TANG, B.; ALMEIDA, F. C. L. Waves motion in elastic structures. In: JR. V. ANS STEFFEN JR., V. L.; SAVI, M. A. (Ed.). **Dynamics of smart systems and structures, concepts and applications**. [S.l.]: Springer, 2016.

BRILLOUIN, L. **Wave propagation in periodic structures**: electric filters and crystal lattices. [S.l.]: Dover Publications, 1953.

CHEN, R.; WU, T. Vibration reduction in a periodic truss beam carrying locally resonant oscillators. **Journal of Vibration and Control**, v. 22, n. 1, p. 2170–285, 2016.

CHENG, Z.; SHI, Z. Composite periodic foundation and its application for seismic isolation. **Earthquake Engineering & Structural Dynamics**, v. 47, n. 4, p. 925–944, 2017.

CREMER, L.; HECKLI, M.; PETERSSON, B. **Structure-borne sound**: structural vibration and sound radiation at audio frequency. 3rd. ed. Berlin: Springer, 2005.

DUHAMEL, D.; MACE, B. R.; BRENNAN, M. J. Finite element analysis of the vibrations of waveguides and structures periodics. **Journal of Sound and Vibration**, v. 294, p. 205–220, 2006.

FAHY, F.; GARDONIO, P. **Sound and structural vibration**: radiation, transmission and response. 2nd. ed. [S.l.]: Elsevier, 2007.

GAN, C.; WEI, Y.; YAN, S. Longitudinal wave propagation in a multi-step rod with variable cross-section. **Journal of Vibration and Control**, v. 22, n. 3, p. 837–852, 2016.

GAOFENG, J.; ZHIFEI, S. A new seismic isolation method and its feasibility study. **Earthquake Engineering and Engineering Vibration**, v. 9, n. 1, p. 75–82, 2010.

GAZALET, J.; DUPONT, S.; KASTELIK J., C.; ROLLAND, Q.; DJAFARI-ROUHANI, B. A tutorial survey on waves propafation in periodic media: Electronic, photonic and phononic crystals. perception of the bloch theorem in real and fourier domains. **Wave Motion**, v. 50, p. 619–654, 2013.

GRAFF, K. F. **Wave motion in elastic solids**. New York: Dover Publications, 1991.

HAGEDORN, P.; DASGUPTA, A. **Vibration and waves in continuos mechanical systems**. [S.l.]: John Wiley & Sons, 2007.

HVATOV, A.; SOROKIN, S. V. Free vibrations of finite periodic structures in pass- and stop-bands of the counterpart infinite waveguides. **Journal of Sound and Vibration**, v. 347, p. 200–217, 2015.

JUNG, W.; GU, Z.; BAZ, A. Mechanical filtering characteristics of passive periodic engine mount. **Finite Elements in Analysis and Design**, v. 46, p. 685–697, 2010.

MACE, B. R.; DUHAMEL, D.; BRENNAN, M. J.; HINKE, L. Finite element prediction of wave motion in structural waveguides. **Journal of the Acoustical Society of America**, v. 117, p. 2835–2843, 2005.

MANKTELOW, K. L. **Disperson analysis of nonLinear periodic structures**. Thesis (PhD) — Institute of Technology, School of Mechanical Engineering, Georgia, 2013.

MEAD, D. J. Wave propagation in continuous periodic structures : research contributions from southampton. **Journal of Sound and Vibration**, v. 190, n. 3, p. 495–524, 1996.

MENCIK, J. M. On the low- and mid-frequency forced response of elastic structures using wave finite elements with one- dimensional propagation. **Computers and Structures**, v. 88, p. 674–689, 2010.

____. New advances in the forced response computation of periodic structures using the wave finite element (wfe) method. **Computational Mechanics**, v. 54, n. 3, p. 789–801, 2014.

NARISETTI, R. K. **Wave propagation in non linear periodic structures**. Thesis (PhD) — Institute of Technology, School of Aerospace Engineering, Georgia, 2010.

NIELSEN, R. B.; SOROKIN, S. V. Periodicity effects of axial waves in elastic compound rods. **Journal of Sound and Vibration**, v. 353, p. 135–149, 2015.

NOBREGA, E. D.; GAUTIER, F.; PELAT, A.; SANTOS, J. M. C. D. Vibration band-gaps for elastic metamaterial rods using wave finite element method. **Mechanical Systems and Signal Processing**, v. 79, p. 192–202, 2016.

OSTACHOWICZ, W.; KUDELA, P.; KRAWCZUK, M.; ZAK, A. **Guided waves in structures for SHM**: the time-domain spectral element method. [S.l.]: John Wiley & Sons, 2012.

PHANI, A. S.; J., W.; FLECK, N. A. Wave propagation in two-dimensional periodic lattices. **Acoustical Society of America**, v. 119, n. 4, p. 1995–2005, 2006.

ROSE, J. L. **Ultrasonic guided waves in solid media**. Cambridge: Cambridge University Press, 2014.

SILVA, P.; MENCIK, J. M.; ARRUDA, J. R. F. Wave finite element-based superelements for forced response analysis of coupled systems via dynamic substructuring. **International Journal for Numerical Methods in Engineering**, 2015.

SINGH, A.; PINES, D. J.; BAZ, A. Active/passive redution of vibration of periodic one-dimensional structures using piezoelectric actuators. **Smart Materials and Structures**, v. 13, p. 698–711, 2004.

SOLAROLI, G.; GU, Z.; BAZ, A.; RUZZENE, M. Wave propagation in periodic stiffened shells: Spectral finite element modeling and experiments. **Jornal of Vibration and Control**, v. 9, p. 1057–1081, 2003.

SONG, Y.; WEN, J.; YU, D.; WEN, X. Suppression of vibration and noise radiation in a flexible floating raft system using periodic structures. **Journal of Vibration and Control**, v. 21, n. 2, p. 217–228, 2015.

SZEFI, J. T. **Helicopter gearbox isolation using periodically layered fluidic isolators**. Thesis (PhD) — Pennsylvania State University, Department of Mechanical and Nuclear Engineering, Pennsylvania, 2003a.

SZEFI, J. T.; SMITH, E. C.; LESIEUTRE, G. A. Formulation and validation of a ritz-based analytical model of high-frequency periodically layered isolators in compression. **Journal of Sound and Vibration**, v. 268, p. 85–101, 2003b.

____. Design and testing of a compact fluidic layered isolator for high-frequency helicopter gearbox isolation. In: AIAA/ASME/ASCE/AHS/ASC STRUCTURES, STRUCTURAL DYNAMICS & MATERIALS CONFERENCE. 45., 2004. **Conference...** [S.l.: s.n.], 2004.

WANG, Z.; MAK, C. M. Optimization of geometrical parameters for periodical structures applied to floating raft systems by genetic algorithms. **Applied Acoustics**, v. 129, p. 108–115, 2018.

XIANG, H. J.; SHI, Z. F. ; WANG, S. J.; MO, Y. L. Periodic materials-based vibration attenuation in layered foundations: experimental validation. **Smart Materials and Structures**, v. 21, 2012.

XIONG, C.; SHI, Z.; XIANG, H. J. Attenuation of building vibration using periodic foundations. **Advances in Structural Enginnering**, v. 15, n. 8, p. 1375–1388, 2012.

XIUCHANG, H.; AIHUA, J.; ZHIYI, Z.; HONGXING, H. Design and optimization of periodic structure mechanical filter in suppression of foundation resonances. **Journal of Sound and Vibration**, v. 330, p. 4689 – 4712, 2011.

YILDIRIM, R. O. Longitudinal elastic wave propagation and energy flux at a discontinuity of two dissimilar semi-infinite circular rods. **JSME International Journal**, v. 37, n. 4, p. 495–501, 1994.

APPENDIX A - EQUATION FOR TRANSMISSION AND REFLECTION

This appendix describes the mathematical development to obtain the transmission (Eq. 82) and reflection (Eq. 94) presented in sections 3.2 and 3.3, respectively. Mathematical manipulations are developed using the relation between the outgoing $\mathbf{a}_{out}$ and incoming $\mathbf{a}_{inc}$ waves given by (see section 3.1)

$$\mathbf{a}_{out} = -\gamma^{-1}\mu\mathbf{a}_{inc} \tag{102}$$

where

$$\mu = [(\mathbf{H}_b)_1 \mid (-\tilde{\mathbf{H}})_2] \tag{103}$$

$$\gamma = [(-\tilde{\mathbf{H}})_1 \mid (\mathbf{H}_b)_2] \tag{104}$$

$$\tilde{\mathbf{H}} = \tilde{\mathbf{T}}_G\mathbf{H}_b = \tilde{\mathbf{T}}_{cell}^N\mathbf{H}_b \tag{105}$$

$$\tilde{\mathbf{T}}_{cell} = \mathbf{H}_c\mathbf{T}_c\mathbf{H}_c^{-1}\mathbf{H}_a\mathbf{T}_a\mathbf{H}_a^{-1} = \tilde{\mathbf{T}}_c\tilde{\mathbf{T}}_a \tag{106}$$

To develop the equation (102) it is necessary to manipulate the equations (106) to (103) as shown:

- **Developing equation** (106):

Consider

$$\mathbf{H}_c = \begin{bmatrix} 1 & 1 \\ jk_cE_cS_c & -jk_cE_cS_c \end{bmatrix} \tag{107}$$

and

$$\mathbf{H}_c^{-1} = \frac{1}{det(\mathbf{H}_c)} \begin{bmatrix} -jk_cE_cS_c & -1 \\ -jk_cE_cS_c & 1 \end{bmatrix} = \ldots = \begin{bmatrix} \frac{1}{2} & \frac{1}{j2k_cE_cS_c} \\ \frac{1}{2} & \frac{1}{-j2k_cE_cS_c} \end{bmatrix} \tag{108}$$

where

$$det(\mathbf{H}_c) = -jk_cE_cS_c - jk_cE_cS_c = -j2k_cE_cS_c \tag{109}$$

Substituting them, it is possible to write:

$$\tilde{\mathbf{T}}_c = \mathbf{H}_c\mathbf{T}_c\mathbf{H}_c^{-1} = \begin{bmatrix} 1 & 1 \\ jk_cE_cS_c & -jk_cE_cS_c \end{bmatrix} \begin{bmatrix} e^{jk_cL_c} & 0 \\ 0 & e^{-jk_cL_c} \end{bmatrix} \begin{bmatrix} \frac{1}{2} & \frac{1}{j2k_cE_cS_c} \\ \frac{1}{2} & \frac{1}{-j2k_cE_cS_c} \end{bmatrix} \tag{110}$$

$$\tilde{\mathbf{T}}_c = \begin{bmatrix} e^{jk_cL_c} & e^{-jk_cL_c} \\ jk_cE_cS_ce^{jk_cL_c} & -jk_cE_cS_ce^{-jk_cL_c} \end{bmatrix} \begin{bmatrix} \frac{1}{2} & \frac{1}{j2k_cE_cS_c} \\ \frac{1}{2} & \frac{1}{-j2k_cE_cS_c} \end{bmatrix} \tag{111}$$

$$\tilde{\mathbf{T}}_c = \begin{bmatrix} \frac{e^{jk_cL_c} + e^{-jk_cL_c}}{2} & \frac{e^{jk_cL_c} - e^{-jk_cL_c}}{j2k_cE_cS_c} \\ j2k_cE_cS_c\frac{e^{jk_cL_c} - e^{-jk_cL_c}}{2} & \frac{e^{jk_cL_c} + e^{-jk_cL_c}}{2} \end{bmatrix} = \begin{bmatrix} \cos(k_cL_c) & \frac{1}{Z_c}\sin(k_cL_c) \\ -Z_c\sin(k_cL_c) & \cos(k_cL_c) \end{bmatrix} \tag{112}$$

Similarly, it is possible to obtain

$$\tilde{\mathbf{T}}_a = \mathbf{H}_a \mathbf{T}_a \mathbf{H}_a^{-1} = ... = \begin{bmatrix} \cos(k_a L_a) & \frac{1}{Z_a}\sin(k_a L_a) \\ -Z_a \sin(k_a L_a) & \cos(k_a L_a) \end{bmatrix} \tag{113}$$

where

$$Z_a = k_a E_a S_a \quad ; \quad Z_c = k_c E_c S_c \tag{114}$$

Also, using the equations (112) and (113), it is possible to get

$$\tilde{\mathbf{T}}_{cell} = \tilde{\mathbf{T}}_c \tilde{\mathbf{T}}_a = ... = \begin{bmatrix} \tilde{T}_{11} & \tilde{T}_{12} \\ \tilde{T}_{21} & \tilde{T}_{22} \end{bmatrix} \tag{115}$$

where

$$\tilde{T}_{11} = \cos(k_c L_c)\cos(k_a L_a) - \frac{Z_a}{Z_c}\sin(k_c L_c)\sin(k_a L_a) \tag{116}$$

$$\tilde{T}_{12} = \frac{1}{Z_a}\cos(k_c L_c)\sin(k_a L_a) + \frac{1}{Z_c}\sin(k_c L_c)\cos(k_a L_a) \tag{117}$$

$$\tilde{T}_{21} = -Z_c \sin(k_c L_c)\cos(k_a L_a) - Z_a \cos(k_c L_c)\sin(k_a L_a) \tag{118}$$

$$\tilde{T}_{22} = -\frac{Z_c}{Z_a}\sin(k_c L_c)\sin(k_a L_a) + \cos(k_c L_c)\cos(k_a L_a) \tag{119}$$

- **Developing equation** (105):

In this work is considered the following relation for power of a 22 matrix (ANDREESCU, 2014)

$$\tilde{\mathbf{T}}_{cell}^N = \alpha \tilde{\mathbf{T}}_{cell} - \beta \mathbf{I} \tag{120}$$

where

$$\alpha = \frac{\Lambda_1^N - \Lambda_2^N}{\Lambda_1 - \Lambda_2}, \quad \beta = \frac{\Lambda_2\Lambda_1^N - \Lambda_1\Lambda_2^N}{\Lambda_1 - \Lambda_2} \tag{121}$$

N is the number of cells, $\Lambda_{1,2}$ are first and second eigenvalues obtained from $\tilde{\mathbf{T}}_{cell}$ matrix and $\mathbf{I}$ is 22 identity matrix. Using the relationship (120), is written the following equation

$$\tilde{\mathbf{H}} = \tilde{\mathbf{T}}_{cell}^N \mathbf{H}_b = \begin{bmatrix} (\alpha\tilde{T}_{11} - \beta) & \alpha\tilde{T}_{12} \\ \alpha\tilde{T}_{21} & (\alpha\tilde{T}_{22} - \beta) \end{bmatrix} \begin{bmatrix} 1 & 1 \\ jZ_b & -jZ_b \end{bmatrix} \tag{122}$$

$$\tilde{\mathbf{H}} = \begin{bmatrix} (\alpha\tilde{T}_{11} - \beta + jZ_b\alpha\tilde{T}_{12}) & (\alpha\tilde{T}_{11} - \beta - jZ_b\alpha\tilde{T}_{12}) \\ (\alpha\tilde{T}_{21} + jZ_b(\alpha\tilde{T}_{22} - \beta)) & (\alpha\tilde{T}_{21} - jZ_b(\alpha\tilde{T}_{22} - \beta)) \end{bmatrix} \tag{123}$$

where

$$Z_b = k_b E_b S_b \tag{124}$$

- **Developing equations** (103) and (104):

From section 3.1, it is possible to write

$$\mu = [(\mathbf{H}_b)_1 \mid (-\tilde{\mathbf{H}})_2] = \begin{bmatrix} 1 & -(\alpha\tilde{T}_{11} - \beta - jZ_b\alpha\tilde{T}_{12}) \\ jZ_b & -(\alpha\tilde{T}_{21} - jZ_b(\alpha\tilde{T}_{22} - \beta)) \end{bmatrix} \tag{125}$$

$$\gamma = [(-\tilde{\mathbf{H}})_1 \mid (\mathbf{H}_b)_2] = \begin{bmatrix} -(\alpha\tilde{T}_{11} - \beta + jZ_b\alpha\tilde{T}_{12}) & 1 \\ -(\alpha\tilde{T}_{21} + jZ_b(\alpha\tilde{T}_{22} - \beta)) & -jZ_b \end{bmatrix} \tag{126}$$

and also

$$\gamma^{-1} = \frac{1}{det(\gamma)} \begin{bmatrix} -jZ_b & -1 \\ (\alpha\tilde{T}_{21} + jZ_b(\alpha\tilde{T}_{22} - \beta)) & -(\alpha\tilde{T}_{11} - \beta + jZ_b\alpha\tilde{T}_{12}) \end{bmatrix} \tag{127}$$

where

$$\eta = det(\gamma) = \alpha(\tilde{T}_{21} - Z_b^2\tilde{T}_{12}) + jZ_b(\alpha(\tilde{T}_{11} + \tilde{T}_{22}) - 2\beta) \tag{128}$$

Substituting the equations (125) and (127) into the equation (102), it is possible to write

$$\mathbf{a}_0 = -\gamma^{-1}\mu\mathbf{a}_i = \mathbf{G}\mathbf{a}_i \tag{129}$$

where

$$\mathbf{G} = -\gamma^{-1}\mu = ... = \begin{bmatrix} \mathbf{G}_{11} & \mathbf{G}_{12} \\ \mathbf{G}_{21} & \mathbf{G}_{22} \end{bmatrix} \tag{130}$$

$$\mathbf{G}_{11} = \frac{j2Z_b}{\eta} \tag{131}$$

$$\mathbf{G}_{12} = \frac{-\alpha[(\tilde{T}_{21} + Z_b^2\tilde{T}_{12}) + jZ_b(\tilde{T}_{11} - \tilde{T}_{22})]}{\eta} \tag{132}$$

$$\mathbf{G}_{21} = \frac{-\alpha[(\tilde{T}_{21} + Z_b^2\tilde{T}_{12}) + jZ_b(\tilde{T}_{22} - \tilde{T}_{11})]}{\eta} \tag{133}$$

$$\mathbf{G}_{22} = \frac{j2Z_b[\alpha^2(\tilde{T}_{11}\tilde{T}_{12} - \tilde{T}_{12}\tilde{T}_{21}) + \alpha\beta(-\tilde{T}_{11} - \tilde{T}_{22}) + \beta^2]}{\eta} \tag{134}$$

Using the equations (78) and (79) and the equation shown above is possible to write

$$\begin{Bmatrix} A_r \\ A_t \end{Bmatrix} = \begin{bmatrix} \mathbf{G}_{11} & \mathbf{G}_{12} \\ \mathbf{G}_{21} & \mathbf{G}_{22} \end{bmatrix} \begin{Bmatrix} 0 \\ A_i \end{Bmatrix} \tag{135}$$

Note that is assumed that there are no incident waves from the rigth side of the structure. Thus,

the equation (135) results in

$$\frac{A_t}{A_i} = \frac{A_{transmitted}}{A_{incident}} = \mathbf{G}_{22} \tag{136}$$

$$\frac{A_r}{A_i} = \frac{A_{reflected}}{A_{incident}} = \mathbf{G}_{12} \tag{137}$$

Substituting the equations (116) to (119) into equations (132) and (134) and considering that $\Omega = \dfrac{\omega L_a}{\pi v_a}$ is non-dimensional frequency, the non-dimensional form is obtained

$$\mathbf{G}_{22} = \frac{j2[\alpha^2 + \beta^2 + \alpha\beta b(\Omega)]}{\eta} \tag{138}$$

and

$$\begin{aligned}\mathbf{G}_{12} = \{-\alpha[(-\kappa_{ab} + \frac{1}{\kappa_{ab}})\sin(\pi\Omega)\cos(\pi\tau\Omega) + (-\kappa_{cb} + \frac{1}{\kappa_{cb}})\sin(\pi\tau\Omega)\cos(\pi\Omega)] \\ -j\alpha[(\kappa_{ca} - \frac{1}{\kappa_{ca}})\sin(\pi\Omega)\sin(\pi\tau\Omega)]\}/\eta\end{aligned} \tag{139}$$

where

$$\begin{aligned}\eta = \alpha[(-\kappa_{ab} - \frac{1}{\kappa_{ab}})\sin(\pi\Omega)\cos(\pi\tau\Omega) + (-\kappa_{cb} - \frac{1}{\kappa_{cb}})\cos(\pi\Omega)\sin(\pi\tau\Omega)] \\ +j[-\alpha\beta b(\Omega) - 2\beta]\end{aligned} \tag{140}$$

$$b(\Omega) = -2\cos(\pi\Omega)\cos(\pi\tau\Omega) + (\kappa_{ca} + \frac{1}{\kappa_{ca}})\cos(\pi\Omega)\sin(\pi\tau\Omega) \tag{141}$$

and

$$\kappa_{ab} = \frac{Z_a}{Z_b} \qquad \kappa_{cb} = \frac{Z_c}{Z_b} \qquad \kappa_{ca} = \frac{Z_c}{Z_a} \tag{142}$$

are impedance parameters and

$$\tau = \frac{L_c v_a}{L_a v_c} \tag{143}$$

is ratio of propagation times parameter.

The equations (138) and (139) can be rewritten in terms of physical and geometric param-

eters of the structure

$$\mathbf{G}_{22} = \frac{j2[\alpha^2 + \beta^2 + \alpha\beta b(\Omega)]}{\eta} \tag{144}$$

$$\begin{aligned}\mathbf{G}_{12} = \{-\alpha[(-S_{ab}\sqrt{E_{ab}\rho_{ab}} + \frac{1}{S_{ab}\sqrt{E_{ab}\rho_{ab}}})\sin(\pi\Omega)\cos(\pi\Omega L_{ca}\sqrt{\frac{\rho_{ca}}{E_{ca}}})+ \\ (-S_{cb}\sqrt{E_{cb}\rho_{cb}} + \frac{1}{S_{cb}\sqrt{E_{cb}\rho_{cb}}})\sin(\pi\Omega L_{ca}\sqrt{\frac{\rho_{ca}}{E_{ca}}})\cos(\pi\Omega)]- \\ j\alpha[(S_{ca}\sqrt{E_{ca}\rho_{ca}} - \frac{1}{S_{ca}\sqrt{E_{ca}\rho_{ca}}})\sin(\pi\Omega)\sin(\pi\Omega L_{ca}\sqrt{\frac{\rho_{ca}}{E_{ca}}})]\}/\eta\end{aligned} \tag{145}$$

where

$$\begin{aligned}\eta = \alpha[(-S_{ab}\sqrt{E_{ab}\rho_{ab}} - \frac{1}{S_{ab}\sqrt{E_{ab}\rho_{ab}}})\sin(\pi\Omega)\cos(\pi\Omega L_{ca}\sqrt{\frac{\rho_{ca}}{E_{ca}}})+ \\ (-S_{cb}\sqrt{E_{cb}\rho_{cb}} - \frac{1}{S_{cb}\sqrt{E_{cb}\rho_{cb}}})\cos(\pi\Omega)\sin(\pi\Omega L_{ca}\sqrt{\frac{\rho_{ca}}{E_{ca}}})] + j[-\alpha b(\Omega) - 2\beta]\end{aligned} \tag{146}$$

and

$$\begin{aligned}b(\Omega) = -2\cos(\pi\Omega)\cos(\pi\Omega L_{ca}\sqrt{\frac{\rho_{ca}}{E_{ca}}}) + (S_{ca}\sqrt{E_{ca}\rho_{ca}} + \frac{1}{S_{ca}\sqrt{E_{ca}\rho_{ca}}})\times \\ \times\sin(\pi\Omega)\sin(\pi\Omega L_{ca}\sqrt{\frac{\rho_{ca}}{E_{ca}}})\end{aligned} \tag{147}$$

where

$$L_{ca} = \frac{L_c}{L_a} \tag{148}$$

$$S_{ab} = \frac{S_a}{S_b} \qquad S_{cb} = \frac{S_c}{S_b} \qquad S_{ca} = \frac{S_c}{S_a} \tag{149}$$

$$E_{ab} = \frac{E_a}{E_b} \qquad E_{cb} = \frac{E_c}{E_b} \qquad E_{ca} = \frac{E_c}{E_a} \tag{150}$$

$$\rho_{ab} = \frac{\rho_a}{\rho_b} \qquad \rho_{cb} = \frac{\rho_c}{\rho_b} \qquad \rho_{ca} = \frac{\rho_c}{\rho_a} \tag{151}$$

are ratios of geometric and physical parameters.

APPENDIX B - TRANSFER MATRIX EIGENVALUE ANALYSIS

This appendix describes the mathematical development to obtain the equation (98). Based on the section 3.4 the relation between the left and right hand sides structure is given by

$$\left\{ \begin{array}{c} u_R \\ F_R \end{array} \right\} = \tilde{\mathbf{T}}_{cell} \left\{ \begin{array}{c} u_L \\ F_L \end{array} \right\} \tag{152}$$

The periodic condition (Eq. 1) for the displacements and forces in a section implies to the following equation (BRILLOUIN, 1953)

$$\left\{ \begin{array}{c} u_R \\ F_R \end{array} \right\} = \Lambda \left\{ \begin{array}{c} u_L \\ F_L \end{array} \right\} \tag{153}$$

From equations (152) and (153) the following eigenvalue problem is defined

$$(\tilde{\mathbf{T}}_{cell} - \Lambda \mathbf{I}) \left\{ \begin{array}{c} u_L \\ F_L \end{array} \right\} = \mathbf{0} \tag{154}$$

where $\tilde{\mathbf{T}}_{cell}$ is given by equation (115), $\mathbf{I}$ is the identity matrix and Λ are the eigenvalues which are associated to the frequency. The nontrivial solution fo this equation requires to solve the determinant function $det(\tilde{\mathbf{T}}_{cell} - \Lambda \mathbf{I}) = 0$.

$$det(\tilde{\mathbf{T}}_{cell} - \Lambda \mathbf{I}) = det \left[\begin{array}{cc} \tilde{T}_{11} - \Lambda & \tilde{T}_{12} \\ \tilde{T}_{21} & \tilde{T}_{22} - \Lambda \end{array} \right] = 0 \tag{155}$$

or

$$\Lambda^2 + (-\tilde{T}_{11} - \tilde{T}_{22})\Lambda + (\tilde{T}_{11}\tilde{T}_{22} - \tilde{T}_{12}\tilde{T}_{21}) = 0 \tag{156}$$

Substituing the equations (116) to (119) from appendix A into equation (156), is obtained

the following equation

$$\Lambda^2 + b(\omega)\Lambda + 1 = 0 \tag{157}$$

where

$$b(\omega) = -2\cos(k_c L_c)\cos(k_a L_a) + (\frac{Z_a}{Z_c} + \frac{Z_c}{Z_a})\sin(k_c L_c)\sin(k_a L_a) \tag{158}$$

The roots of the equation (157) are the eigenvalues of the matrix $\mathbf{T}_{cell}$.

Considering that $\Omega = \dfrac{\omega L_a}{\pi v_a}$ is non-dimensional frequency, it is obtained the equation (158) in non-dimensional form

$$b(\Omega) = -2\cos(\pi\Omega)\cos(\pi\tau\Omega) + (\kappa_{ca} + \frac{1}{\kappa_{ca}})\cos(\pi\Omega)\sin(\pi\tau\Omega) \tag{159}$$

where

$$\kappa_{ca} = \frac{Z_c}{Z_a} \tag{160}$$

are impedance parameters and

$$\tau = \frac{L_c v_a}{L_a v_c} \tag{161}$$

is ratio of propagation times parameter. Note that the equation (159) is a terms of the equations proposed to relation of transmission and reflection shown in appendix A. In addition, this equation is rewritten in terms of physical and geometric parameters of the structure, i.e.,

$$\begin{aligned} b(\Omega) = -2\cos(\pi\Omega)\cos(\pi\Omega L_{ca}\sqrt{\frac{\rho_{ca}}{E_{ca}}}) + (S_{ca}\sqrt{E_{ca}\rho_{ca}} + \frac{1}{S_{ca}\sqrt{E_{ca}\rho_{ca}}})\times \\ \times \sin(\pi\Omega)\sin(\pi\Omega L_{ca}\sqrt{\frac{\rho_{ca}}{E_{ca}}}) \end{aligned} \tag{162}$$

where

$$S_{ca} = \frac{S_c}{S_a} \qquad L_{ca} = \frac{L_c}{L_a} \qquad E_{ca} = \frac{E_c}{E_a} \qquad \rho_{ca} = \frac{\rho_c}{\rho_a} \tag{163}$$